UNIVERSITY OF OKLAHOMA

GRADUATE COLLEGE

PERFORMANCE CHARACTERISTICS OF SELECTED ASPHALT MIXES: A LABORATORY AND FIELD STUDY

A THESIS

SUBMITTED TO THE GRADUATE FACULTY

in partial fulfillment of the requirements for the

Degree of

MASTER OF SCIENCE

By

SINNIAH KARUPPIAH NAVARATNARAJAH
Norman, Oklahoma
2006

Downloaded from SHAREOK. Persistent Handle URL: http

UNIVERSITY OF OKLAHOMA
LIBRARIES

THESIS
NAV
Cop. 2

PERFORMANCE CHARACTERISTICS OF SELECTED ASPHALT MIXES: A LABORATORY AND FIELD STUDY

A THESIS APPROVED FOR THE
SCHOOL OF CIVIL ENGINEERING AND ENVIRONMENTAL SCIENCE

BY



©Copyright by SINNIAH KARUPPIAH NAVARATNARAJAH 2006
All Rights Reserved.

ACKNOWLEDGEMENT

A journey is easier when you travel together. Interdependence is certainly more valuable than independence. This thesis is the result of two and half years of work whereby I have been accompanied and supported by many people. It is a pleasant aspect that I now have the opportunity to express my gratitude for all of them.

The first person I would like to thank is my supervisor, Dr. Musharraf M. Zaman. I have been in his project since 2004 when I started my graduate study. During these years I have known Dr.Zaman as a sympathetic and principle-centered person. His overly enthusiastic attitude and integral view on research and his mission for providing 'only high-quality work and not less', has made a deep impression on me. I owe him a lot of gratitude for having shown me this way of research.

I would like to thank my promoter and co-advisor, Dr. Naji Khoury, who kept an eye on the progress of my work and always was available when I needed his advice and help. His guidance and support made my working and learning experience, a very special one. I would also like to thank Dr. Robert Nairn, the other member of my thesis committee who monitored my work and made efforts in reading and providing me with valuable comments on earlier versions of this thesis.

I am grateful to Oklahoma Department of Transportation (ODOT) and Oklahoma Department of Environmental Quality (ODEQ) for providing necessary funding for this research work and support during field testing. I would like to thank Danny Gierhart of ODOT and Chau Yih Cheong of Burgess Engineering for their support and arrangement during field testing. I am also thankful to Mike Schmitz for his valuable assistance whenever I needed in the laboratory.

During this work I have collaborated with many colleagues for whom I have great regard, and I wish to extend my warmest thanks to Rajul, Wasi, Pranshoo, Charbel and Kunal for their support and encouragement.

I am also thankful to Susan Williams, Molly Smith, Brenda Finch, Audre Carter and Karen Kelly for their support for my graduation.

I have met so many teachers in my life and this is the time to thank all of them for their guidance in each step of my school life. A special thanks goes to Mr. Jeevarajah, my mathematics teacher, I am really glad that I have come to know him in my life.

Finally, I feel a deep sense of gratitude for my father and mother who formed a part of my vision and taught me the good things that really matter in life. They taught me the value of hard work by their own example. I would like to share this moment of happiness with them. I also am grateful for my sister and brother for rendering me the sense and the value of brotherhood. I am glad to be one of them.

TABLE OF CONTENTS

ACKNOWLEDGEMENT iv
LIST OF TABLES viii
LIST OF FIGURES x
ABSTRACT xiii

CHAPTER 1 1
INTRODUCTION 1
1.1. Introduction 1
1.2. Resilient Modulus 2
1.3. Rutting Effect on HMA Pavements 3
1.4. Problem Statement 6
1.5. Hypothesis and Objectives 7
1.6. Thesis Format 8

CHAPTER 2 11
LITERATURE REVIEW 11
2.1. General 11
2.2. Cyclic Indirect Tension Resilient Modulus Test 11
2.3. Factors Affecting Indirect Tension Resilient Modulus 12
2.3.1. Effect of Loading 13
2.3.2. Effect of Temperature 14
2.3.3. Effect of Air Voids 15
2.4. Permanent Deformation or Rutting 17
2.5. Non-destructive Testing Techniques 19
2.6. Fatigue Cracking 21
2.7. Permeability of HMA 22
2.8. Performance of Chat in Flexible Pavements 23

CHAPTER 3 27
RESEARCH APPROACH 27
3.1. General 27
3.2. Sources of Materials 27
3.3. Laboratory Testing 28
3.3.1. Cyclic Indirect Tension Resilient Modulus Test 28
3.3.1.1. Sample Preparation for M_R Testing 31
3.3.1.2. M_R Test Procedure 31
3.3.1.3. Accuracy of Deflection Value in M_R Calculation 33
3.3.2. APA Rut Test 33
3.3.3. Fatigue Test 35
3.3.4. Permeability Test 36
3.3.5 Laboratory Seismic Modulus Test 37
3.4. Field Testing 38
3.4.1. Falling Weight Deflectometer (FWD) Test 38

3.4.2. Ground Penetrating Radar (GPR) 40
3.4.3. Spectral Analysis of Surface Waves (SASW) 40

CHAPTER 4 56
RESULTS AND DISCUSSION 56
4.1. General 56
4.2. Laboratory tests 56
4.2.1. Cyclic Indirect Tension Resilient Modulus Test 56
4.2.1.1. Variation of M_R with Stress Ratio 56
4.2.1.2. M_R Values at Selected Stress Ratios 60
4.2.1.3. Effect of Binder Content on Resilient Modulus 61
4.2.1.4. Effect of Air Voids on Resilient Modulus 62
4.2.1.5. Effect of Aggregate Sizes on Resilient Modulus 63
4.2.1.6. Variation of M_R with Temperature 64
4.2.1.7. A Model to Predict Resilient Modulus 65
4.2.2. APA Rut Test 68
4.2.2.1. Effect of Binder Content on Rut Depth 69
4.2.2.2. Effect of Air Voids on Rut Depth 70
4.2.2.3. Effect of Percentage Fines on Rut Depth 71
4.2.2.4. General Model to Predict Rutting Potential 71
4.2.3. Correlations between M_R and APA Rut 72
4.2.4. APA Fatigue Test 74
4.2.5. Permeability Test 76
4.2.6. Laboratory Seismic Modulus Test 79
4.2.7. Relative Comparison between M_R and E_S 80
4.3. Field Non-Destructive Tests 81
4.3.1. Falling Weight Deflectometer Test 81
4.3.3. Spectral Analysis of Surface Waves (SASW) test 83
4.3.4. Ground Penetrating Radar (GPR) test 84

CHAPTER 5 135
CONCLUSIONS AND RECOMMENDATIONS 135
5.1. Conclusions 135
5.2. Recommendations 139

REFERENCES 140

APPENDIX A: Mix Design Sheets 150
APPENDIX B: Test Procedures by MTS FlexTest Controller 155
APPENDIX C: APA Rut Results 163
APPENDIX D: Model Verification 167

LIST OF TABLES

Table 2.1: Summary of Resilient Modulus Testing Literature Review 25
Table 3.1: Test Matrix for the Laboratory Tests Conducted 42
Table 3.2: Test Matrix for Non-Destructive Field Tests 42
Table 3.3: Summary of Mix Properties for the Collected Loose HMA Mixes 43
Table 3.4: Number of Loading Cycle Used in Each Stress Sequence 43
Table 4.1: Measured M_R for Tar Creek Base Mix Laboratory Specimens 86
Table 4.2: Measured M_R for Tar Creek Surface Mix Laboratory Specimens 87
Table 4.3: Measured M_R for Tar Creek Cores 88
Table 4.4: Measured M_R for Davis Base Mix Laboratory Specimens 89
Table 4.5: Measured M_R for Davis Cores 90
Table 4.6: Measured M_R for OKC Base Mix Laboratory Specimens 91
Table 4.7: Measured M_R for OKC Cores 92
Table 4.8: Linear Model Parameters for Tar Creek Specimens ($M_R = A + BR$) 93
Table 4.9: Linear Model Parameters for Davis Specimens ($M_R = A + BR$) 93
Table 4. 10: Linear Model Parameters for OKC Specimens ($M_R = A + BR$) 94
Table 4.11: Semi-Log Model Parameters for Tar Creek Specimens ($M_R = A\ B^R$) 94
Table 4.12: Semi-Log Model Parameters for Davis Specimens ($M_R = A\ B^R$) 95
Table 4.13: Semi-Log Model Parameters for OKC Specimens ($M_R = A\ B^R$) 95
Table 4.14: Log-Log Model Parameters for Tar Creek Specimens ($M_R = AR^B$) 96
Table 4.15: Log-Log Model Parameters for Davis Specimens ($M_R = AR^B$) 96
Table 4.16: Log-Log Model Parameters for OKC Specimens ($M_R = AR^B$) 97
Table 4.17: Average M_R for the Stress Ratios 0.20, 0.35 and 0.50 98
Table 4.18: Materials and Mix Properties 99
Table 4.19: Percentage Difference in M_R Values of Field Cores with Respect to Laboratory Specimens 99
Table 4.20: Measured and Predicted Model Parameters 100
Table 4.21: Sensitivity Check for M_R Model by Changing Each Variable by 20% 101
Table 4.22: Matrix of APA Rut Results 102
Table 4.23: Predicted Rut Depth from Material and Mix properties 103
Table 4.24: Predicted M_R and APA Rut Depth at 2000 and 8000 Loading Cycles 104

Table 4.25: Models for Predicted M_R and Rut Depth at 2000 and 8000 Loading Cycles 104
Table 4.26: APA Fatigue Results 105
Table 4. 27: Measured and Predicted Fatigue Cycles 105
Table 4.28: Permeability Test Results 106
Table 4.29: Comparison of Measured and Predicted Permeability Values 106
Table 4.30: Laboratory Seismic Modulus Test Results for Davis Cores 107
Table 4.31: Seismic Modulus and Predicted M_R for the Davis Cores 108
Table 4.32: FWD Back-Calculated Moduli for Tar Creek Site 109
Table 4.33: FWD Back-Calculated Moduli for Davis Site 110
Table 4.34: FWD Back-Calculated Moduli for OKC Site 110
Table 4.35: Comparison of Modulus from FWD Test and M_R by Semi-Log Model (Davis Site) 111
Table 4.36: Comparison of Modulus from FWD Test and M_R by Semi-Log Model (Tar Creek Site) 111
Table 4.37: Comparison of Modulus from FWD Test and M_R by Semi-Log Model (OKC Site) 111
Table 4.38: Moduli and HMA Thicknesses from SASW Test for Tar Creek Site 112
Table 4.39: Comparison of FWD and SASW Moduli for Tar Creek Site 112

LIST OF FIGURES

Figure 1.1: A Photographic View of Field Rutting 10
Figure 3.1: Location of Project Sites 44
Figure 3.2: Collection of Loose HMA Mix from the Tar Creek Site 44
Figure 3.3: Field Asphalt Coring Machine 45
Figure 3.4: Cyclic Indirect Tension Resilient Modulus Test Specimen 45
Figure 3.5: A Diametrically Loaded Cylindrical Specimen 46
Figure 3.6: Heavy Duty Asphalt Saw 46
Figure 3.7: Heavy Duty Laboratory Coring Machine 47
Figure 3.8: Computer Controlled MTS Digital Data Acquisition System 47
Figure 3.9: LVDTs Attached to the Cyclic Indirect Tension Resilient Modulus Test Specimen 48
Figure 3.10: Temperature Chamber and Loading Setup Connected with the MTS Frame 48
Figure 3.11: APA Rut Sample Mold and Molds Secured in the Sample Tray 49
Figure 3.12: APA Fatigue Sample Molds Secured in the Sample Tray 49
Figure 3.13: Karol-Warner's Falling Head Permeameter 50
Figure 3.14: Laboratory Seismic Test Setup 51
Figure 3.15: A Typical Plot of the Transfer Function (Nazarian et al., 2003) 51
Figure 3.16: FWD Device Used in the Tar Creek Site 52
Figure 3.17: FWD Device Used in the Davis and Eastern Ave. Project Site 52
Figure 3.18: Typical Force Output from a FWD Test (Bandara and Briggs, 2004) 53
Figure 3.19: Typical FWD Location of Loading Plate and Deflection Sensors (Bandara and Briggs, 2004) 53
Figure 3.20: The GPR Equipment USed at Tar Creek Site 54
Figure 3.21: Principle of GPR (after USDOT, 2005b) 54
Figure 3.22: A Photographic View of a SASW Test 55
Figure 3.23: Plan View of the SASW Test Setup 55
Figure 4.1: Variation of M_R with Stress Ratio (Davis specimen at 41°F) 113
Figure 4.2: Variation of M_R with Stress Ratio (Davis specimen at 77°F) 113
Figure 4.3: Variation of M_R with Stress Ratio (Davis specimen at 104°F) 114

Figure 4.4: Frequency Diagram for Linear Model from 53 Observations 114
Figure 4.5: Frequency Diagram for Semi-Log Model from 53 Observations 115
Figure 4.6: Frequency Diagram for Log-Log Model from 53 Observations 115
Figure 4.7: Variation of M_R with Stress Ratio for Laboratory specimen at T = 41°F 116
Figure 4.8: Variation of M_R with Stress Ratio for Laboratory specimen at T = 77°F 116
Figure 4.9: Variation of M_R with Stress Ratio for Laboratory specimen at T = 104°F .. 116
Figure 4.10: Variation of M_R with Stress Ratio for Field Cores at T = 41°F 117
Figure 4.11: Variation of M_R with Stress Ratio for Field Cores at T = 77°F 117
Figure 4.12: Variation of M_R with Stress Ratio for Field Cores at T = 104°F 117
Figure 4.13: Variation of M_R with Binder Content (Laboratory Specimens) 118
Figure 4.14: Variation of M_R with Binder Content (Field Cores) 118
Figure 4.15: Variation of M_R with Air Voids (Laboratory Specimens) 119
Figure 4.16: Variation of M_R with Air Voids (Field Cores) 119
Figure 4.17: Variation of M_R with Percentage Passing No. 200 Sieve (Laboratory Specimens) 120
Figure 4.18: Variation of M_R with Percentage Passing No. 200 Sieve (Field Cores) 120
Figure 4.19: Variation of M_R with Temperature for Laboratory specimens at R = 0.20 121
Figure 4.20: Variation of M_R with Temperature for Laboratory specimens at R = 0.35 121
Figure 4.21: Variation of M_R with Temperature for Laboratory specimens at R = 0.50 122
Figure 4.22: Variation of M_R with Temperature at R = 0.35 (Laboratory Specimens) .. 122
Figure 4.23: Variation of M_R with Temperature at R = 0.35 (Field Cores) 123
Figure 4.24: Average Decrease of M_R when Temperature increases from 41°F to 104°F 123
Figure 4.25: Calculated and Predicted Model Parameter A for Power Model 124
Figure 4.26: Calculated and Predicted Model Parameter B for Power Model 124
Figure 4.27: Calculated and Predicted M_R from Power Model ($M_R = A B^R$) 125
Figure 4.28: Calculated and Predicted Rut Depths 125

Figure 4.29: Variation of Rut Depth at 2000 Cycles with M_R at R = 0.20 and T = 77°F 126
Figure 4.30: Variation of Rut Depth at 2000 Cycles with M_R at R = 0.35 and T = 77°F 126
Figure 4.31: Variation of Rut Depth at 2000 Cycles with M_R at R = 0.50 and T = 77°F 126
Figure 4.32: Variation of Rut Depth at 8000 Cycles with M_R at R = 0.20 and T = 77°F 127
Figure 4.33: Variation of Rut Depth at 8000 Cycles with M_R at R = 0.35 and T = 77°F 127
Figure 4.34: Variation of Rut Depth at 8000 Cycles with M_R at R = 0.50 and T = 77°F 127
Figure 4.35: Comparison Between Calculated and Predicted Fatigue Cycles 128
Figure 4.36: Comparison Between Calculated and Predicted Permeability Values 128
Figure 4.37: FFT generated Transfer Function for NDT Results (Core # 1; Hit # 2) 129
Figure 4.38: Laboratory Seismic Modulus for Davis Cores 129
Figure 4.39: Box Plot for Seismic Modulus for Davis Cores (57 Observations) 130
Figure 4.40: Average Laboratory Seismic Modulus for Davis Cores 130
Figure 4.41: FWD Back-calculated Modulus for Tar Creek Site 131
Figure 4.42: FWD Back-calculated Modulus for Davis Site 131
Figure 4.43: FWD Back-calculated Modulus for OKC Site 132
Figure 4.44: Comparison of Laboratory M_R at R = 0.20, E_{FWD} at 9 kip Load for Davis Site 132
Figure 4.45: GPR Thickness Profile for South Lane, Tar Creek Site 133
Figure 4.46: GPR Thickness Profile for North Lane, Tar Creek Site 134

ABSTRACT

A combined laboratory and field study was undertaken to investigate the performance characteristics of some Hot Mix Asphalt (HMA) mixes that are commonly used by Oklahoma Department of Transportation (ODOT). Four different types of loose HMA mixes collected from three project sites, namely, Davis, Tar Creek and Oklahoma City (OKC) were examined with a series of laboratory testing, namely resilient modulus (M_R), APA rut, fatigue and permeability. Field cores were retrieved from the sites and laboratory tests, namely, resilient modulus, APA rut and seismic modulus were performed. Field non-destructive tests were also performed in this study.

The laboratory resilient modulus tests were performed with varying stress level and at three selected temperatures, namely 5°C, 25°C and 40°C, as recommended in the ASTM D 4123 test methods. The test results indicate that the resilient modulus is a function of applied stress and temperature. Also, the results showed that the resilient modulus values vary with mix properties, namely binder content, binder type, air voids, percentage passing No. 200 sieve, among others. In reviewing the results, the laboratory Davis specimens resulted in the highest average resilient modulus values, followed by the OKC specimens, the Tar Creek base mix specimen, and then the Tar Creek surface mix specimen, in general, for all three temperatures. The resilient moduli of the field cores were comparatively lower than that of laboratory specimens. This is due to the differences in compaction represented by laboratory gyratory compaction and field compaction, and the resulting differences in mix properties of the specimens. A model to predict resilient modulus of HMA from the stress ratio, temperature and aforementioned specific mix properties was developed. The model was tested for its fitting as well as

predicting capabilities. APA rut test results showed that the Tar Creek mixes are susceptible to rutting potential. Comparatively lower rut depths were obtained for the Davis and the OKC mixes. The difference in specific mix properties, namely, binder content, air voids and percentage passing No. 200 sieve were identified as the reason for this changes.

A model was developed to predict the rutting potential with these varying mix properties. Attempts were made to correlate APA rut depths with resilient moduli. APA rut depths at 2000 and 8000 repeated cycles were correlated with the M_R values at three selected temperatures (5°C, 25°C and 40°C) and three specific stress ratios (0.20, 0.35 and 0.50). Scattered R-squared values were obtained for the correlation of each aforementioned parameters. This may be due to the differences between resilient modulus and APA rut testing parameters and mechanisms. Rutting is expected to occur at high temperatures and with a large number of load repetitions (due to plastic flow and other mechanisms), whereas resilient modulus should present stress-strain properties of HMA under cyclic loading at intermediate temperatures and lower loading cycles.

The laboratory seismic modulus test showed that the seismic modulus values were 6 to 10 times higher than the M_R values with different stress ratios. This is due to the differences in strain level and strain rates involved in these two test methods. The back-calculated modulus from Falling Weight Deflectometer (FWD) data showed that the Davis results are well comparable with that of laboratory M_R values. Significant scatter was observed for similar comparison for the Tar Creek and the OKC sites. It is expected that the predictive models and the comparison between laboratory and field modulus

results will be a helpful tool for implementing the Superpave mix design and the 2002 AASHTO design guide.

CHAPTER 1

INTRODUCTION

1.1. Introduction

Pavement design and evaluation for construction and rehabilitation purposes require a careful evaluation of a number of factors including material properties, traffic characteristics and environmental conditions, among others. Undoubtedly, material properties are one of the most significant factors in the structural design and performance of pavements (Barksdale et al., 1997). Existing pavement design procedures, namely, AASHTO (1993) and the Asphalt Institute (AI) recognize the resilient modulus (M_R) as the primary mechanistic property to evaluate the performance of pavement materials under vehicular loading and environmental conditions. Specifically, these design methods require the evaluation of M_R of Hot Mix Asphalt (HMA) with temperature as well as the M_R of subgrade soil with moisture. In the new AASHTO 2002 design guide, the dynamic modulus is used to characterize the HMA mixes and the M_R to characterize the subgrade soil behavior.

With the movement toward the new mechanical-empirical (M-E) based design procedure (AASHTO 2002 Design Guide), predictive equations have been developed to estimate the dynamic modulus of the HMA layer as a function of properties such as mix type, aggregate structure, binder specification, compacted mixture volumetric, and mix temperature (Crovetti et al., 2005). Studies have been performed to correlate the resilient modulus with the dynamic modulus of HMA. For example, Loulizi et al. (2006) conducted a study that compared resilient modulus and dynamic modulus for two types of HMA mixes, typically used by the Virginia Department of Transportation (VDOT). A

strong relationship was observed in that study between the dynamic modulus performed at 5 Hz and the resilient modulus performed with a loading time of 0.03 sec. Another study by Crovetti et al. (2005) reported that the laboratory test equipment and procedures for determining the dynamic modulus of HMA mixtures are still in the development stage. That study also noted that a regression model that correlates M_R of HMA mixes with temperature will be a good comparative measure for their dynamic modulus counterpart.

In addition to the aforementioned studies, the current dynamic modulus protocol (ASTM D 3497) calls for the axial compression testing of HMA specimens having a diameter of 100 mm (4 in) and a height of 150 mm (6 in). Performing dynamic modulus tests may be quite a difficult task in the case of field cores, since it is often impossible to obtain this size specimen from actual pavements (Kim et al., 2004). Thus, the advantage of the current protocol for indirect tension (IDT) resilient modulus test, ASTM D 4123 appears to be more appropriate and relatively simple for the evaluation of existing HMA pavements by performing the test on field cores (Kim et al., 2004). As such, it is reasonable to utilize standardized equipment and procedures for measuring the M_R of HMA mixtures. The present study pertains to this topic.

1.2. Resilient Modulus

It is well known that most paving materials are not elastic but experience some permanent deformation after each load application. However, if the load is rapid and/or small compared to the strength of the material and is repeated for a large number of cycles, the deformation under each load repetition is almost completely recoverable

(Huang, 2004). The elastic modulus corresponding to the recoverable strain under the repeated load is known as resilient modulus, M_R. Mathematically, M_R is defined as:

$$M_R = \frac{\sigma_d}{\varepsilon_r} \qquad (1.1)$$

where σ_d is applied deviator stress and ε_r is recoverable (resilient) strain.

Several studies (see e.g., Brown and Foo, 1989; Almudaiheem and Al-Sugair, 1991; Ali and Lobez, 1996; Katicha, 2003; Tarefder, 2003; Tarefder and Zaman, 2003; Crovetti et al., 2005) have highlighted the importance of resilient modulus and have evaluated the M_R with temperature and mix properties. Although several procedures have been used by those studies and others to determine the resilient modulus, only one procedure has been standardized by ASTM (ASTM D 4123). The test consists of a haversine-shaped cyclic load pulse applied in the vertical diametric plane of a cylindrical specimen through a loading strip. The resultant recoverable horizontal deformation measured by a surface-gage-point mounted linear variable differential transducer (LVDT) and the applied load are used to calculate the resilient modulus. Consequently, the ASTM D 4123 test procedure is used herein to evaluate the resilient modulus of selected HMA mixes.

1.3. Rutting Effect on HMA Pavements

Permanent deformation is one of the most important types of load-associated distresses occurring in a flexible pavement system (Huang, 2004). It is associated with rutting in the wheel path, which develops gradually as the number of load repetitions increases. Rutting in HMA pavements has been a major problem nation-wide for many years. It is becoming a greater problem especially with greater wheel loads and higher tire pressure. Rutting normally appears as longitudinal depressions in the wheel paths,

accompanied by small upheavals to the side (Figure 1.1)[†]. The width and depth of the rutting profile is highly dependent upon the pavement structure (layer thickness and quality of materials), traffic composition and quantity, as well as the environmental condition at the site. Studies have been conducted (see e.g., Collins et al., 1995; Christopher et al., 1999; Choubane et al., 2000; Kandhal, 2002) to relate laboratory asphalt pavement analyzer (APA) rut depths to actual field rutting. A study by Srinivasan (2004) evaluated the indirect tensile (IDT) strength to identify HMA rutting potential. A strong correlation between IDT strength and APA rutting potential was observed in that study. A different study by Anderson et al. (2002) examined the relationship of Superpave gyratory compaction-related properties to HMA rutting behavior. It was concluded that the testing temperature and the air voids have a significant effect on the HMA rutting potential. In particular, the rut depth decreased with an increase in air voids and an increase in testing temperature, and these variables are therefore believed to be key factors that affect rutting potential.

Two types of strain are developed in HMA pavements under repeated traffic loading. One is the elastic strain which is completely recoverable under each loading cycle, and it is related to the stiffness or modulus of the HMA material. The other strain is the plastic strain, which accumulates with repeated loading cycles and is related to permanent deformation (rutting). It is logical to question if an HMA mix with high resilient modulus exhibits low rut potential and vise versa. In a broader sense, one may question if rutting potential could be correlated with resilient modulus of HMA mixes. So far, no systematic studies have been undertaken to answer these questions. This is partly because the field of resilient modulus testing for HMA materials is largely unexplored.

[†] Figures are presented at the end of each chapter

Limited studies have been conducted to examine correlations between rutting potential and resilient modulus (see e.g., Brown and Cross, 1989; Tarefder, 2003; Tarefder and Zaman, 2003; Bhasin et al., 2005). Brown and Cross (1989) reported that there is no good corelation (R-squared = 0.01) between HMA layer rutting and indirect tension resilient modulus. Their study concluded that there is no reason to expect a good relationship between these parameters since rutting is due to compressive stress and resilient modulus test measures tensile properties of the HMA mixes. Tarefder (2003) and Tarefder and Zaman (2003) conducted a study to correlate APA rut depth at 8000 loading cycles with the cyclic indirect tension resilient modulus at three different temperatures (0°C, 23°C and 40°C). The highest R-squared value obtained for the regression equation relating rutting and resilient modulus at 40°C was 0.27. Overall, a poor correlation was obtained for each test temperature. The reason stated for this poor correlation was the mechanistic differences (stress level, strain, temperature, loading cycles, mechanisms, etc.) between resilient modulus and APA rut. Their study also noted that if indirect tension resilient modulus test is performed at a higher temperature it would be interesting to see whether the correlation between resilient modulus and APA rut improves.

In the present study, a series of resilient modulus and APA rut tests are conducted for selective HMA mixes that are commonly used in Oklahoma. Results are organized as resilient modulus at different stress levels and different temperatures and the APA rut values at different loading cycles. These laboratory data are then used to examine if rutting potential could be correlated with resilient modulus by different combinations of stress level, temperature and loading cycle.

1.4. Problem Statement

Material properties have been recognized as one of the most vital factors in the structural design and performance of HMA pavements (see e.g., Barksdale et al., 1997). The 1986 and 1993 AASHTO design guides have highlighted the importance of pavement materials and have recognized the resilient modulus of each layer as the most vital parameter in the design. Asphalt materials are considered as one of the most complicated groups among the six groups classified in the new pavement design guide (PDG) namely, asphalt materials, PCC materials, chemically stabilized materials, non-stabilized granular materials, subgrade soils, and bedrock. This is due to the fact that the HMA mix behavior can be heavily influenced by temperature, stress level and mix type. Currently, Oklahoma Department of Transportation (ODOT) does not have any data base for resilient modulus even for the most widely used HMA mixes. Therefore, generating a data base for HMA mix behavior with respect to the aforementioned influencing factors and finding correlations between resilient modulus and APA rut can have positive impacts on the transportation community's continued effort to implement the Superpave mix design and the 2002 AASHTO design guide.

Non-Destructive Testing (NDT) of pavements has made substantial progress during the past two decades (see e.g., Abdallah et al., 2001; Nazarian et al., 2004; Shalaby et al., 2004). The newer pavement design and rehabilitation selection methods increasingly use non-destructive testing procedures for structural evaluation (Abdallah et al., 2001). With the rapid advancement of hardware and software technology, non-destructive testing instrumentation and data analysis techniques are being continually improved. Most algorithms currently used to determine the remaining life of pavements rely on stiffness parameters determined from NDT devices. One major area of continual improvement is

the reliable and rapid extraction of stiffness parameters from nondestructive field data. Therefore, combining non-destructive and laboratory test data can provide a wealth of information not available from a single device. More specifically, integrating data from both the laboratory destructive tests and field non-destructive test methods may yield more robust, consistent and accurate modulus profiles. Therefore, a correlation between laboratory resilient modulus and back-calculated modulus from non-destructive field tests is expected to be a helpful tool for implementation of the new AASHTO 2002 pavement design guide.

1.5. Hypothesis and Objectives

The main hypotheses of this study are:

1. The indirect tension resilient modulus of HMA mixes is a function of applied stress, temperature, and materials and mix properties.
2. The HMA performance characteristics, namely, APA rut, fatigue and permeability are dependent on materials and mix properties.
3. The indirect tension resilient modulus may be correlated with APA rut depth.
4. Indirect tension resilient modulus can be correlated with back-calculated modulus from field tests.

To verify these hypotheses, laboratory and field tests were conducted in the present study on four different HMA mixes collected from three different sites. Specific objectives of the current study are given below:

1. Determine the cyclic indirect tension resilient modulus of laboratory specimens and field cores at different stress levels and different temperatures.

2. Correlate the M_R values with specific mix properties, namely air voids, binder content, specific gravity and percentage passing No. 200 sieve and test parameters, namely temperature and applied stress.
3. Determine the rutting, fatigue cycles and permeability of loose HMA mixes collected from selected field sites and compacted in the laboratory. Correlate results with selected material and mix properties, namely air voids, binder content, specific gravity and percentage passing No. 200 sieve.
4. Examine correlations, if any, between resilient modulus and APA rut depth.
5. Determine the modulus of field cores using a non-destructive technique, namely laboratory seismic modulus test. Compare the seismic modulus values with the resilient modulus values from cyclic indirect tension test.
6. Determine the modulus of HMA layer using a non-destructive technique namely, Spectral Analysis of Surface Waves (SASW) test. Compare the SASW modulus values with the back-calculated modulus values from Falling Weight Deflectometer (FWD) tests.
7. Determine back-calculated modulus of the HMA layer from FWD data for all three sites, and compare the laboratory resilient modulus from field cores with the corresponding FWD modulus.

1.6. Thesis Format

This thesis is based on a laboratory and field study for selective HMA mixes that are commonly used by Oklahoma Department of Transportation (ODOT). The performance characteristics tests (resilient modulus, APA rut, fatigue and permeability) of these selected HMA mixes were performed by a series of laboratory tests for

laboratory and field compacted (i.e., core) HMA specimens. A series of non-destructive field tests were also performed in this study.

To document the results obtained from the present study, this thesis is divided into five chapters. Chapter 1 is an introduction to the research subject with pertinent background information. This chapter also presents the problem statement and objectives of this study. Chapter 2 presents the literature review on resilient modulus, APA rut, fatigue and permeability testing. Factors affecting the resilient modulus and APA rut results are also discussed. A literature review on laboratory and field non-destructive testing techniques for the evaluation of elastic modulus is also presented. In Chapter 3, the laboratory experimental methodology used in this study is outlined. This chapter includes a section on material sources and their properties. A detailed test matrix of this study is also presented. Further, experimental methodology for non-destructive testing in the field is presented. Chapter 4 is devoted to the discussion of the test results obtained from both laboratory and field test programs. Chapter 5 presents the conclusions of this study and recommendations for future studies.



Figure 1.1: A Photographic View of Field Rutting

CHAPTER 2

LITERATURE REVIEW

2.1. General

This chapter provides an overview of the previous studies on HMA performance characteristics by laboratory and field testing. It also presents a brief discussion on the performance of chat material in HMA pavements. Non-destructive testing techniques are also discussed because of their relevance to the present study.

2.2. Cyclic Indirect Tension Resilient Modulus Test

The modulus of HMA has been presented in the literature in several different forms including dynamic modulus, stiffness and resilient modulus (M_R) in both compression and tension. The M_R is more appropriate for use in multi-layer elastic theories, as reported by Huang (2004). Therefore, the measurement of M_R of HMA material has been the subject of considerable research. It has been determined by two approaches: (1) predict the M_R using physical and mechanical properties of the mixture using available correlations, and (2) determine the resilient modulus by laboratory testing.

The M_R measurement by an indirect tension test is considered most promising in terms of repeatability compared to the evaluation of resilient modulus from triaxial testing (Barksdale et al., 1997; Tarefder et al., 2004). A pavement layer is generally believed to exhibit anisotropy in which radial properties are constant in all directions but are different from properties in the vertical direction. Due to the anisotropy of HMA mixes, the resultant discrepancy in resilient modulus between diametral testing and triaxial testing can be quite pronounced. Wallace and Monismith (1986) carried out tests on HMA cores taken from San Diego test road. It was shown that as a result of placement and compaction efforts, the material was about twice as stiff in the radial direction

compared to the vertical direction. An HMA layer of typical thickness was subjected to a bending action, which is primarily resisted by the radial rather than the vertical stiffness of the HMA layer. Therefore, for vertical cores taken from an actual pavement, the diametral test or flexural bending test should give a more relevant assessment of the stiffness of the HMA layer than tests performed in the vertical direction (Barksdale et al., 1997). The main advantage of the test is its failure to completely simulate the stress conditions encountered in practice. The diametral test is believed to simulate the tensile stress condition existing in the bottom of the HMA layer reasonably well. This test has additional advantages since thin cores can be tested, which permits additional measurements over the depths of thick HMA layers (Barksdale et al., 1997).

Originally indirect tension tests were used to measure rupture strain in concrete (Blakey and Beresford, 1955). They were thereafter adapted to determine the elastic properties (Young's modulus (E) and Poisson's ratio (ν)) of HMA (Wright, 1955; Hondros, 1959). Kennedy and Hudson (1968) first suggested the use of indirect tension test for stabilized materials, while Schmidt (1972) used the test to determine the resilient modulus of HMA. Since then, indirect tension testing has become the main setup selected by most engineers for evaluation of resilient moduli of HMA (Brown and Foo, 1989). A summary of resilient modulus tests conducted by different researchers and associations is presented in Table 2.1.[‡]

2.3. Factors Affecting Indirect Tension Resilient Modulus

Several factors affect the results of resilient modulus testing. Applied load, test temperature and air voids are among the important factors. A number of studies (see e.g.,

[‡] Tables are presented at the end of each chapter

Brown and Foo, 1989; Almudaiheem and Al-Sugair, 1991; Ali and Lobez, 1996; Katicha, 2003; Tarefder, 2003) have been conducted on resilient modulus by varying these factors, as discussed below.

2.3.1. Effect of Loading

The repeated-load indirect tension test for determining resilient modulus of HMA mixes is conducted by applying compressive cyclic load using a haversine shaped pulse. The load is applied vertically in the vertical diametral plane of a cylindrical specimen. The applied cyclic load and resulting recoverable horizontal deflection of the specimen are measured and, with an assumed Poisson's ratio corresponding to test temperature, is used to calculate M_R. The test procedure is described in the ASTM D 4123. As recommended by ASTM D 4123, the load magnitude should range from 10 to 50% of the indirect tensile strength of the specimen.

Almudaiheem and Al-Sugair (1991) used a load ranging from 10 to 30% of the indirect tensile strength of a specimen. The upper limit was reduced from the 50% indirect tensile strength, as recommended by ASTM D 4123, to 30% to ensure the stress within the samples did not exceed the elastic range. Also, three different binder contents were used to see if the change in M_R is affected by the percentage of binder in the mix. The study suggested that a larger load (closer to 50% of the indirect tensile strength of the specimen) should be used in the test because it yields a smaller resilient modulus value, which in turn results in a more conservative design. It also reported that this is particularly important for mixes with a lower binder content.

To analyze the effect of stress level on resilient modulus, Brown and Foo (1989) performed a study on laboratory prepared specimens and field cores. In that study a linear

model was developed to predict resilient modulus at a stress ratio (applied stress divided by indirect tensile strength) of 15%. To evaluate the effect of stress level on M_R, the resulting modulus ratio defined as (M_R/Predicted M_R at 15% stress ratio) of each specimen tested was plotted against the percentage of applied stress corresponding to tensile strength of the specimen. It was concluded that the amount of stress applied to the sample during testing has significant effect on the measured resilient modulus. The study also recommended characterization of HMA mixes at a stress ratio of 15%. The following linear model was reported from the study involving combined field and laboratory specimens:

$$Y = -0.0238X + 1.36 \quad (2.1)$$

where Y is the modulus ratio and X is the stress ratio (in percentage). From the model it was reported that a change in stress from 15% to 10% of tensile strength at 25°C will increase the measured M_R by approximately 12%.

2.3.2. Effect of Temperature

The resilient modulus of HMA decreases significantly with increasing temperature (see e.g., Bonnaure et al., 1982; Roque and Buttlar, 1992; Barksdale et al., 1997; Katicha, 2003; Tarefder and Zaman, 2004). Asphalt binders are highly sensitive to temperature, which affects the resilient and viscous properties as well as aging characteristics of a binder (Shalaby et al., 2004).

A correlation between resilient modulus and temperature was reported by Katicha (2003). It was found that the resilient modulus decreases with increasing temperature, and it is best represented by an exponential model shown below:

$$M_R = \alpha\, e^{-\beta T} \quad (2.2)$$

where α and β are model parameters. An R-squared value of 0.97 was reported for this model. It was also reported that the model parameters α and β are functions of binder and mix properties. Also, it developed a relationship for α and β with respect to bulk specific gravity, air voids, binder content and fine to binder ratio. This current study is slightly different than the study by Katicha (2003). The resilient modulus of HMA mixes are correlated with stress ratio, and the model parameters are reported as a function of temperature and material properties.

Ali and Lobez (1996) found that the back-calculated HMA layers' elastic modulus could be well correlated (R-squared = 0.72) to the layer temperature based on data collected at site 48SA (SHRP No. 481077) located at southbound lanes on U.S. Highway 287 in Texas. The following model was reported in that study:

$$E = e^{9.372-0.0361T} \tag{2.3}$$

where T is temperature in °C at a point 25 mm below the pavement surface, and E represents elastic modulus in MPa. Another study by Salem (2004) reported that the HMA modulus could be related to the pavement temperature with an exponential function in the form:

$$E = K_1 e^{K_2 T} \tag{2.4}$$

where T is pavement temperature in °C and K_1 and K_2 are model parameters. An R-squared value of 0.8 was obtained in that study.

2.3.3. Effect of Air Voids

Both literature and experience have shown that specimens compacted using gyratory compactors tend to have a non-uniform air void distribution along both the diameter and the height (Harvey et al., 1994). To obtain a uniform air void distribution

within a specimen, the final test specimen should be cored and cut off the top and bottom parts of the gyratory compacted sample (Chehab et al., 2000).

A brief preliminary study was conducted by Chehab et al. (2000) on cylinders 75 mm in diameter cored from both 100 mm and 150 mm diameter specimens to compare their air void distribution. This study revealed that in the case of 100 mm compacted specimens, sections in the middle of the 75 mm core had higher air void content than those at the top and bottom. This distribution was opposite to that found in 75 mm diameter cores taken from 150 mm diameter specimens. This finding and the fact that the Superpave gyratory compactor (SGC) had been originally designed for compacting 150 mm diameter specimens suggest that 100 mm diameter specimens are not being compacted as effectively as those having 150 mm diameter.

Tarefder (2003) performed triaxial and diametral resilient modulus tests for Superpave gyratory compacted samples. In that study it was reported that the air voids of 12.1% and 8.6% show slightly lower triaxial resilient modulus than those of the samples with 4.2% and 4.7% air voids. It was also reported that the air voids have higher influence on the diametral resilient modulus values than that of triaxil resilient modulus values. The study recommended that the resilient modulus samples be cored from the 150 mm diameter SGC sample to 100 mm diameter core to reduce the density gradient in the final specimen.

Loulizi et al. (2005) conducted a study to compare the resilient modulus and dynamic modulus of HMA as material properties for flexible pavement design. Two types of mixes (surface mix (SM-9.5A) and base mix (BM-25.0)) were prepared for that study, according to Superpave mix design. The study reported that the mix type did not

have any significant effect (p-value of 0.637 > 0.05) even though there are major differences between the two mixes, especially in the void content (2.6% difference in the void content between two mixes).

2.4. Permanent Deformation or Rutting

Permanent deformation or rutting is one of the main failure mechanisms in HMA pavements. Total permanent deformation at the surface is the accumulation of permanent deformation in all of the HMA and unbound layers in the pavement system (AASHTO, 2002). Excessive permanent deformation can occur in mixtures that lack adequate stiffness and/or strength at high temperatures. Significant rutting occurs during hot weather, when the surface of flexible pavements can reach a temperature of 60°C or higher. Furthermore, this mode of distress is also associated with relatively high traffic levels; the greater the number of vehicles and greater the proportion of heavy trucks, the greater the potential for permanent deformation (Srinivasan, 2004; Christensen et al., 2000). Rutting normally appears as longitudinal depression in the wheel paths accompanied by small upheavals to the sides. The width and depth of the rutting profile is highly dependent upon the pavement structure (layer thickness and quality), traffic matrix and quantity as well as the environment at the design site (AASHTO, 2002). In the transverse profile, rutting along the wheel path modifies drainage characteristics and reduces runoff capability. Water can accumulate in traffic lanes, creating conditions for hydroplaning of vehicles, reducing skid resistance of the surface course and unsafe traffic conditions.

Numerous studies have been conducted to compare results of APA rut testing to actual field performance. Most of these studies have been able to relate APA rut depths to

actual field rutting (see e.g., Collins et al., 1995; Christopher et al., 1999; Choubane et al., 2000; Kandhal, 2002). A joint study by the FHWA and WesTrack evaluated the APA results to predict rutting performance on mixtures placed at full scale pavement (Williams et al., 1999). Data from 10 test sections from WesTrack exhibited a strong correlation (R-squared = 0.91) between APA and field rutting.

Srinivasan (2004) conducted a study to evaluate ITD strength to identify HMA rutting potential. The objective of that research was to study if rutting potential can be evaluated with equipment readily available to state highway agencies. In that study, rutting potential was evaluated with the Asphalt Pavement Analyzer (APA). The parameters that were evaluated as independent variables include the IDT strength, volumetric parameters, compaction slope, and the compacted aggregate resistance. IDT strength was measured using the Marshall Stabilometer with a split tensile head and with the samples at 60°C. The main factors included in that experiment were binder type, binder content, sand content, nominal maximum aggregate size and gradation. The study reported that the analysis of variance demonstrated significant effects of all the main factors and their interactions on rutting potential. Further, a strong correlation (R-squared = 0.78) between rutting potential and indirect tensile strength as measured with the stabilometer was obtained in that study. In the present study, which is technically similar to the study by Srinivasan (2004), the rutting potential is correlated with resilient modulus and the resilient modulus correlated with stress ratio (applied stress / tensile strength).

Asworth (2003) performed a study about the key factors that affect rutting potential in samples prepared with materials from New Brunswick, Canada. Four variables that are

believed to play an active role in permanent deformation performance were therefore examined in that study. The variables included in that study were test temperature, air voids, aggregate source and course aggregate content. The study suggested that air voids and test temperature are key factors that affect rutting potential. The course aggregate content was also identified as a key factor, but it was reported that it did not exhibit predictable results. The study therefore suggested a need for a larger sample size and further testing. In the present study, in addition to the aforementioned variables, the specific gravity of binder, specific gravity of aggregate and percentage fines are included as key factors that affect rutting potential.

2.5. Non-destructive Testing Techniques

Non-Destructive Testing (NDT) of pavements has made substantial progress during the past two decades (see e.g., Abdallah et al., 2001; Nazarian et al., 2004; Shalaby et al., 2004). Most algorithms currently used to determine the remaining life of pavements rely on stiffness parameters determined from NDT devices. One major area of continual improvement is the reliable and rapid extraction of stiffness parameters from nondestructive field data. Two of the most common NDT methods used are the deflection-based method and seismic-based method (Bandara et al., 2004). The Falling Weight Deflectometer (FWD) is currently the most common structural evaluation tool for the deflection-based NDT method (Abdallah et al., 2001). Deflection bowls are used to back calculate the modulus profiles of pavements using the inverse theory. The Spectral Analysis of Surface Waves (SASW) is one of the most common seismic based methods of NDT (Abdallah et al., 2001). In the SASW method, time records obtained with

vibration sensors are used to obtain an experimental dispersion curve, which, through an inversion procedure, provides an estimate of the elastic modulus profile of the pavement.

To determine pavement layer thickness and moduli by SASW method, Nazarian et al. (1988) performed a field study at the Pavement Test Facility of Texas A&M University in Bryan. The SASW test was performed at nine sites, and the primary objective of that study was to evaluate the effectiveness of the SASW method in determining thickness of various layers of different materials comprising the pavement systems and to study moduli variations in similar materials at carefully controlled pavement sites. The study concluded that the overall, moduli and thicknesses determined by the SASW tests seem very reasonable. The study also reported that the comparison of modulus values from the SASW and FWD tests at the same sites show several general points. Also, moduli of the top pavement layer exhibit less scatter in SASW tests than in FWD tests because of the higher sensitivity of the SASW method to properties. One of the conclusions made in that study was that the moduli obtained by the two methods compare well when the predominant pavement layers are thick and stiff. In such cases both tests are performed in the linear range.

Shalaby et al. (2004) performed a study to compare back-calculated modulus and laboratory resilient modulus of HMA mixes. Eight test sites were constructed for the study by using two types of HMA mixes that are commonly used in Manitoba, Canada. From the FWD field analysis and indirect tensile laboratory testing of the field cores, the following conclusions were made: (1) laboratory stiffness modulus values were considerably lower than FWD back-calculated values, and (2) laboratory results underestimate the stiffness compared with FWD results. Their study also reported that

there are no standardized test procedures and no consensus on various test parameters. Therefore, the resilient modulus values can vary greatly depending on the selected mix design and test methods.

2.6. Fatigue Cracking

Fatigue cracking in HMA mixtures is a primary cause of failure, along with rutting, thermal cracking and moisture damage. Fatigue cracking is the phenomenon of fracture under repeated or fluctuating stress having a maximum stress value less than the tensile strength of the material (Roberts et al., 1996; Healow, 1998). An understanding of the fatigue behavior of a HMA mixture is required to improve its design and performance. However, accurate prediction and evaluation of fatigue damage is a difficult task because HMA mixture typically demonstrate inelastic behavior and are composed of irregularly shaped and randomly oriented aggregate particles (Kim et al., 2006). This type of failure generally occurs when the pavement has been stressed to the limit of its fatigue life by repetitive axle load applications.

Fatigue resistance is closely related to compacted air voids (see e.g., Finn and Epps, 1980; Huber and Heiman, 1987; Kandhal et al., 1991). HMA with relatively low density (high air voids) has low cohesion and tends to lose aggregate rather easily. Where pockets of segregation occur and fine aggregate is absent, stress from traffic and weather tends to strip the binder, leaving the aggregate particles relatively free to break away. Generally speaking, an increase in compacted air voids will effectively reduce fatigue life as the compacted mix is less resistant to the cumulative effects of repeated loading (Healow, 1998). Finn and Epps (1980) quantified the adverse effects of inadequate compaction on fatigue life and show that a 1% increase in air voids may reduce the

fatigue life of HMA by the order of 35%. Epps and Monismith (1972) explained the two primary factors contributing to maximum fatigue resistance in HMA: binder content and air void content. Binder content is limited on the high side by stability requirements during mix design, and the optimum binder content should approach this upper limit. Adequate compaction during construction will leave the HMA layer at design density with void content approaching 4% from the high side. In order to develop more effective analytical design methods for pavements, increased knowledge of material properties as well as deterioration mechanisms, such as fatigue cracking as a performance test, is very important.

2.7. Permeability of HMA

Permeability of HMA continues to generate considerable interest in the asphalt materials, design and construction community. It is generally agreed that excess moisture in HMA pavements is potentially detrimental to pavement performance because of such phenomena as stripping in the HMA mixture and softening or weakening in underlying unbound layers. Developing an ability to measure the flow of water through HMA layer is not a new topic (Cruz, 2000). In recent years, however, a number of new test methods for measuring the permeability of HMA have been developed (or refined) for both laboratory and field (in-place) applications (Colley et al., 2001; Prowell et al., 2002; Brandon et al., 2004; Hall, 2004). Most laboratory-based methods for estimating the permeability of HMA feature either a constant-head or a falling-head type test (Kanitpong et al., 2003; Mohammad et al., 2003).

McWilliams (1986) observed that the size and shape of the void structure of hot-mix asphalt mixtures depends on the aggregate gradation, compaction effort, and the

amount of the mineral filler or fine sand. The binder content, shape, and texture of the aggregate also have an influence on the void characteristics in a HMA mixture. Other researchers (Choubane et al., 1998; Huang et al., 1999; Cooley and Brown, 2000; Maupin, 2000) reported that the air void content, aggregate nominal maximum size and mixture gradation are the major factors that influence the permeability of HMA mixtures. Among these, air void is the most critical factor in the permeability of a hot-mix asphalt mixture.

Kantipong et al. (2002) performed a study to evaluate the permeability of HMA mixes prepared by using the aggregates from different sources. The study reported that the aggregate source is shown to have a significant effect on the permeability. Aggregate shape affects size of voids, shape, and connectivity of voids, and hence, directly influences the permeability.

2.8. Performance of Chat in Flexible Pavements

Numerous waste materials result from manufacturing operations, service industries, sewage treatment plants, households, and mining. Legislation has been enacted in recent years to either mandate the use of some waste materials in road construction or to examine the feasibility of such usage (Kandhal, 1996). The use of waste materials in hot mix asphalt for pavement application has always been an attractive choice for the asphalt industry. A waste material that can be easily incorporated in hot mix asphalt and that will provide a better performing pavement has been an important subject among the pavement designers and engineers for a long time.

The Tri-State Mining District in northeast Oklahoma, southeast Kansas and southwest Missouri was the site of substantial zinc and lead ore extraction since the late

18th century. This activity in Oklahoma resulted in a total of approximately165 million tons of chat (i.e., chert fragments) of which about 75 million tons is currently stockpiled in large quantities on the surface of the Tar Creek Superfund Site (Wahnee et al., 2000; Hughes, 2002; Wasiuddin et al., 2005; Teredesai et al., 2005; Teredesai, 2005; Wasiuddin et al., 2006a; Wasiuddin et al., 2006b). A systematic study was conducted by Wasiuddin et al. (2005) to develop HMA mix designs that would incorporate raw chat in HMA for base course and surface course applications in an environmentally safe manner. A total of six mix designs were pursued in that study with different percentages of raw chat. Three surface mixes with 40%, 60% and 80% chat and three base mixes with 40%, 50% and 70% raw chat in the mix were prepared and performance characteristics tests were performed. The study concluded that the use of raw chat in hot mix asphalt showed great potential for both surface course and base course applications by meeting the Superpave mix design requirements. These designs also met the performance test requirements for a surface mix, as specified by ODOT in its standards and specification. Wasiuddin et al. (2005) also concluded that the use of raw chat in hot mix asphalt is a promising effort and as much as 80% and 50% raw chat can be used in an S5 type Superpave surface mix and S3 type Superpave base mix, respectively, as far as the engineering properties are concerned.

Table 2.1: Summary of Resilient Modulus Testing Literature Review

Reference	Load Level	Temperatures	Pulse	M_R Value Used	Model Used or Comparison
ASTM D 4123, (1982)	10 to 50% of ITS	5, 25, and 40 °C	Haversine Load Duration: 0.1 sec Frequency: 0.33 to 1 Hz	Average M_R at 5, 25, and 40 °C	-
Brown and Foo (1989)	10, 15, and 20 % of ITS	4, 25, and 40 °C	Haversine Load Duration: 0.1 sec Frequency: 1 Hz	Average M_R at 4, 25, and 40 °C	Linear Model: Modulus ratio wrt 15% stress (Y) vs. % of stress (X) Y= -0.0238X+1.36
Hossain et al., (1992)	Load between 90 to 120 lb, with majority around 100 lb.	77 and 104 °F	Haversine Load Duration: 0.1 to 0.4 sec Frequency: 0.33, 0.5, and 1 Hz	Average M_R at 77, and 104 °F (ASTM D4123)	Compare with FWD test results
SHRP P07 (Nov 1992)	30, 15, 5% of indirect tensile strength for test temperatures of 41, 77, 104 °F	41, 77, and 104 °F	Haversine Load Duration: 0.1 s Frequency: 1 Hz	Four of the last five cycles used (Values shall be within 15% of average)	-
Zhou et al., (1992)	10 to 50% of ITS (ASTM D 4123)	42, 73, and 95 °F	Haversine Load Duration: 0.1 sec Frequency: 0.33 to 1 Hz	Average M_R at 42, 73, and 95 °F (ASTM D4123)	Compare with FWD test results

Table 2.1 (Cont'd): Summary of Resilient Modulus Testing Literature Review (Cont'd)

Katicha (2003)	Load applied in a way to limit the strain between 150 and 500 microstrains.	5, 25, and 40 °C	Haversine Load Duration: 0.1 and 0.3 sec Frequency: 1 Hz	Average of last five cycles used (Values shall be within 5% of any two loading cycles)	Temperature Model $M_r = \alpha.e^{-\beta.T}$ $\alpha = 17621$ $\beta = 0.0464$
Tarefder (2003)	Triaxial M_R Test: 20 to 30 psi Indirect Tensile M_R Test: 25 to 35 psi (10 to 40 % of ITS)	0, 25, and 40 °C	Haversine Load Duration: 0.1 sec Frequency: 1 Hz	-	Triaxial and Diametral M_R comparison Used in Rut correlation model
Shalaby et al., (2004)	Varies	10 and 25 °C	Haversine Load Duration: 0.3 sec Frequency: 1 Hz	Four of the last five cycles used (Values shall be within 15% of average)	Compare with FWD back-calculated test results

CHAPTER 3

RESEARCH APPROACH

3.1. General

This chapter presents the research approach adopted in this study. The sources of materials, sample preparation, laboratory test procedures and field test procedures are outlined in the following sections. A test matrix with number of specimens tested in each laboratory test is included in Table 3.1. Table 3.2 shows the different non-destructive field tests performed at each site.

3.2. Sources of Materials

The main objective of this study was to examine the performance characteristics of selected HMA that are typically used in Oklahoma. Behavior of chat-asphalt used in the Tar Creek test road project was also evaluated. In the process of achieving this objective four different asphalt mixes were collected from three different project sites (refer to Figure 3.1): (1) Davis (HW # 7, Davis, OK); (2) OKC (Eastern Ave., Oklahoma City, OK); and (3) Tar Creek (Test Road Project, Miami, OK). Bulk HMA mixes were collected from field during pavement construction, as shown in Figure 3.2. These bulk mixes were used to prepare specimens in the laboratory. Field cores were also retrieved from each project site for laboratory testing. Base HMA mixes were collected from all three project sites. In addition to base mix, surface mix was also collected from the Tar Creek site. Also, in terms of materials, the Tar Creek project site contains Chat material in the HMA mix. A summary of mix properties for the collected loose HMA mixes is shown in Table 3.3. Additional information on the asphalt mixes is presented in the design sheets attached in Appendix A.

3.3. Laboratory Testing

Laboratory tests included in this study are resilient modulus (M_R), APA rut, fatigue and permeability. Two types of specimens were prepared in the laboratory: (1) cylindrical specimens and (2) beam specimens. Cylindrical specimens were compacted using a Superpave Gyratory Compactor (SGC) and then tested for M_R, indirect tensile (IDT) strength, APA rut, and permeability. The Asphalt Vibratory Compactor (AVC) was used to compact beam specimens for the fatigue test. The field specimens consisted of two sets: Set 1 consisted of specimens having a diameter of 100 mm (4 in); and Set 2 consisted of specimens having a diameter of 150 mm (6 in). Figure 3.3 shows a photographic view of coring a specimen in the field. Specimens in Set 1 were tested for M_R and IDT strength, while specimens in Set 2 were only tested for APA rut. The field cores from the Davis site were also tested for laboratory seismic modulus.

3.3.1. Cyclic Indirect Tension Resilient Modulus Test

The resilient modulus is a measure of the elastic modulus of a linear visco-elsatic material at a given stress state (Huang, 2004). It is mathematically defined as the applied deviator stress (σ_d) divided by the recoverable (resilient) strain (ε_r) that occurs when the applied load is removed from the test specimen (Equation 1.1). According to Brown et al. (1989), the ASTM D 4123 testing protocol suffers from the lack of accuracy and precision. Therefore, the expression for evaluating diametral or indirect tension M_R, as derived by Tarefder (2003), is used in this study. The derivation below is reproduced from Tarefder (2003), with the final expression for M_R corrected.

If a plastic disk or cylinder is loaded diametrically, as shown in Figure 3.5, from the theory of elasticity, it is possible to determine the elastic modulus of the material. It can

be shown that this load gives rise to a uniform tensile stress along the horizontal diametral plane of the cylinder (Timeshenko and Goodier, 1970). The expression for the total normal stress on the vertical plane, σ_x and the total normal stress on the horizontal plane, σ_y can be expressed as follows:

$$\sigma_x = \frac{2P}{\pi t d}\left[1 - \frac{16d^2x^2}{(d^2 + 4x^2)^2}\right] \tag{3.1}$$

$$\sigma_y = \frac{2P}{\pi t d}\left[1 - \frac{4d^4}{(d^2 + 4x^2)^2}\right] \tag{3.2}$$

where
P = applied load,
x = distance from the origin along the abscissa (horizontal),
y = distance from the origin along the ordinate (vertical),
t = thickness of the cylinder, and
d = diameter of the cylinder.

Assuming plane stress condition and elastic behavior, the expression for the horizontal strain, ε_x can be given as:

$$\varepsilon_x = \frac{1}{E}\left[\sigma_x - \nu(\sigma_y + \sigma_z)\right] \tag{3.3}$$

where

E = Young's modulus,
σ_z = stress along z-direction, which is zero, and
ν = Poisson's ratio.

Under short duration dynamic loads on a viscous material such as hot mix asphalt, the viscous effects are generally small and the apparent Young's modulus (E) is

frequently referred as the resilient modulus (M_R) (Tarefder, 2003). By substituting σ_x and σ_y from Equation (3.3), the following expression can be obtained:

$$\varepsilon_x = \frac{2P}{M_R \pi t d}\left[\frac{(4d^4\nu - 16d^2x^2)}{(d^2 + 4x^2)^2} + (1-\nu)\right] \tag{3.4}$$

The total horizontal deformation, Δh is given by:

$$\Delta h = \int_{(-d_g/2)}^{(d_g/2)} \varepsilon_x dx \tag{3.5}$$

where d_g is the gauge length of the horizontal LVDT. By substituting ε_x and integrating between the limits of gauge length, the following expression can be obtained and used to calculate the M_R of a HMA specimen in tension.

$$M_R = \frac{2P}{\Delta h \pi t d}\left\{\frac{(3+\upsilon)d^2 d_g + (1-\upsilon)\left\{d_g^3 - 2d\left(d^2 + d_g^2\right)\tan^{-1}\left(\frac{d_g}{d}\right)\right\}}{d^2 + d_g^2}\right\} \tag{3.6}$$

In this testing approach, the diametral vertical load, and deformation along vertical and lateral directions are measured using two LVDTs. Each LVDT has a stroke length of 2.54 mm (0.1 in). The M_R value is determined from the deviatoric stress and recoverable horizontal deformation. An assumed Poisson's ratio values of 0.2, 0.35, and 0.5 were used for test temperatures of 5°C (41°F), 25°C (77°F) and 40°C (104°F), respectively, as suggested by Barksdale et al. (1997) and the SHRP Protocol P07 (SHRP, 1992). The Poisson's ratio of each specimen was evaluated from the test results as the ratio of the measured lateral and vertical deformations.

3.3.1.1. Sample Preparation for M_R Testing

Both laboratory prepared cylindrical specimens and field cores of 100 mm (4 in) diameter and 75 mm (3 in) height were used in the testing program. In order to get laboratory prepared test specimens, the following steps were followed, as described in the ASTM D 4123 test method. First, the theoretical maximum specific gravity (G_{mm}) test for each asphalt mixes was performed on reference samples in accordance with the AASHTO T 209-04 test method. Then the loose HMA mix was heated in an oven for approximately two hours at a temperature of 149°C (300°F). The heated loose mix was then compacted in a 150 mm (6-in) diameter cylindrical mold and a height of approximately 100 mm (4 in) using a Superpave gyratory compactor. In order to obtain specimens of specific height (75 mm or 3in), as shown in Figure 3.4, both ends of the SGC compacted specimens were trimmed using a heavy duty asphalt saw (Figure 3.6). After trimming, the remaining part was cored using a heavy duty asphalt coring machine, as shown in Figure 3.7.

Field cores were extracted from the field by using a 100 mm (4 in) coring rig. The final test specimens of 75 mm (3 in) thickness were prepared in the laboratory by trimming both ends of the specimen using a heavy duty asphalt saw. For both laboratory prepared specimens and field cores, the bulk specific gravity (G_{mb}) was evaluated by using the CoreLok sealing method, in accordance with OHD L-45 test method.

3.3.1.2. M_R Test Procedure

The M_R test procedure consisted of applying six stress sequences, as listed in Table 3.4. Each test sequence consisted of a haversine-shaped load pulse having a duration of 0.1 sec and a rest period of 0.9 sec. An electro-hydraulic test system manufactured by

Material Testing System (MTS) was used to load the specimen. The load-deformation response was recorded for 50th and the last 5 cycles of each stress sequence by using a computer-controlled FlexTest SE Test Controller (see Figure 3.8). The FlexTest SE digital servo-controller from MTS is made up of a powerful array of reliable, flexible and easy-to-use controllers designed to address the full spectrum of material and component testing needs (MTS, 2005). Basic capabilities include station configuration editing, the creation of up to four parameters sets per configuration, auto-zeroing, control mode switching with hydraulics on, and adaptive control. The controller provides a self-contained, single-channel control, and can be linked to other controllers for multi-channel testing.

Table 3.4 shows the number of loading cycles used in each sequence. A 22.2 kN (5 kips) load cell was used for samples at 40°C (104°F) and a 97.9 kN (22 kips) load cell was used for samples at 5°C (41°F) and 25°C (77°F) temperatures. The vertical and horizontal deformations were measured by two LVTDs having a stroke length of 2.54 mm (0.1 in), attached in the diametrically perpendicular direction of one face of the specimen, as shown in Figure 3.9. A gauge length of approximately 80 mm (3.15 in) was used to mount the LVDTs on one face of the specimen. M_R tests were conducted within a temperature chamber, as shown in the Figure 3.10. The samples were kept in the temperature chamber for a time period of 18 to 24 hours for the specimen to reach and maintain the required test temperature. A set of four samples were prepared for test at each temperatures (5°C, 25°C, and 40°C). One sample was tested for indirect tensile strength and other three samples were tested for resilient modulus at each temperature. The applied stress level was chosen according to the tensile strength of the sample of

each set. A load corresponding to 0.10 stress ratio (applied stress divided by tensile strength) was used for the conditioning sequence. For the remaining five sequences, a starting load at the first sequence corresponding to a stress ratio of 0.20 was used and a 0.10 stress ratio increment in each subsequent sequence was applied. In order to make full contact between specimen and loading strip, 10% of the peak applied load was used as the seating load in each loading cycle. The resilient modulus was calculated from the average recoverable deflection and average load from the last five cycles of each sequence. A sample of the MTS test software and a tutorial explaining "How to Run Indirect Tensile Resilient Modulus Test" and "How to Run Indirect Tensile Strength Test", developed by the author, are attached in Appendix B.

3.3.1.3. Accuracy of Deflection Value in M_R Calculation

The accuracy of deflection measurement in M_R calculation depends on the resolution of the data acquisition system and LVDTs. In the current study, using ±2.54 mm (± 0.1 in) LVDTs and 16-bit data acquisition, the resolution of the measured displacement was $0.2/2^{16} = 3 \times 10^{-6}$ in. The expected displacement for HMA specimen is generally between 25.4×10^{-4} (10^{-4} in) to 25.4×10^{-3} (10^{-3} in). So, the deviation of displacement or maximum relative error was in the range of $3 \times 10^{-6}/10^{-4}$ and $3 \times 10^{-6}/10^{-3}$ (3% - 0.3%). Based on this calculation, the possible error associated with the M_R calculation considered negligible.

3.3.2. APA Rut Test

The Asphalt Pavement Analyzer (APA) is a multi-functional Loaded Wheel Tester that has been successfully used for evaluating permanent deformation (rutting), fatigue

cracking and moisture susceptibility of HMA mixes (Kandhal and Mallick, 1999). The APA has the capability of testing both rectangular and cylindrical specimens. A typical APA rut test uses three beam specimens or six cylindrical specimens. Each beam specimen is 75 mm (3 in) tall, 125 mm (5 in) wide and 300 mm (12 in) long (see Figure 3.12). Each cylindrical specimen is 150 mm (6 in) in diameter and 75 mm (3 in) in height. Both SGC samples and field cores can be tested. In this study six SGC cylindrical specimens from each mix and six field cores from each site were used for laboratory rut testing. Laboratory cylindrical specimens were compacted from each loose HMA mix type. The weight of the loose mix was chosen to obtain 7% air voids, in accordance with the OHD L-43 test method. The compacted specimens were kept overnight at room temperature and then bulk specific gravity tests were performed in accordance with the OHD L-45 test method. Subsequently, the compacted specimens were placed in the molds, as shown in Figure 3.11 and preconditioned at 64°C (147.2°F) for a minimum of 6 hours, inside the APA test chamber. This was done by switching on APA chamber and setting the duration of preconditioning time. Following preconditioning, the desired vertical wheel load (445 N or 100 lbs) was applied and the hose pressure was set at 690 kPa (100 psi). The APA was allowed to run for 8000 loading cycles in accordance with the OHD L-43 test method. The rut depth was measured as a function of load cycles by the automated rut depth measuring system. Manual measurements were taken by digital measuring gauge as a check on the automatic system rut depth measurement. The average rut depths of six specimens (three sets) were reported as the rut depth of the mixture, as recommended by the OHD L-43 test method.

3.3.3. Fatigue Test

Fatigue failure generally occurs when a pavement is stressed to the limit of its fatigue life by repetitive axle load applications. Fatigue cracking is often associated with loads that are too heavy for the pavement structure or more repetitions of a given load are imposed than provided for in the design. Fatigue cracking is generally considered to be more of a structural problem than just a material problem (Brown et al., 2001). It is usually caused by a number of pavement factors that occur simultaneously. In addition to repeated heavy loads, poor sub-grade drainage can contribute to high deflections in a pavement, which is also one of the principal causes of fatigue cracking.

The Asphalt Pavement Analyzer (APA) is capable of testing fatigue life of asphalt specimens. Fatigue cracking resistance of HMA can be determined by subjecting beam specimens to a repeated wheel loads and contact pressures. The automated data acquisition system in APA plots the vertical deformation of the beam from which the fatigue life is evaluated. In this study, a set of three 125 mm x 300 mm x 75 mm (5 in x 12 in x 3 in) beam specimens were prepared from each type of HMA mix. The weight of loose mix was chosen so as to get a targeted air void of 7 ± 1% in these specimens. The compacted specimens were kept over night at room temperature and then bulk specific gravity test (G_{mb}) was performed in accordance with the AASHTO T166 test method. The APA wheels were calibrated by using a pre-calibrated load cell to a 1113 ± 4.5 N (250 ± 1 lb) load and the cycle counter was preset to 50,000 cycles. Then the specimens were placed in the testing molds, as shown in Figure 3.12, and secured in the APA sample tray. The temperature of the APA was set to the test temperature (20°C) and the specimens were allowed to condition at the test temperature for one hour before starting

the test. The APA was started and allowed to run for the preset number of cycles. The APA stop automatically at the end of the test cycle or when all three beams have failed in fatigue. After the APA stopped, the number of cycles completed for each specimen was recorded from the test data sheet and reported as the fatigue life of the HMA mix.

3.3.4. Permeability Test

It is generally agreed that excess moistures in HMA pavements is potentially detrimental to pavement performance because of phenomena such as stripping in the HMA layers and softening or weakening in underlying unbound layers. Most laboratory-based methods for estimating permeability of HMA feature either a constant head or a falling head type test (e.g., Kantipong, et al., 2003; Mohammad, et al., 2003). In this study, a relatively simple laboratory method involving a falling head device, shown in Figure 3.13 and manufactured by Karol-Warner, was used according to the OHD L-44 test method. Two specimens having 150 mm (6 in) diameter and 75 mm (3 in) height were prepared using the Superpave Gyratory Compactor for each type of HMA mix. The weight of loose mix was chosen so as to obtain a target air void of 7 ± 1%. The compacted samples were kept overnight at room temperature and then bulk specific gravity (G_{mb}) test was performed in accordance with the OHD L-45 test method. Then the permeability test was performed, as described in the OHD L-44 test method. The time taken for the meniscus of water to drop in the graduated cylinder from the initial timing mark (65-cm) to lower timing mark (0-cm) was recorded to nearest 0.1 second. The test was performed three times for each specimen and the lowest time was recorded. For samples having a test time approaching 30 min during the first run without the water level reaching the lower timing mark, the water level at 30 min was recorded and then the

test was performed one more time. The coefficient of permeability (k) was calculated by using the following equation (OHD L-44, 2003).

$$k = \frac{aL}{At} \ln\left(\frac{h_1}{h_2}\right) C \qquad (3.7)$$

where

k = coefficient of permeability, cm/s
a = inside cross-sectional area of the buret, cm^2
L = average thickness of the test specimen, cm
A = average cross-sectional area of the test specimen, cm^2
t = elapsed time between h_1 and h_2, sec
h_1 = initial head across the test specimen, cm
h_2 = final head across the test specimen, cm
C = temperature correction for viscosity of water

For the permeability calculation, the mark and the time record which results in the highest coefficient of permeability was used and reported as the permeability of that HMA specimen.

3.3.5 Laboratory Seismic Modulus Test

The laboratory seismic modulus test was performed on field cores from the Davis site. The test consisted of placing an accelerometer at one end of the specimen and tapping the other end with a hammer having a load cell attached to it, as shown in Figure 3.14. Both the accelerometer and hammer are connected to a data acquisition system that is connected to a portable computer. A software developed by Khanna (2006) was used to acquire and process the time records from the accelerometer and the load cell. The response measured with the accelerometer contains an oscillation that corresponds to the standing wave energy trapped within the specimen (Nazarian et al., 2003; Teredesai, 2005).

The frequency of oscillation was determined by transforming the two signals (acceleration and load) into frequency domain using the Fast–Fourier Transform (FFT) technique and then normalizing the acceleration amplitude with the load amplitude. The variation of normalized amplitude as a function of frequency, which is called transfer function, contains peaks that correspond to the oscillation of the standing waves. A typical plot of the transfer function is shown in Figure 3.15. The transfer function in Figure 3.15 shows two distinct peaks. The first peak corresponds to shear resonance (f_s), while the second peak corresponds to longitudinal resonance (f_p). Knowing the resonant frequency (f_p, Hz), mass density (γ/g, $(lb/in^3)/(in/s^2)$), and the length of the specimen (l, inches), the laboratory seismic modulus (E_S, psi) could be determined using the following equation (Nazarian et al., 2003):

$$E_S = \frac{\gamma}{g}(2F_L L)^2 \qquad (3.8)$$

3.4. Field Testing

A non-destructive field test, called Falling Weight Deflectometer (FWD) test, was performed at all three pavement sites. In addition to FWD test, Ground Penetrating Radar (GPR) test and Spectral Analysis of Surface Wave (SASW) test were performed at the Tar Creek site.

3.4.1. Falling Weight Deflectometer Test

Falling Weight Deflectometer (FWD) is one of the most popular equipment for pavement deflection measurement and evaluation of existing pavement structures (Abdallah et al., 2001). The impulse load is generated by a falling mass from one or more predetermined heights that typically last for 25 to 30 ms. The resulting load pulse is

transmitted to the pavement as a half sine wave (Bandara and Briggs, 2004). The FWD test was conducted in accordance with the ASTM D 4694 test standard. The peak deflections and load magnitude are captured, reported and automatically stored in the system.

Figure 3.16 shows the FWD device used at the Tar Creek site. The test consisted of applying two different loads: one 44.5 kN (10 kip) and the other 80 kN (18 kip), falling from two different heights of 100 mm (4 in) and 396 mm (15.6 in), respectively. Each load is impounded five times at each location. Figure 3.17 shows the FWD device used in the Davis and the OKC sites. This equipment used three different loads (40 kN (9 kip), 53 kN (12 kip), and 80 kN (18 kip)) falling four times per load at each location from a constant height. The resulting load pulse is transmitted to the pavement as a half sine wave. A time-history plot of a typical FWD load pulse is shown in Figure 3.18. The peak deflections and load magnitude were captured, reported and automatically stored by the system. Deflections were measured with seven velocity transducers (sensors) that are mounted on a bar, as shown in Figure 3.19. They are automatically lowered to the pavement surface during testing. One transducer is located in the center of the loading plate and others are spaced at 0, 0.2, 0.3, 0.5, 0.6, 0.9 and 1.5 m (0, 8, 12, 18, 24, 36 and 60 in.) from the center, as recommended by the Federal Highway Administration. The resulting deflections form a "basin" whose depth and shape were used to calculate the material properties (moduli (E_{FWD})) of the constituent pavement layers (Bandara and Briggs, 2004). The results of the FWD tests were processed using a compute program, *Modulus 5.0*, developed by Liu et al. (2000). The results of the FWD tests are discussed in Chapter 4.

3.4.2. Ground Penetrating Radar (GPR)

A Ground Penetrating Radar (GPR) technique was used to determine the thicknesses of the pavement structure, specifically, the AC layer and the stabilized base course. GPR is a pulse-echo method for measuring pavement layer thicknesses (USDOT, 2005a). It works like an ultrasound device, but uses radio waves rather than sound waves to penetrate the pavement (USDOT, 2005a). Antennas mounted on a moving truck are used to transmit short pulses of radio wave energy into the pavement, as shown in Figure 3.20. As this energy travels down through the pavement structure, echoes are created at boundaries of dissimilar materials (such as the asphalt-base interface). The arrival time and strength of these echoes can be used to calculate pavement layer thickness (Teredesai, 2005; Nazarian et al., 2006). Figure 3.21 shows a typical transmitted radio wave and a reflected wave. It is important to note that GPR is one of the most rapid techniques for data collection, among all the geophysical methods, in terms of both wave propagation and sampling rates (scans/second) (USDOT, 2005b). A GPR analysis can be performed at walking or slow driving speeds for QA assessments and condition assessments of a pavement structure (Teredesai, 2005). Results of the GPR tests performed at the Tar Creek site are discussed in Chapter 4.

3.4.3 Spectral Analysis of Surface Waves (SASW)

Spectral Analysis of Surface Waves (SASW) is a non-destructive field test to evaluate the modulus of different layers in a pavement. It can also be used to determine the profile of a pavement structure. This method of seismic testing developed for determining small strain Young's modulus profiles at a pavement site and small strain shear modulus profile at a soil site (Nazarian, et al., 1988; Teredesai, 2005). The method

is based on the dispersive characteristic of Rayleigh waves when traveling through a layered medium (Geovision, 2004). The SASW test is performed on the surface, allowing for less costly measurements than with traditional borehole methods (Bandara and Briggs, 2004).

SASW tests were performed at three selected locations on the Tar Creek site. The test consisted of striking the surface of a pavement with a hammer and recording the resultant stress wave-time histories using two receivers (geophones) at known offsets or known distances. Figure 3.21 shows a photographic view of a SASW test in progress. It is important to note that different sizes of hammers were used for different source-receiver geometries so that different wavelengths are achieved. Also, spacing between the receivers was varied to sample different pavement layers. The wave arrival histories at different spacing were analyzed to determine the pavement layer thicknesses and moduli (Nazarian et al., 1988). Once the shear wave velocity profiles are determined, shear and Young's modulus (modulus of elasticity) of the materials (E_{SASW}) are calculated through the use of mathematical equations. The equations are incorporated in the *WinSASW*, a computer program developed at the University of Texas at Austin (Joh, 1996). This software was used in this study to evaluate the aforementioned properties. Figure 3.23 shows the positions of sources (hammer) and receivers (accelerometer and geophones) used to perform the SASW test. The results of the SASW tests are discussed in Chapter 4.

Table 3.1: Test Matrix for Laboratory Tests Conducted

Project Site	Mix Type/ Field Core	Number of Specimens for Laboratory Test				
		Resilient Modulus	APA Rut	APA Fatigue	Permeability	Seismic Modulus
Tar Creek	Surface Mix	9	6	3	2	-
	Bse Mix	9	6	3	2	-
	Cores	6	6	-	-	-
Davis	Base Mix	9	6	3	2	-
	Cores	6	6	-	-	19
OKC	Base Mix	8	6	3	2	-
	Cores	6	6	-	-	-
Total		53	42	12	8	19

Table 3.2: Test Matrix for Non-Destructive Field Tests

Project Site	Field Non-Destructive Tests		
	FWD	SASW	GPR
Tar Creek	√	√	√
Davis	√	-	-
OKC	√	-	-

FWD – Falling Weight Deflectometer
SASW – Spectral Analysis of Surface Waves
GPR – Ground Penetrating Radar

Table 3.3: Summary of Mix Properties for the Collected Loose HMA Mixes

Project Site	Mix Type	Aggregate Type	Binder Type	AC (%)
Tar Creek	Surface Mix (S5)	Lime Stone with 80% raw chat	PG 64-22 OK	6.9
	Base Mix (S3)	Lime Stone with 50% raw chat	PG 64-22 OK	5.6
Davis	Base Mix (S2)	Lime Stone	PG 64-22 OK	4.5
OKC	Base Mix (S2)	Lime Stone	PG 64-22 OK	4.3

Table 3.4: Number of Loading Cycle Used in Each Stress Sequence

Sequence ID	Number of Cycles
C	200
S1	100
S2	100
S3	100
S4	100
S5	100



Notes: 1. Davis (HW #7, Davis, OK); **2. OKC** (Eastern Ave., Oklahoma City, OK); and **3. Tar Creek** (Test Road Project, Miami, OK)

Figure 3.1: Location of Project Sites



Figure 3.2: Collection of Loose HMA Mix from the Tar Creek Site



Figure 3.3: Field Asphalt Coring Machine

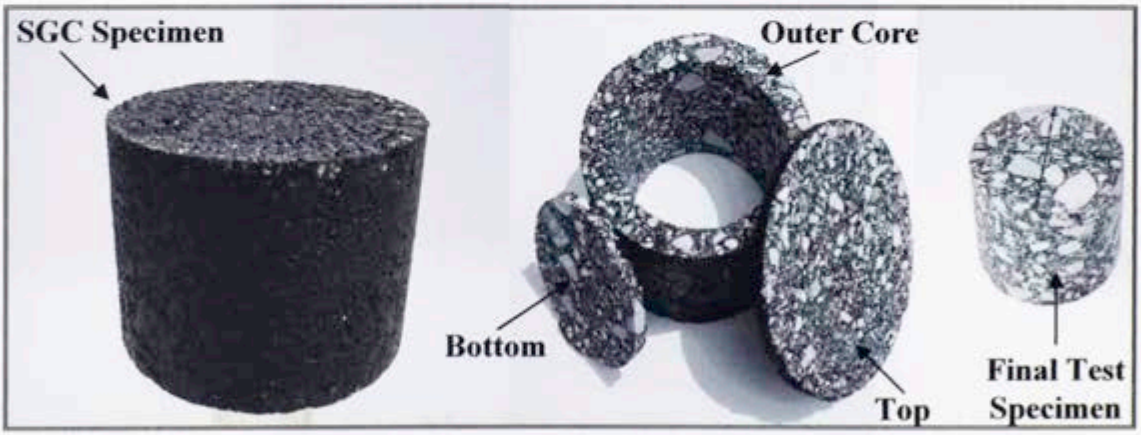


Figure 3.4: Cyclic Indirect Tension Resilient Modulus Test Specimen

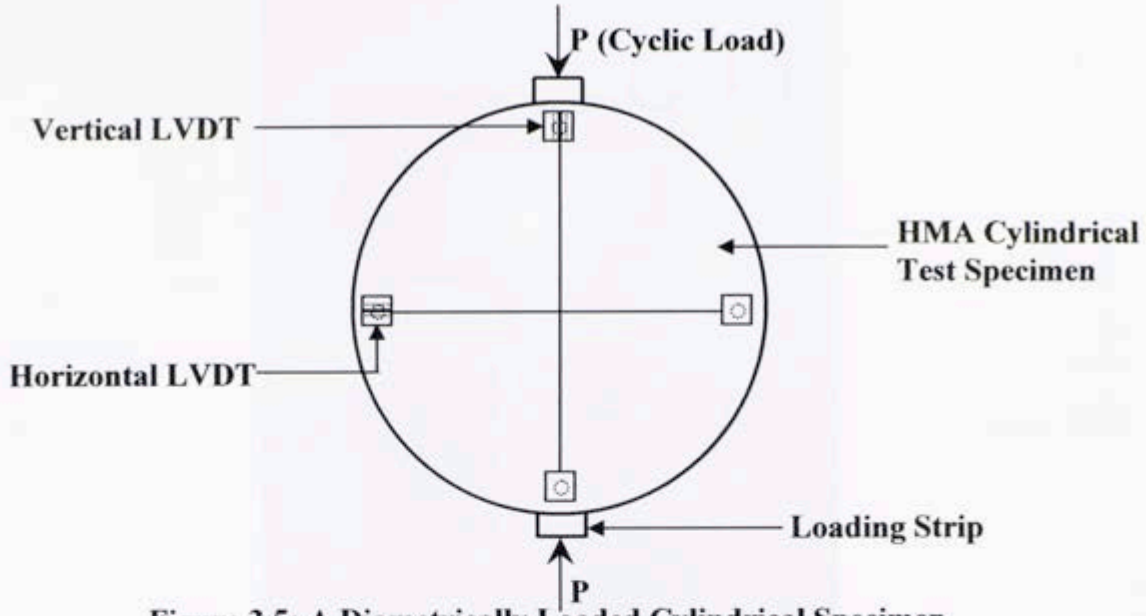


Figure 3.5: A Diametrically Loaded Cylindrical Specimen



Figure 3.6: Heavy Duty Asphalt Saw

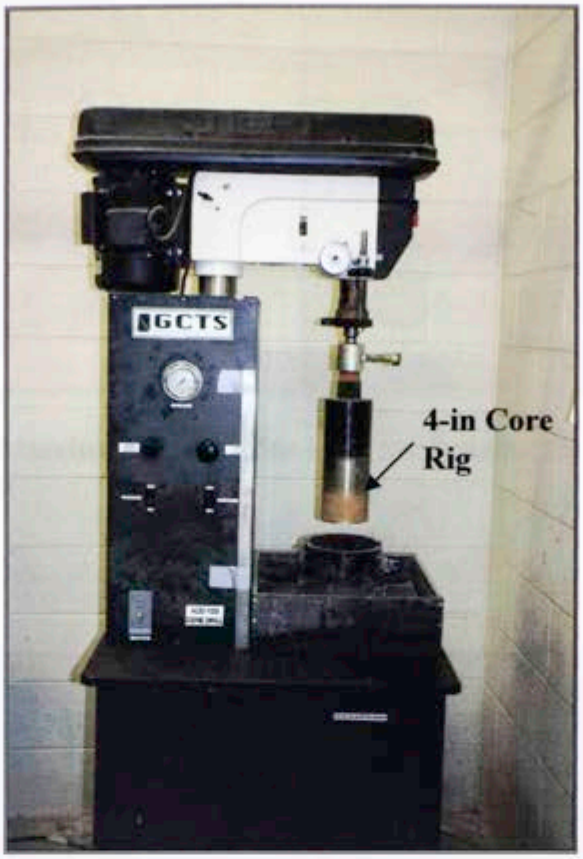


Figure 3.7: Heavy Duty Laboratory Coring Machine



Figure 3.8: Computer Controlled MTS Digital Data Acquisition System

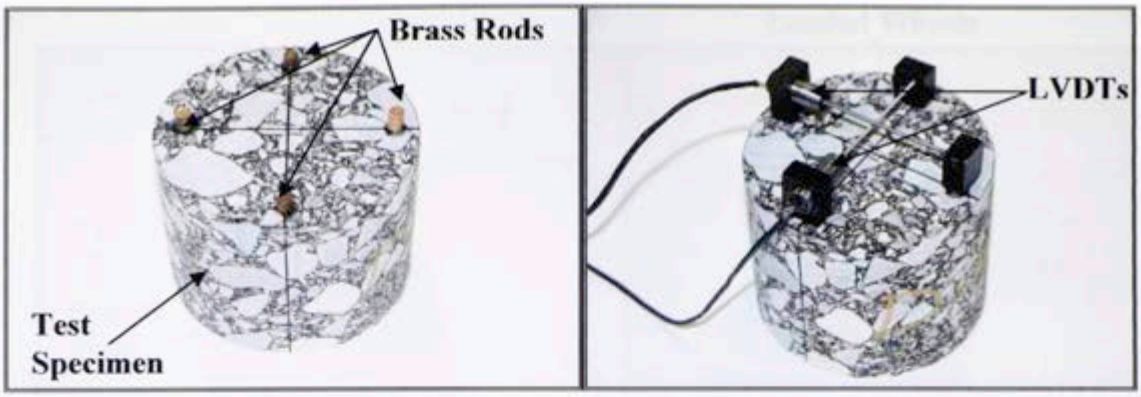


Figure 3.9: LVDTs Attached to the Cyclic Indirect Tension Resilient Modulus Test Specimen

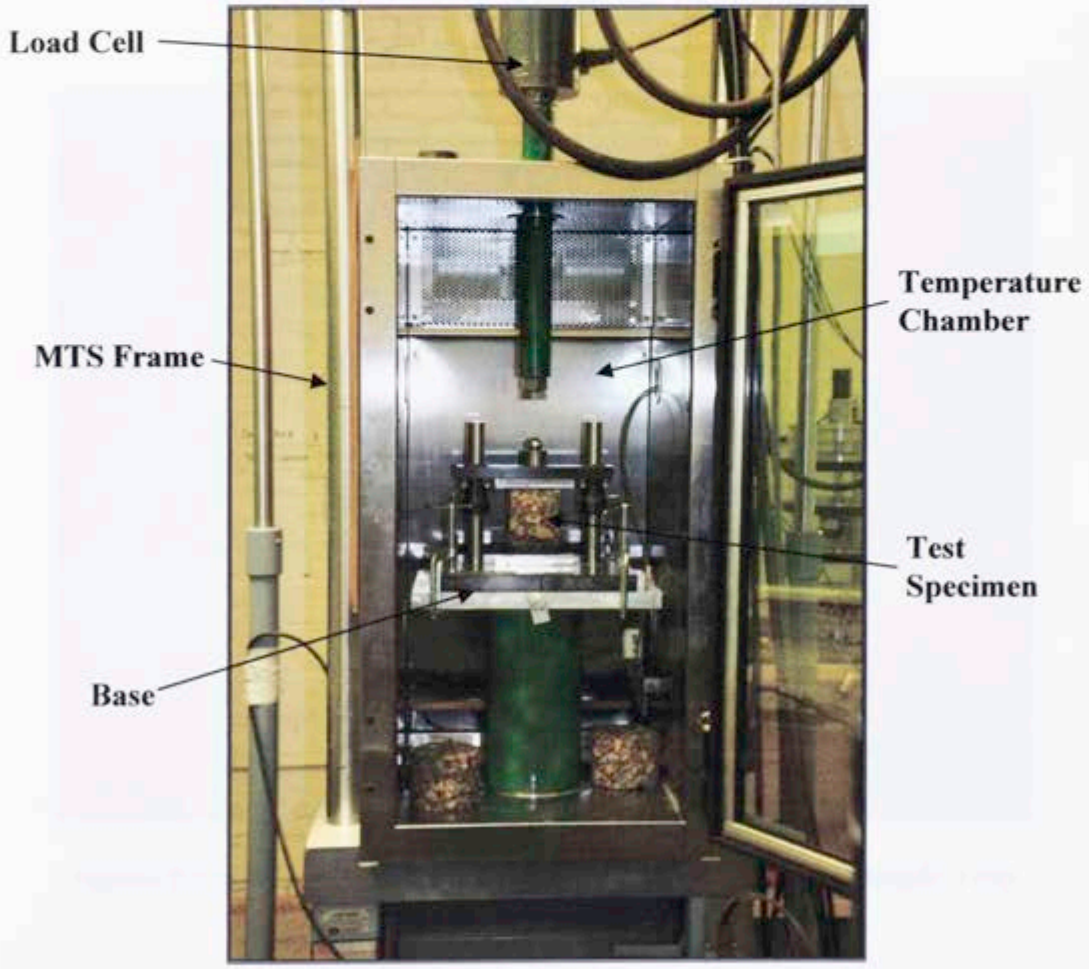


Figure 3.10: Temperature Chamber and Loading Setup Connected with the MTS Frame

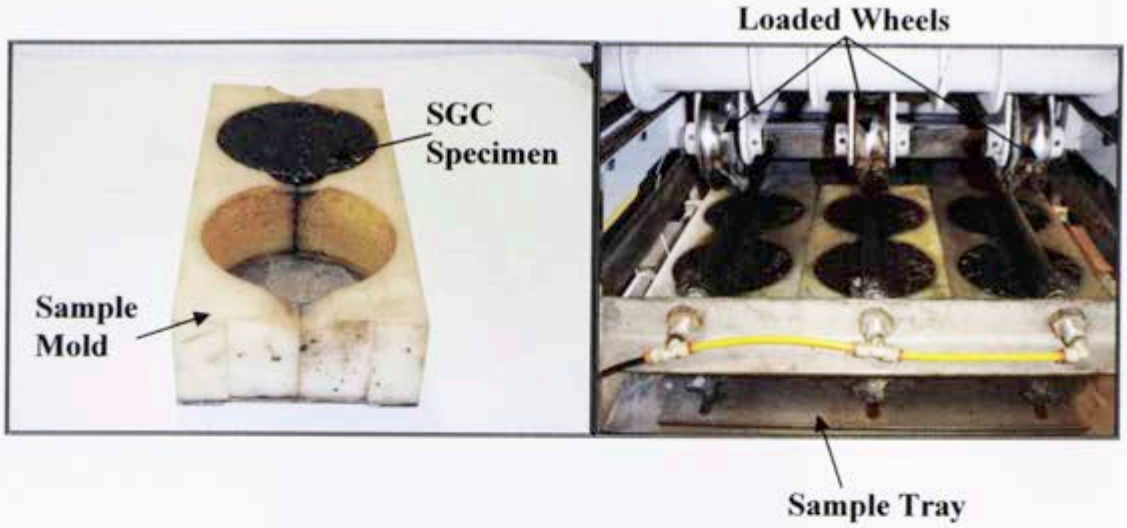


Figure 3.11: APA Rut Sample Mold and Molds Secured in the Sample Tray

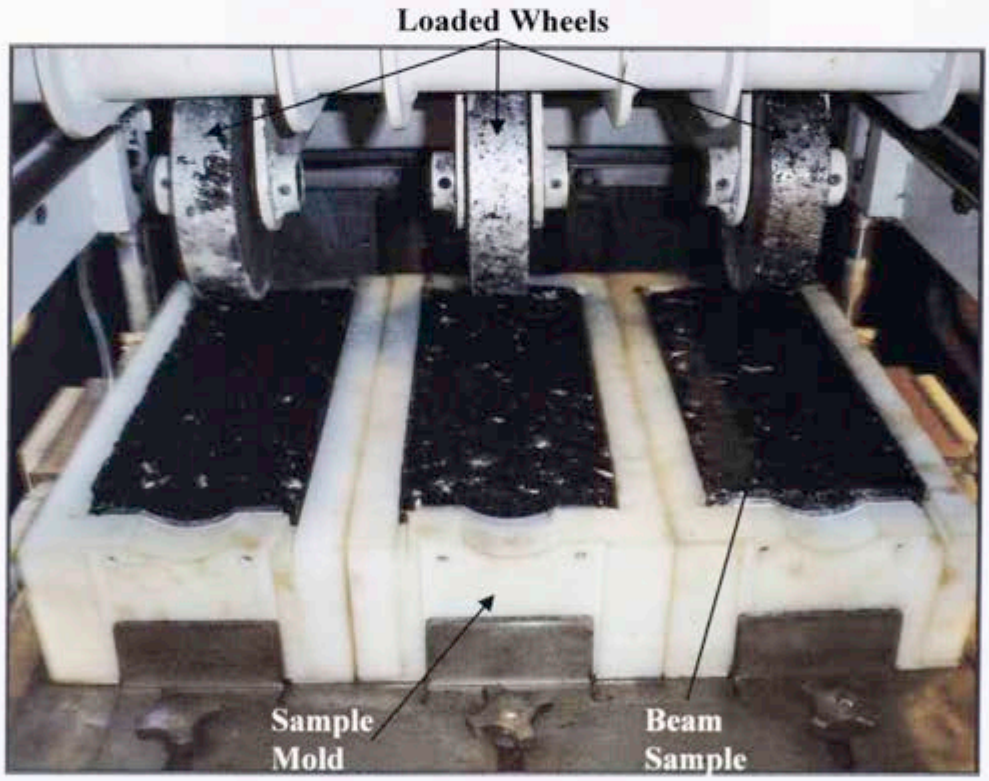


Figure 3.12: APA Fatigue Sample Molds Secured in the Sample Tray

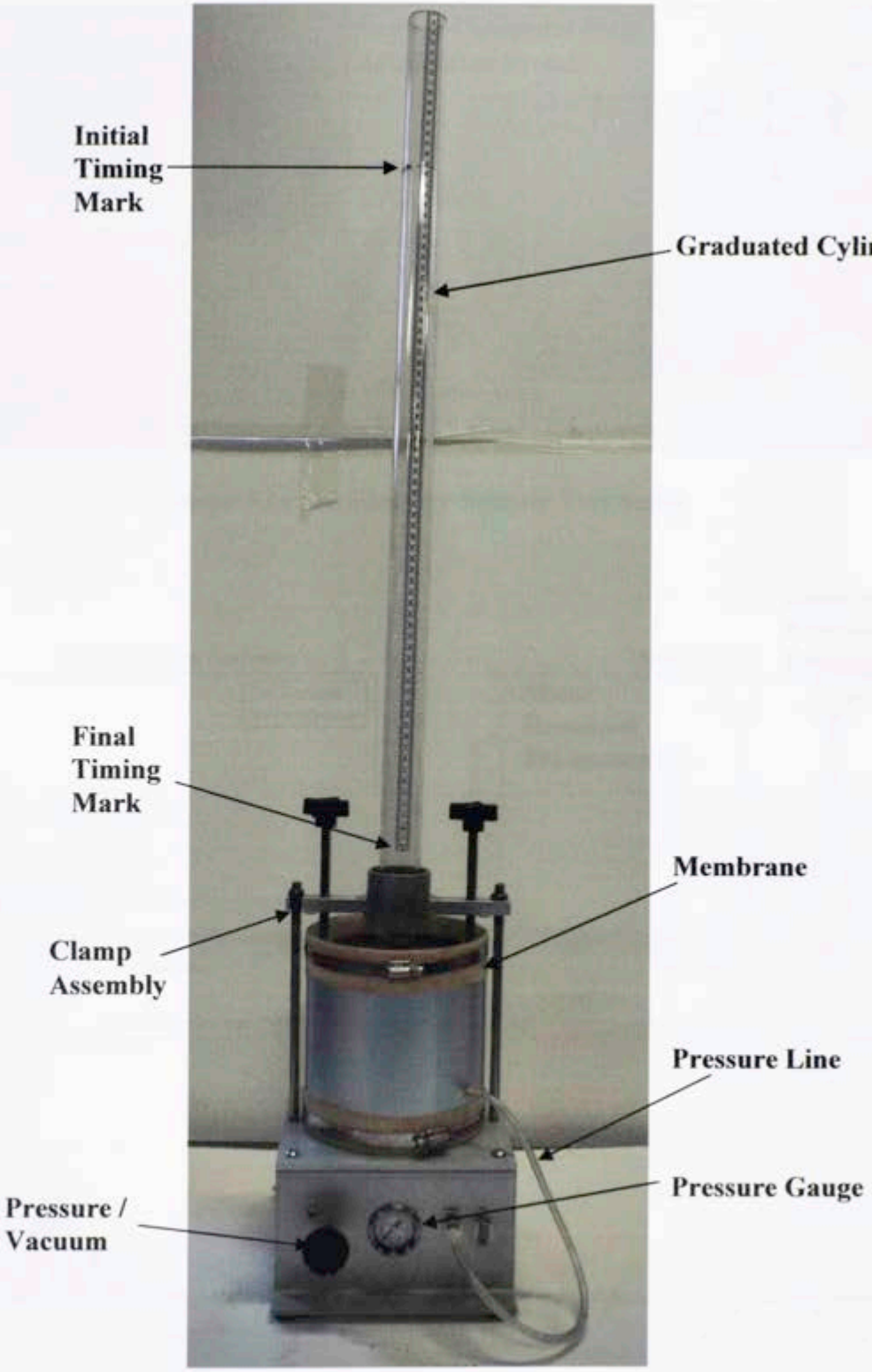


Figure 3.13: Karol-Warner's Falling Head Permeameter

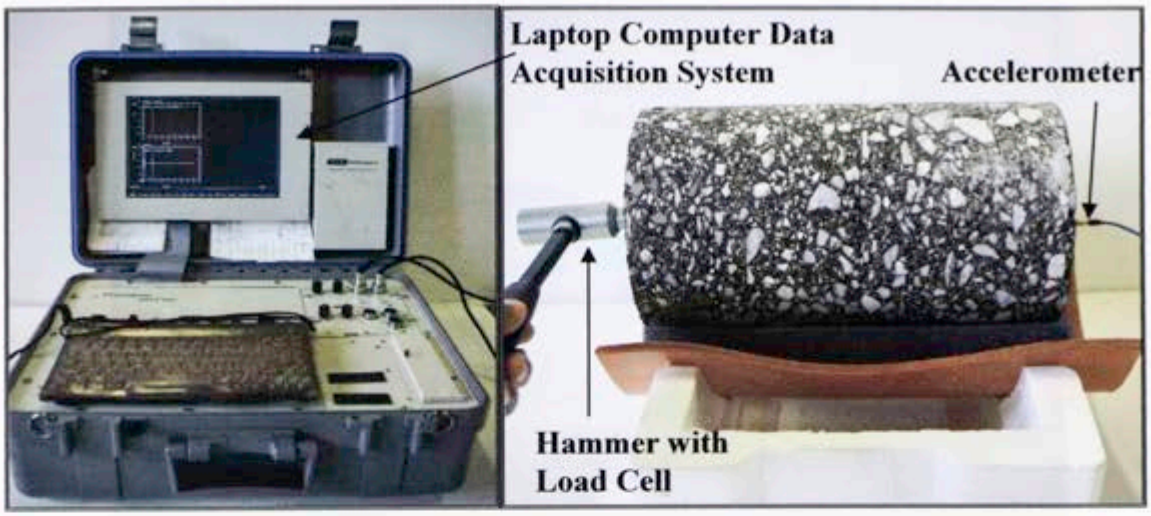


Figure 3.14: Laboratory Seismic Test Setup

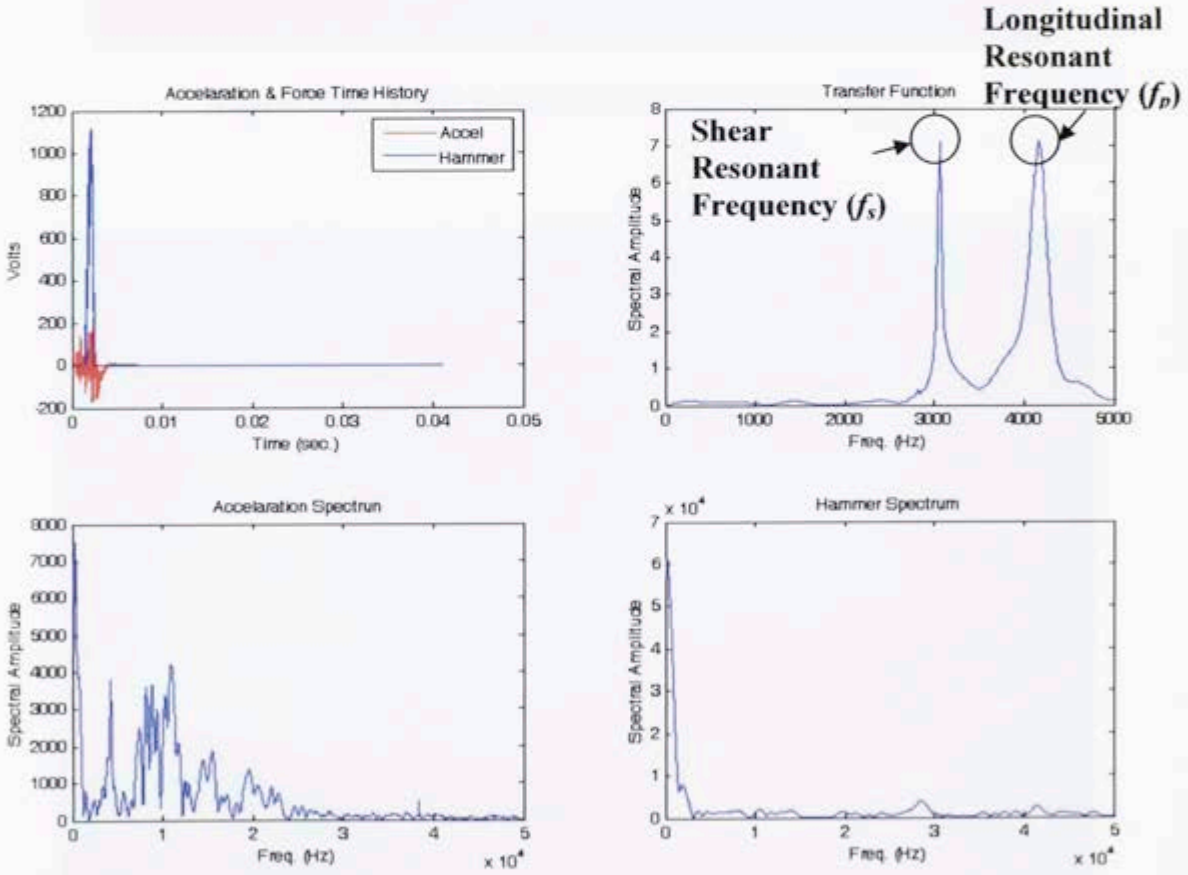


Figure 3.15: A Typical Plot of the Transfer Function (Nazarian et al., 2003)

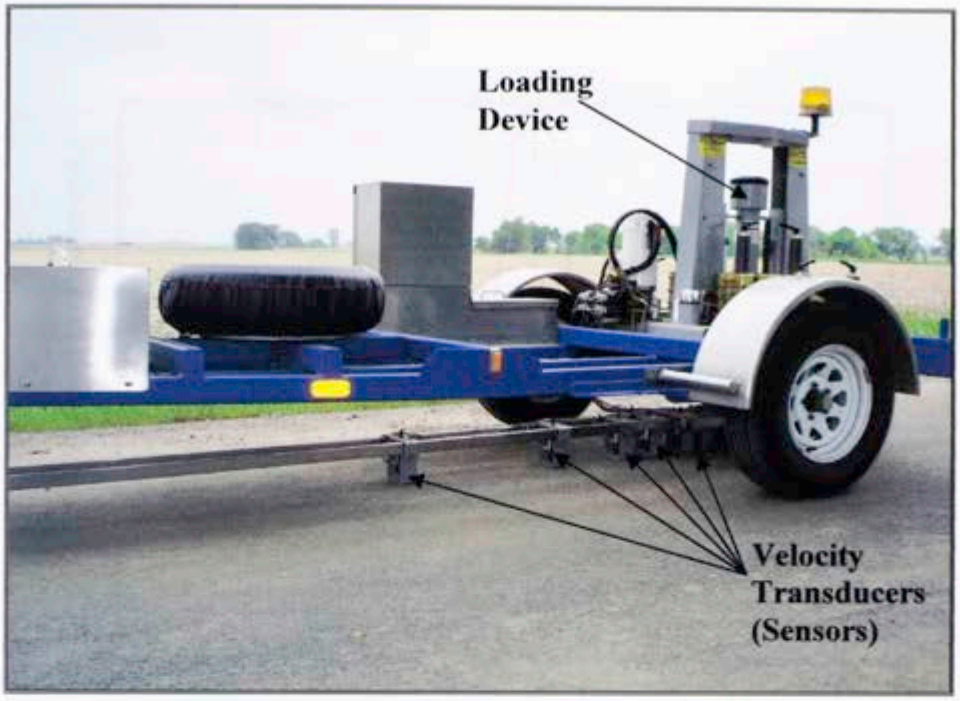


Figure 3.16: FWD Device Used in the Tar Creek Site



Figure 3.17: FWD Device Used in the Davis and Eastern Ave. Project Site

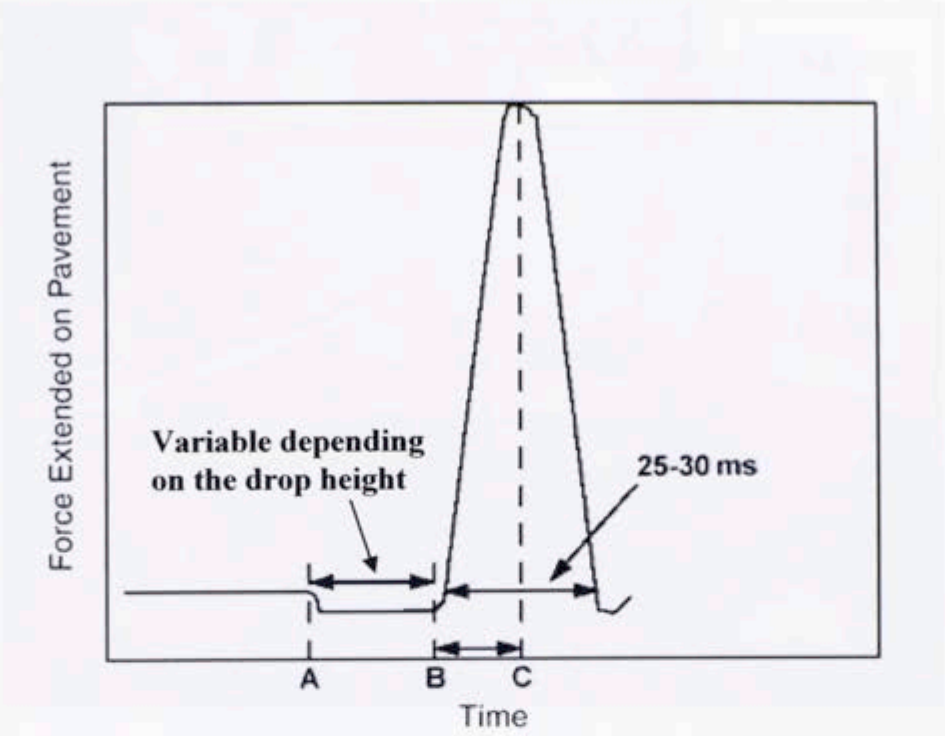


Figure 3.18: Typical Force Output from a FWD Test (Bandara and Briggs, 2004)

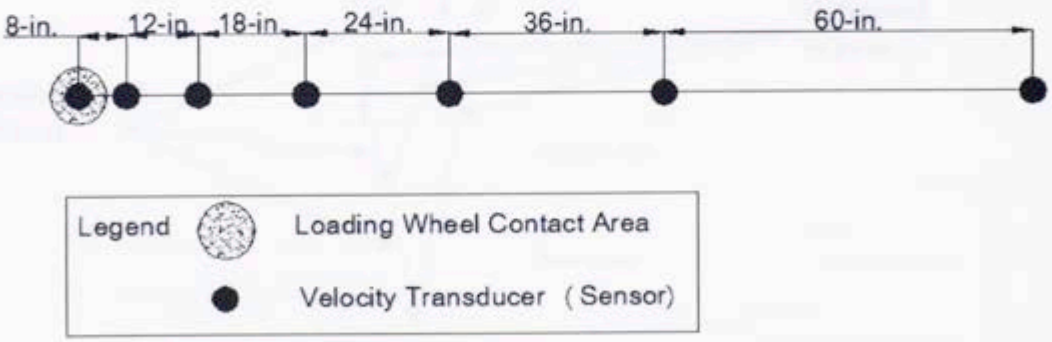


Figure 3.19: Typical FWD Location of Loading Plate and Deflection Sensors (Bandara and Briggs, 2004)



Figure 3.20: The GPR Equipment USed at Tar Creek Site

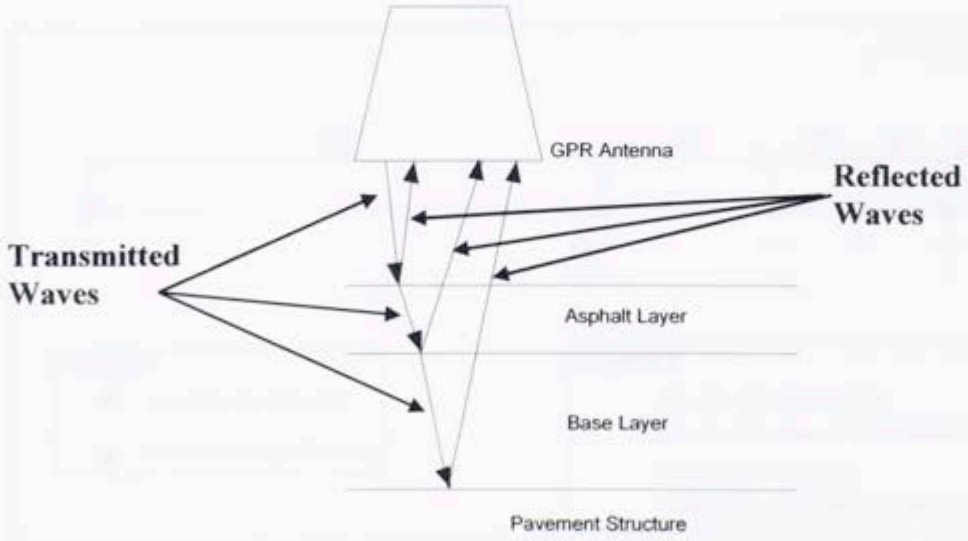


Figure 3.21: Principle of GPR (after USDOT, 2005b)



Figure 3.22: A Photographic View of a SASW Test

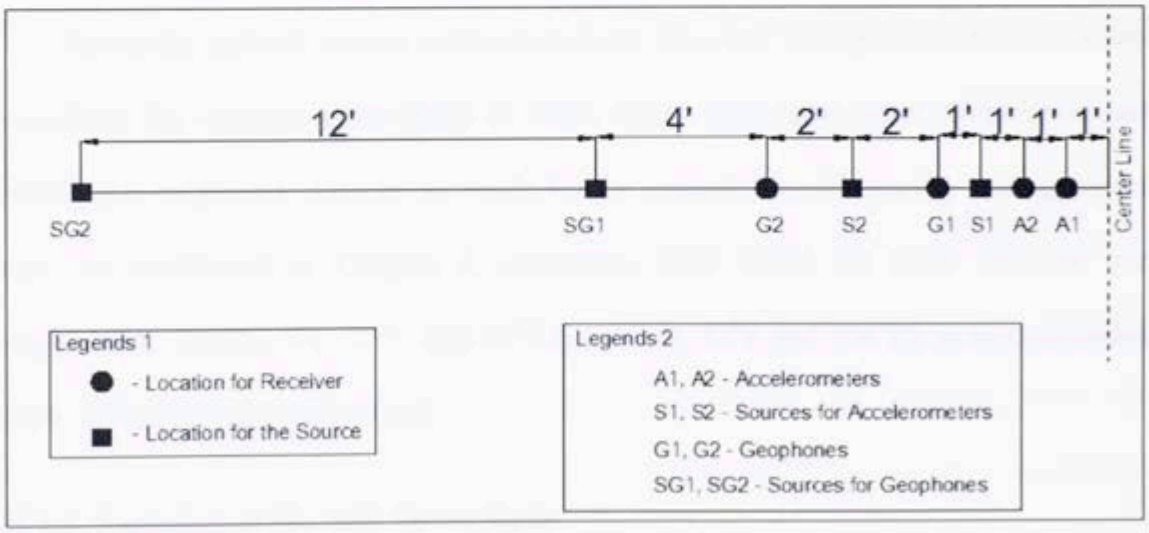


Figure 3.23: Plan View of the SASW Test Setup

CHAPTER 4

RESULTS AND DISCUSSION

4.1. General

The laboratory and field test results are presented and discussed in details in this chapter. It consists of two sections. The first section presents the test results for the laboratory prepared specimens and field cores. The second section presents the field test results namely, Falling Weight Deflectometer (FWD) and Spectral Analysis of Surface Waves (SASW).

4.2. Laboratory tests

The laboratory results for cyclic indirect tension resilient modulus test, APA rut test, fatigue test and permeability test along with the laboratory seismic modulus test are presented and discussed in the following sections.

4.2.1. Cyclic Indirect Tension Resilient Modulus Test

The cyclic indirect tension resilient modulus (M_R) test was performed in this study to evaluate the variation of modulus of HMA mixes with stress ratio, temperature and specific mix properties, namely, air voids, binder content, specific gravity and aggregate sizes. As mentioned in Chapter 3, specimens were tested for three different test temperatures, namely, 5°C, 25°C and 40°C (i.e., 41°F, 77°F and 104°F), as recommended by the ASTM D 4123 test method.

4.2.1.1. Variation of M_R with Stress Ratio

Previous studies (Hossain et al., 1992; Zhou et al., 1992; Shalaby et al., 1997; Tarefder, 2003; Tarefder and Zaman, 2003) were undertaken to evaluate the variation of resilient modulus of HMA mixes with test temperature, air voids, binder content and binder grade,

among others. The resilient modulus values were generally evaluated at only one specific stress level. Tarefder (2003) and Tarefder and Zaman (2003) reported the resilient modulus at a specific stress level between 10% and 40% of the indirect tensile strength (ITS). In a similar study, Hossain et al. (1992) used an average load of 445 N (100 lb) to calculate the resilient modulus of HMA pavement cores. In these studies, no attempts were made to examine the variation of M_R with stress level.

A study by Barksdale et al. (1997) noted that the modulus of HMA mixes, at a temperature higher than 25°C, is highly influenced by the stress state. In that study, it was also reported that SHRP P07 recommended the evaluation of resilient modulus at different stress levels, namely, 5%, 15% and 30% of the indirect tensile strength. The tests were performed at three different temperatures 5°C, 25°C and 40°C (i.e., 41°F, 77°F and 104°F). Another study by Brown and Foo (1989) stated that the stress applied to the specimen has significant effect on the M_R value. In that study, the resilient modulus tests were conducted in accordance with the ASTM D 4123 test method. Specimens were subjected to stress levels corresponding to 10%, 15% and 20% of indirect tensile strength.

In the present study, the variations of resilient moduli under various stress levels were examined. The resilient modulus values for different stress ratios (applied stress/indirect tensile strength), at different temperatures, for all the mixes are summarized in Tables 4.1 through 4.7. It is evident that the resilient modulus, in general, decreases with the increase in stress ratio. For example, the M_R value of Tar Creek base specimen (TC-B-M_R-6) at 25°C (77°F) exhibited a decrease from approximately 3861 MPa (560 ksi) to 3068 MPa (445 ksi) as the stress ratio increased from 0.21 to 0.35. The

variation of M_R values with the stress ratio for the Davis base mix specimens tested at 5°C, 25°C and 40°C (i.e., 41°C, 77°F and 104°F) are graphically illustrated in Figures 4.1 through 4.3. As depicted in these figures, the M_R values decreased with the stress ratio. For example, The M_R values decreased approximately 17% as the stress ratio increased from 0.30 to 0.50 for specimens tested at 5°C (41°F). The resilient modulus exhibited a similar behavior with stress ratio at temperatures 25°C (77°F) and 40°C (104°F). Also, the OKC base mix exhibited the same behavior with the stress ratio, as can be seen from Table 4.6. A similar trend has been reported in the literature. For example, Brown and Foo (1989) reported that the resilient modulus exhibited a decrease with the increase in the stress ratio. Almudaiheem and Al-Sugair (1991) reported a decrease in resilient modulus with increasing stress ratio from approximately 10% to 30%. Also, Boudreau et al. (1992) reported that the resilient modulus depends on the percentages of indirect tensile stress applied.

It has been recognized that the state of stress and deformations at any location within a pavement structure, due to traffic loading, is a function of moduli (Witczak, 2000). Also, the modulus, in turn, is a function of the state of the stress. As a result, a predictive model correlating M_R with state of stress is expected to be beneficial to pavement design. These models may also be useful in the finite element analysis of pavements. Thus, it was decided to evaluate the performance of three potential models in predicting M_R of HMA mixes with the stress ratio, R. The following three models were evaluated:

Linear Model: $M_R = A + B\,R$ (4.1)

Semi-Log Model: $M_R = A\,B^R$ or $\log(M_R) = \log(A) + R\log(B)$ (4.2)

Log-Log Model: $M_R = A\,R^B$ or $\log(M_R) = \log(A) + B\log(R)$ (4.3)

where, "*A*" and "*B*" are model parameters that were evaluated from test data. Each model was then used to predict the resilient modulus values of the 53 test specimens. It is important to note that, other studies have used some of those models. For example, Brown and Foo (1989) used a similar linear model to correlate resilient modulus with stress ratio. Results showed that M_R values decreased approximately 12% as the stress ratio increased from 10% to 15%, for samples tested at 25°C (77°F). In Huang (2004), the dynamic modulus in of HMA mixes under flexural stress was predicted using a similar semi-log model. It was reported, in that study, that the dynamic stiffness modulus decreases with an increase in dynamic load magnitude, due to relatively large strain in the flexural test.

Tables 4.8 through 4.16 show the model parameters and the R-squared values for all the mixes, using the aforementioned models. The R-squared value, also known as coefficient of determination, was used to compare the relative performance of each model in predicting the resilient modulus of HMA with stress ratio. A frequency plot for the coefficient of determination (R-squared) for each regression model was generated, as shown in Figures 4.4 through 4.6. From Figures 4.4 and 4.5, one can see that 47 out of 53 R-squared values for the linear and semi-log models varied between 0.7 and 1.0. Comparatively, the log-log model revealed a total of 41 out of 53 R-squared values varying between 0.7 and 1.0. The R-squared value was the only indicator used here to evaluate the performance of these models. In view of these results, the linear and semi-log models were considered better in predicting the M_R values than the log-log model. Although both models revealed high R-squared values, only the semi-log model was used subsequently to determine the resilient modulus at specific stress ratios, namely, 0.20,

0.35 and 0.50. These stress levels were used since they fall within the range specified by the ASTM D 4123. The resilient modulus at those specific stress ratios were used to evaluate the performance of the four selected mixes in the subsequent sections.

4.2.1.2. M_R Values at Selected Stress Ratios

The M_R values for the laboratory mixes at the aforementioned stress ratios, i.e., 0.20, 0.35 and 0.50, are summarized in Table 4.17 and graphically illustrated in Figures 4.7 through 4.12. In comparing these results, laboratory Davis specimens resulted in the highest average resilient modulus values, followed by the OKC specimens, the Tar Creek base mix specimens, and then the Tar Creek surface mix specimens, in general. For example, the average M_R value of the Davis specimens (laboratory compacted) at a temperature of 25°C (77°F) and a stress ratio of 0.20 is approximately 26%, 39% and 74% higher than the corresponding values of the OKC base, the Tar Creek base and the Tar Creek surface specimens, respectively, as shown in Figure 4.8. The corresponding average M_R values are 9,811 MPa (1423 ksi) for the Davis base, 7,288 MPa (1057 ksi) for the OKC base, 5,992 MPa (869 ksi) for the Tar Creek base and 2,565 MPa (372 ksi) for the Tar Creek surface specimens. From Figure 4.7 through Figure 4.12, it is clear that the Davis mix would perform better compared to all the other mixes. While the OKC base, the Tar creek base are expected, based on this resilient modulus values, to have the similar performance. The Tar Creek surface mix appears to have the lowest performance compared to the other mixes. The difference in M_R values is believed to be due to the difference in the specific mix properties, namely, binder content, binder grade, air voids, nominal maximum aggregate size (NMAS) and percentage of fines, among others. A summary of the mix properties is presented in Table 4.18. Attempts have been made to

evaluate the effect of each individual property on the behavior of resilient modulus values of these mixes, as discussed in the following sections. Also, a regression model depicting the combined effect of these properties was developed.

4.2.1.3. Effect of Binder Content on Resilient Modulus

Figure 4.13 shows the variation of resilient modulus with the binder contents for laboratory compacted specimens. It is evident that the highest resilient modulus corresponds to specimens with a binder content of 4.5%. Specimens with a higher binder contents exhibited lower M_R values, as shown in Figure 4.13. As also depicted in this figure, the resilient modulus of specimens with a binder content of 4.3% have a lower resilient modulus values than the corresponding values at a binder content of 4.5%. A similar qualitative trend was also obtained for field cores, as shown in Figure 4.14. For example, an increase in M_R value for the Davis cores (binder content 4.3%) than the OKC cores (binder content 4.5%) and a decrease in M_R value for the Tar Creek cores (binder content 5.6%) than the Davis cores (binder content 4.5%) are seen.

The increase in resilient modulus as the binder content increased from 4.3% to 4.5% could be attributed to the fact that a slight increase in binder content increases the binder film thickness between aggregate particles, thereby, an increased proportion of asphalt acts to resist the applied stress and thus increase the resilient modulus. A similar explanation was given by Tarefder (2003). A decrease in resilient modulus as the binder content increased beyond 4.5% would be attributed to the fact that additional asphalt (more than the optimum binder content) would increase the binder film thickness between particles excessively and decrease the internal friction of the aggregate, thus making the HMA specimen to undergo a large strain with applied load. Materials can

flow laterally due to the loss of aggregate interlock (Roberts et al., 1996), thus reducing resilient modulus values. It is also worth noting that the difference in resilient modulus (increase or decrease) due to the binder content may be attributed to other properties previously listed, because other mix properties are not identical. The effect of various binder contents on the same mix, by fixing the other properties, was not addressed in this study. A future study may be undertaken to address this issue.

4.2.1.4. Effect of Air Voids on Resilient Modulus

Figure 4.15 and Figure 4.16 show the variation of resilient modulus values with air voids for the laboratory specimens and field cores, respectively. Results showed that no specific trend is evident between the resilient modulus and the air voids. This is consistent for all three temperatures. For example, laboratory specimen with air voids of 6.4% has an average resilient modulus higher than the corresponding values of laboratory specimen with 6.3%, 6.7% and 8.0% air voids. Also, laboratory specimens with air voids of 6.3% have a lower M_R value than the laboratory specimen with 6.7% air voids and a higher M_R value than the laboratory specimen with 8.0% air voids. The range of air void variation within the laboratory specimens are lower (6.0% to 8.0%) in this study. Therefore, a study with changing air voids within a comparatively higher range, keeping other variables unchanged, would give a clear conclusion for the effect of air voids on resilient modulus.

A trend was observed for resilient modulus between the laboratory specimens and field cores. As one can see from Table 4.19, the laboratory resilient modulus values were higher than that of field cores except for some selective specimens. This is due to the fact that the field core densities are lower than those of the laboratory prepared specimens.

Difference in compaction imparted by a laboratory gyratory compactor and a vibratory compactor in the field compaction is the primary reason for this variation. Table 4.19 shows that M_R of laboratory specimens could be as high as 76% of the field cores. Therefore, we can conclude that the increasing air voids (decreasing density) significantly decreases the resilient modulus values. This suggests that homogeneity is more successfully achieved for specimens compacted in the laboratory than for field core, which can vary depending upon the compaction quality. This is consistent with the study by Katicha (2003). The present study showed that densities of the field cores are much lower than those of laboratory prepared specimens, therefore, the average resilient modulus of field core is lower than that of laboratory prepared specimens. Also, the present study showed that the predicted resilient moduli decrease with increasing void ratios. Similar conclusions were made by Crovetti et al. (2005). That study reported that the resilient modulus values decrease at a given temperature, as the percent air voids increase.

4.2.1.5. Effect of Aggregate Sizes on Resilient Modulus

. With regard to the NMAS of the aforementioned mixes, the OKC and the Tar Creek base mixes, with an NMAS of 25 mm (1 in), were coarser than the Davis and the Tar Creek surface mixes. The NMAS was 19 mm (¾ in) for the Davis mix and 12.5 mm (½ in) for the Tar Creek surface mix. A study by Mindess et al. (2002) reported that the larger the NMAS, the higher the strength. However, in this study, the effect of aggregate size on resilient modulus is not clear and could not be adequately investigated. This is due to the fact that the Davis base mix with a NMAS of 19 mm (¾ in), which is less than

the NMAS (25 mm (1 in)) of the Tar Creek base and the OKC base mixes, exhibited a higher resilient modulus values.

The percentage of aggregate passing No. 200 sieve for the Tar Creek surface mix and the Davis base mix were higher and are 6.0% and 5.9%, respectively, as shown in Figure 4.17 and Figure 4.18. These values for the Tar Creek base mix and the OKC mix are comparatively lower and are approximately 4.9% and 4.7%, respectively. But, the resilient modulus for the Tar Creek surface mix specimens is lower than the Davis mix specimens followed by the OKC mix and the Tar Creek base mix specimens. A study by Crovetti et al. (2005) reported that the resilient modulus increases at a given temperature, as the aggregate passing No. 200 sieve increases. In the present study, no clear trend could be identified for variation in resilient modulus with percentage fines. This may be attributed to the change in other mix properties.

4.2.1.6. Variation of M_R with Temperature

The variation of resilient modulus values with temperature for all the mixes is presented in Table 4.17 and graphically illustrated in Figures 4.19 through Figures 4.23. The resilient modulus decreased significantly with increasing in temperature for all mixes. For example, resilient modulus (at stress ratio 0.35) decreases from 11,935 MPa (1731 ksi) to 1,103 MPa (160 ksi) as the temperature increased from 5°C to 40°C (41°F to 104°F) for the Tar Creek base mix. The Davis specimens exhibited a decrease in M_R values from 15,410 MPa (2235 ksi) to 3,172 MPa (460 ksi) as the temperature varied from 5°C to 40°C (41°F to 104°F). It is an indication that the variation in M_R values, due to temperature, varied from one mix to another. A similar behavior for HMA mixes has been reported in previous studies. For example, Katicha (2003) reported that the resilient

modulus decreases with increasing temperature and the variation can be best represented by an exponential model, as was discussed in Chapter 2. A decrease in M_R values with an increase in temperature was also reported by Tarefder (2003) and by Tarefder and Zaman (2003).

The performance of each mix due to temperature was examined. Figure 4.24 shows the average percentage reduction (PR) in M_R for all the laboratory specimens and field cores. As depicted in Figure 4.24, the average percentage reductions in MR for laboratory specimens are 87% for the Tar Creek base, and the Davis and the OKC base mixes. For the Tar Creek surface mix, the percent reduction is 89%. For the field cores the average percentage reduction for the Tar Creek and the Davis cores are 87% and for the OKC cores the reduction is 93%. A similar percentage reduction for different HMA mixes has been reported in the literature (Salem, 2004; Katicha, 2003; and Ali and Lobez, 1996). For example, Katicha (2003) reported that the percentage reduction due to temperature varied between 78% and 90%. Based on these results, it may be concluded that the Tar Creek surface mix was more susceptible to temperature than the other mixes, if the percent reduction in M_R ought to be used as an indicator of temperature susceptibility. It is believed that the temperature susceptibility of the HMA specimens may be attributed to the binder content in the mixes, since the Tar Creek surface mix has the higher binder content compared to the other mixes.

4.2.1.7. A Model to Predict Resilient Modulus

From the aforementioned results, it is evident that resilient modulus varies with stress level, temperature, material properties and mix properties. This is consistent with Katicha (2003) that the difference in measured resilient modulus is believed to be due to

the difference in properties of various mixes, namely, air voids, binder content, specific gravity of materials and percentage fines. To this end, it was decided to develop a general model correlating resilient modulus with stress ratio, temperature and aforementioned specific mix properties. The employed semi-log model (Equation 4.6) includes two model parameters ("A" and "B"). The parameter "A" represents the resilient modulus at a stress ratio of zero, while "B" represents the sensitivity of resilient modulus to stress ratio changes. These model parameters were correlated with temperature, material properties and specific mix properties, namely air voids, binder content, specific gravity and percentage fines. The actual model parameters "A" and "B", shown in Tables 4.11 through 4.13, were used to develop a general model as a function of the aforementioned properties. The SAS statistical software was used for this purpose. The stepwise method at a level of 0.15 was used in developing model for "A" and "B". The stepwise method consists of entering or removing one variable at a time in the regression model, to attain a better R-squared value. The employed stepwise method showed that the model parameter "A" was related to temperature, percentage of air voids, percentage of binder content and percentage of material passing No. 200 sieve. Parameter "B" was found to be only related to temperature and percentage air voids. The relationships for predicted model parameters "A" and "B" are presented in Equations 4.9 and 4.10, respectively.

$$A = 3048.96 - 23.12\,T - 148.36\,A_v - 280.39\,AC + 443.04\,N_{200} \qquad (4.4)$$

$$B = 0.803 - 0.010\,T + 0.053\,A_v \qquad (4.5)$$

where,

T = temperature, in °F,
A_v = air voids, in %,
AC = binder content, in %, and

N_{200} = aggregate passing No. 200 sieve, in %.

The analysis of variance (ANOVA) of this predicted model parameter yields an F value of 35.1 and an R-squared value of 0.75 with a P_r value less than 0.0001, for parameter "A". Parameter "B" model had an F-value of 38.4 and R-squared value of 0.61 with a P_r less than 0.0001, which indicates that the model is considered statistically significant in predicting the variation of model parameters with aforementioned specific mix properties. A comparison between the calculated and the predicted model parameters "A" and "B" are summarized in Table 4.20 and illustrated in Figure 4.25 and Figure 4.26. From Figure 4.25, the predicted "A" can be correlated with the measured "A" with a straight line regression having a slope of approximately 1.0 and an R-squared value of 0.75. For parameter "B", the predicted "B" is correlated with a line of slope 1.002 and an R-squared value of 0.6, as shown in Figure 4.26. Thus, the proposed model to predict the resilient modulus with other engineering properties can be expressed as follows:

$$M_R = (3048.96 - 23.12\,T - 148.36\,A_v - 280.39\,AC + 443.04\,N_{200}) \times (0.803 - 0.010\,T + 0.053\,A_v)^R \quad (4.6)$$

From the developed regression model, it is evident that M_R values of HMA mixes depends on the temperature, air voids, binder content and percentage passing No. 200 sieve. The sensitivity of each variable was checked with by increasing each variable by 20% with respect to the reference value shown in Table 4.21. It is evident that the temperature and percentage passing No. 200 sieve are more sensitive variables than the others. A decrease of 34% and an increase of 33% were obtained for the variables temperature and percentage passing No. 200 sieve, respectively.

Finally, the proposed model was used to estimate resilient modulus. The average resilient modulus was compared to the calculated values for all the mixes. The M_R values were plotted with the calculated M_R values shown in Figure 4.27. As a result, the predicted M_R can be correlated with the corresponding actual values with a straight line regression having a slope of approximately 0.98 (fairly close to 1.0) and an R-squared value of 0.84. It is an indication that such a model could be a good indicator in making performance predictions of M_R due to the variation of stress level, temperature, material properties and mix properties.

4.2.2. APA Rut Test

The APA rut test results for laboratory prepared and field cores are shown in Table 4.22. A total of 42 specimens were tested in this study and the reported APA rut values correspond to 8000 loading cycles. The APA rut values with number of loading cycles are graphically shown in Appendix C. From the test results for all three HMA base mixes it is evident that the Tar Creek base mix showed a high rut value of 4.9 mm (0.2 in) for specimens with an average air void of 7.0%. Comparatively, the OKC and the Davis base mixes exhibited lower rut values. The average rut value for specimens from the Davis mix was 2.7 mm (0.1 in) with a standard deviation of 0.4 mm (0.02 in). As for the OKC base mix, the average value was 2.4 mm (0.1 in) with a standard deviation of 0.05 mm (0.002 in). The average air voids for the Davis and the OKC specimens was approximately 7.0%. For all these base mixes, the rut values are less than the Oklahoma Department of Transportation (ODOT) design rut requirement (5 mm or 0.2 in). Only one surface mix (i.e., the Tar Creek surface mix) was tested in this study for APA rut. An average rut value of 7.6 mm (0.3 in) was obtained for the Tar Creek surface mix with an

average air void of 7.9%. From Table 4.22, one can see that the Tar Creek cores with an average air void 8.0% had a higher rut depth of 9.5 mm (0.4 in), followed by the OKC cores 5.6 mm (0.2 in) and then the Davis cores 3.1 mm (0.1 in). Consequently, one can conclude that the Tar Creek mixes are more susceptible to rutting potential than the OKC and the Davis mixes.

4.2.2.1. Effect of Binder Content on Rut Depth

The binder contents varied from one mix to another. Among the base mixes, the Tar Creek base mix had a 5.6%, which is higher than the binder content used for the Davis (4.5%) and the OKC (4.3%) HMA base mixes. Eliminating the affect of other properties such as air voids, specific gravity and percentage fines, one can conclude that a higher binder content produces a larger rut depth. This is also true for the Tar Creek surface mix with a binder content of 6.9%, which gives comparatively higher rut depths than the other mixes. This is consistent with Roberts et al. (1996) that a high binder content is expected to produce higher rut depth. It is due to the fact that an increase in binder content would increase the binder film thickness between particles and would decrease the internal friction of the aggregate. Thus, making the mix tender and more susceptible to rutting, because materials can flow laterally due to the loss of aggregate interlock (Roberts et al., 1996). Similar observations were also reported by Tarefder (2003), Tarefder and Zaman (2003) and Wasiuddin et al. (2005). Wasiuddin et al. (2006) reported in a study that a trial blend for a base mix with 70% chat material has high rut value due to the higher binder content used in the mix. This is consistent with the current study, the Tar Creek surface mix contained a higher chat percentage (80%) than the Tar Creek base mix (50%). The binder content used in the Tar Creek surface mix was higher than that in the

Tar Creek base mix. The increased binder content led to increased rut depths in the surface mix specimens. The reason for the higher binder content in the Tar Creek surface mix could be attributed to the higher amount of N_{200} in the mix requiring more to coat the aggregate. However, N_{200} is not the only factor, the overall gradation is also an effective factor for higher binder content in the Tar Creek surface mix. Specifically, although the N_{200} value for the Tar Creek surface mix and the Davis base mix are approximately same (6.0% and 5.9%, respectively), overall the Tar Creek surface mix is finer than the other three mixes, as can be seen from Figure A.1 in Appendix A.

4.2.2.2. Effect of Air Voids on Rut Depth

From the present study, effects of air voids on the rut depth could not be identified since the laboratory prepared specimens were compacted at average air voids approximately of 7±1 %, as recommended in the OHD L-43 test method. Due to limited scope of this study, no attempts were made to investigate the variation of rut depths with varying air voids. The air voids of the laboratory specimens varied between 6% to 8%. In a similar study by Tarefder (2003) and by Tarefder et al. (2003) reported that there is no significant effect on rut depth for the specimens air voids varying between 6% to 8%. But, the air voids of the Tar Creek cores varied between 6.9% to 9.6%. Therefore, if we compare the rut depth of the Tar Creek laboratory specimens with the Tar Creek filed cores, we can observe that the rut depths are reduced with decreasing air voids. This is due to the fact that specimens having smaller air voids create a more homogeneous binder-aggregate structure. Therefore, reduced air voids can lead to increased stiffness and reduced rut potential of HMA mixes.

4.2.2.3. Effect of Percentage Fines on Rut Depth

The variation of rut depth with percentage fines in mixes could not be clearly examined in this study. For example, the percentage fines (passing No. 200 sieve) for the Davis base mix and the Tar Creek surface mix are approximately the same (5.9% and 6.0%, respectively). However, the average rut depth of the Tar Creek surface mix specimens is higher (7.6 mm, i.e., 0.3 in) than the average rut depth of the Davis base mix specimens (2.7 mm, i.e., 0.1 in). Also, the Tar Creek base mix specimens with percentage passing No. 200 sieve of 4.9%, exhibited an average rut depth of 4.9 mm (0.2 in), which is higher than the Davis base mix specimens but lower than the Tar Creek surface mix specimens. This may be attributed to the variation of other mix properties in these mixes. Therefore, no clear conclusions could be drawn with respect to the effect of percentage fines on the rutting potential. A study by Teng (1998) reported that the increase in percentage fines reduces excess binder in the HMA mixes, consequently reduces the rut depth. Overall, the present study support this observation.

4.2.2.4. General Model to Predict Rutting Potential

Based on the aforementioned results, it was decided to develop a regression model correlating rutting potential with specific mix properties, namely, air voids, binder content and percentage fines. The stepwise method at a 0.15 level was used for this purpose. The following rut model was developed:

$$Log\ (Rut) = 0.676 + 0.179\ AC - 0.178\ N_{200} \qquad (4.7)$$

where:

Rut = rut depth, in mm,
AC = binder content, in %, and
N_{200} = aggregate passing No. 200 sieve, in %.

The ANOVA of this model yield an F value of 11.6 with a P_r of less than 0.0006 and an R-squared value of 0.56, which indicates that the model may be considered statistically significant in predicting the variation of rut depth with specific mix properties, namely binder content and percentage fines. From this model, it is clear that the increasing binder content increases the rut depth and an increase in percentage fines decreases the rut depth. This observation is consistent with the observation reported by Tarefder (2003), Tarefder and Zaman (2003) and Teng (1998). Binder content is the only common variable in the rut models reported by Tarefder (2003) and Tarefder and Zaman (2003) and the rut model developed here. The other properties, namely, air voids and specific gravity were not included in this model due to statistical insignificance in the model. Table 4.23 shows a summary of measured and predicted rut depths. A comparison between the predicted rut depths and the actual rut depths is illustrated in Figure 4.28.

4.2.3. Correlations between M_R and APA Rut

The average rut depths of the six specimens tested from each laboratory specimens and field cores were correlated with the M_R values at temperatures 5°C, 25°C and 40°C (i.e., 41°F, 77°F and 104°F). The average value of M_R at three stress levels (R = 0.20, 0.35 and 0.50) were used to develop a model correlating M_R and rut depth. A linear model similar to the one employed by Tarefder (2003) and Tarefder and Zaman (2003) was used. The models were developed using M_R values at different stress ratios and temperatures with the APA rut depths at different numbers of loading cycles, namely 2000 and 8000, as shown in Table 4.24. The linear models along with coefficient of determination (R-squared) are shown in the Table 4.25 and are graphically illustrated in Figures 4.29 through 4.34. From Table 4.25, comparatively a high R-squared value of

0.72 was obtained for rut at 2000 loading cycles and M_R at 40°C (104°F) and a stress ratio of 0.50. A low R-squared value of 0.54 was obtained for rut at 2000 loading cycles and M_R at 5°C (41°F) and a stress ratio of 0.20. The obtained R-squared values for different temperature and stress levels for M_R and different loading cycles for rut depth did not show a clear trend. This may be due to the testing parameters and mechanisms involved in these two types of testing. Rutting is expected to occur at high temperatures and with large number of load repetitions, whereas modulus should present stress-strain properties of HMA mixes at intermediate temperatures and lower loading cycles (Tarefder, 2003; Tarefder and Zaman, 2003). Also, rutting measures the consolidation and plastic flow characteristics of HMA mixes under repeated loading, whereas resilient modulus represents the elastic stress-strain behavior under cyclic loading. These differences in test parameter and different mechanisms result in different correlation coefficients. This is also evident from the study by Brown and Cross (1989), Tarefder (2003), Tarefder and Zaman (2003) and Bhasin et al. (2005).

Brown and Cross (1989) reported that there is no good relation (R-squared = 0.01) between HMA rutting and indirect tension resilient modulus. That study also noted that there is no reason to expect a good relationship to exist between these parameters since rutting is due to compressive stress and resilient modulus test measures tensile properties of the HMA mixes. Tarefder (2003) and Tarefder and Zaman (2003) conducted a study to correlate APA rut at 8000 loading cycles with the indirect tension resilient modulus at three temperatures (0°C, 23°C and 40°C). The highest R-squared value of 0.27 was obtained for the regression equation relating rutting and resilient modulus at 40°C. Overall, a poor correlation was obtained for each test temperature. The reason stated for

this poor correlation was the mechanistic differences (stress level, strain, temperature, loading cycles etc.) between modulus and rut tests. But, comparatively high R-squared values were obtained in the present study. This may be due to the stress levels used in the resilient modulus testing between these two studies. A stress level of 20 psi to 30 psi was used by Tarefder (2003) and Tarefder and Zaman (2003), while in the present study the stress level varied between 20 psi to 150 psi.

4.2.4. APA Fatigue Test

A total of 12 beam specimens (3 specimens from each HMA mix) were tested for APA fatigue. The results are summarized in Table 4.26. From the number of fatigue cycles shown in Table 4.26, it is evident that both the Tar Creek surface and base mixes show a high fatigue cycle of approximately 49,000. Comparatively, the Davis and the OKC mixes exhibited lower fatigue cycles of approximately 20,000 and 27,000, respectively. The results indicate that the Tar Creek specimens exhibited a greater fatigue resistance than the Davis and the OKC specimens. This can possibly be attributed to many factors such as air voids, aggregate type and binder content, among others.

Higher binder contents will result in a mix having a greater tendency to deform elastically (or at least deform) rather than fracturing under repeated load. The optimum binder content, as determined by mix design, should be high enough to prevent excessive fatigue cracking. The use of an asphalt binder with a lower stiffness will increase a mixture's fatigue life by providing greater flexibility (Roberts et al., 1996). However, the potential for rutting must also be considered in the selection of the asphalt binder amount. A study by Buchanan (2000) reported that increasing effective binder content is the most likely influential factor in greater fatigue resistance of a granite-HMA mix. In the present

study, a similar observation can be made for both the Tar creek base and surface mixes. The effective asphalt content used in these mixes was higher compared to the Davis and the OKC mixes. Therefore a greater fatigue resistance was observed for both the Tar Creek base and surface mixes. A study by Kun et al. (2006) reported that fatigue failure under repeated loading is due to a combination of several mechanisms, among which damage growth, relaxation due to viscoelasticity, and healing of micro cracks play an essential role. The increase in the binder content helps healing of micro cracks. This is also evident from the present study, the increase in binder content in the Tar Creek mixes increased the fatigue life. A separate study by Tangella et al. (1990) reported that the binder content has a significant effect on the fatigue life of HMA mixes. According to that study, the optimum binder content to obtain maximum fatigue life is generally higher than the design based on rutting considerations.

In the present study, it was decided to develop a statistical model to evaluate the effect of specific mix properties namely, air voids, binder content, specific gravity and percentage fines on the fatigue resistance of HMA mixes. A stepwise method was employed at a 0.15 level. The final model obtained from this effort is given below:

$$N_f = 826568 - 3371\,A_v - 279230\,G_{se} - 3234\,N_{200} \qquad (4.8)$$

where:

N_f = number of fatigue cycles,
A_v = air voids, in %,
G_{se} = specific gravity of aggregate, and
N_{200} = aggregate passing No. 200 sieve, in %.

The predicted model yields an R-squared value of 0.98 and an F value of 148.2 with a P_r less than 0.001, which indicates that the predicted model is considered statistically significant. The predicted and calculated fatigue cycles for each specimen tested are

shown in Table 4.27. Figure 4.35 shows the predicted fatigue cycles from the model against the calculated fatigue cycles. It can be seen from the model that increasing air voids, specific gravity of aggregate and aggregate passing No. 200 sieve reduce the number of fatigue cycles since these all variables have a negative coefficient in the model. Inadequate compaction results in increased air voids and subsequently reduced stiffness of HMA specimens (Hughes, 1989). Therefore, the higher the air voids the lower the number of fatigue cycles. This is also evident from the study by Harrigan et al. (2002). That study reported that a 1% increase in air voids will results in a 10% decrease in fatigue life. An increase in percentage fines reduces the effectiveness of the binder in the HMA mixes, therefore it reduces the fatigue life of HMA pavements. This is consistent with the study by Teng (1998). It was reported by Teng (1998) that at low dust to binder ratio values, additional fines act as an asphalt binder extender, and causes the fatigue performance to decline.

4.2.5. Permeability Test

The permeability test results for all mixes are summarized in Table 4.28. All the mixes exhibited the permeability values below the maximum design permeability of 125 x 10^{-5} cm/s (49 x 10^{-5} in/s), as recommended by ODOT. Among the different type of mixes, the Tar Creek surface mix and the OKC base mix showed higher permeability values. The average permeability value for the Tar Creek surface mix was 10.8 x 10^{-6} cm/s (4.3 x 10^{-6} in/s). This value is consistent with similar values reported by Wasiuddin et al. (2005). That study reported a permeability value of 12.0 x10^{-6} cm/s (4.7 x 10^{-6} in/s) for a similar type of HMA specimen. The OKC base mix showed an average permeability value of 14.8 x 10^{-6} cm/s (5.8 x 10^{-6} in/s), which is higher than the corresponding value of

the Tar Creek surface mix. Comparatively, the Tar Creek base and the Davis base mixes showed a lower permeability values of approximately 2.4×10^{-6} cm/s (0.9×10^{-6} in/s) and 3.0×10^{-6} cm/s (1.2×10^{-6} in/s), respectively. It is evident that the gradations of the mixes and the amount of interconnected and opened air voids are the key factors that affect the permeability. The gradation curves for all four HMA mixes are shown in Appendix A along with the mix design sheets. From the lower portion of the gradation curve (the portion representing percentage passing of the smaller particles with size less than 1 mm) the OKC mix is of coarser gradation, followed by the Tar Creek surface, the Davis and the Tar Creek base mixes. Therefore, the permeability values of the OKC base mix and the Tar Creek surface mix are greater than the Davis and the Tar Creek base mixes.

From the results, shown in Table 4.28, even a slight change in air voids, approximately 1% in the Tar Creek surface mix and the OKC base mix, changes the permeability values approximately by 50%. Therefore, it is evident that the air voids is one of the key factors affecting the permeability of HMA mixes. It is evident that the size of air voids increase, the potential for interconnected air voids also increases. This is also evident from the study by Mallick et al. (2003) that a slight change in air voids causes a major change in permeability. Mallick et al. (2003) also reported that mixes with larger NMAS mixes have more potential to be permeable. But, it depends on whether a gradation is fine or coarse graded for a given NMAS. The combination of larger NMAS and less fine aggregate to fill the air voids likely results in coarse graded mixes having more interconnected voids. This factor is consistent with the results obtained from the present study. The percentage fines in the Tar Creek surface mix and the OKC base mixes are comparatively lower than the Davis base mix and the Tar Creek base mix. This

leads to an increase in interconnected open air voids in the specimens and it eventually increases the permeability values.

A statistical model was developed to correlate the permeability with specific mix properties, namely air voids, binder content, specific gravity and percentage fines using the stepwise method. The developed model is shown below:

$$k_{Pred} = 8.10 + 5.48\,A_v - 7.15\,N_{200} \qquad (4.9)$$

where:

k_{pred} = permeability, in 10^{-6} cm/s,
A_v = air voids, in %, and
N_{200} = aggregate passing No. 200 sieve, in %.

As expected, the air voids and percentage passing No. 200 sieve are well correlated with the permeability with an R-squared value of 0.96. From the developed model, it is clear that an increase in air voids increase the permeability, as expected. Also, lesser the amount of N_{200} particles in the mix, higher the permeability. This is consistent with the factors discussed previously. The ANOVA of this statistical model yields an F value of 55.3 with a P_r less than 0.0004, which indicates that the model is considered statistically significant in predicting the variation of permeability with mix properties, namely air voids and percentage fines. Table 4.29 shows a comparison between the predicted and calculated permeability values. Also, a comparison between the predicted and obtained permeability is illustrated in Figure 4.36. From this figure, it is evident that the values are close to the 45° line, which indicates that such a model could be a good indicator in making performance prediction of laboratory permeability due to the aforementioned specific mix properties.

4.2.6. Laboratory Seismic Modulus Test

Nineteen field cores from the Davis site were tested for laboratory seismic modulus test. A total of three hits were performed on each specimen resulting in 57 modulus values. Figure 4.37 shows the Fast Fourier Transform (FFT) generated transfer function for a selective hit on Core #1. The graph shows two clearly visible peaks. The first peak corresponds to shear resonance frequency, while the second peak corresponds to the longitudinal resonance frequency. These peaks were identified in accordance with the procedure described by Nazarian et al. (2003). The resonant frequency corresponding to the second peak was used for the calculation of seismic modulus (E_S), using Equation 3.8. A summary of the frequency and the seismic modulus values obtained from three hits on each specimen is presented in Table 4.30 and graphically illustrated in Figure 4.38. Statistical analysis was performed to identify possible outliers using the box plot and whiskers method (McClave et al., 2001). Eight values out of 57 were identified as outliers, as shown in Figures 4.38 and 4.39. The outliers were removed from the final results. Figure 4.39 shows the final plot of average seismic modulus for each core. The seismic modulus values varied between 41,368 MPa (6,000 ksi) and 68,947 MPa (10,000 ksi) with an average value of 58,336 MPa (8,461 ksi) and a standard deviation of 7,177 MPa (1,041 ksi). This gives a coefficient of variance (CV) of 12%. Nazarian et al. (2002) noted that the seismic modulus is more sensitive to the aggregate skeleton and to the grain-to-grain contact between aggregates. Even for a same type of mix, the seismic modulus is dependent on how the aggregates particles and air voids are distributed inside the specimen.

Only the Davis cores were tested for laboratory seismic modulus because of limited scope of this study, since the specimen dimensions are restricted for this type of tests. Bai

et al. (2004) reported that typically a height/diameter (H/D) ratio of 2 or greater is recommended for this test. In order to obtain a H/D ratio of 2 for a 100 mm (4 in) specimen, the HMA thickness should be at least 200 mm (8 in). But, the HMA lift thicknesses for the Tar Creek and the OKC sites are approximately 100 mm (4 in). To this end, there are no results available to compare the seismic modulus for different HMA mixes.

4.2.7. Relative Comparison between M_R and E_S

Six out of the nineteen Davis cores were tested for both seismic modulus and the laboratory M_R. In order to compare the seismic modulus and M_R, the M_R values at room temperature approximately 25°C or 77°F and different stress ratios (R = 0.20, 0.35 and 0.50) were used. A summary of the seismic modulus and the corresponding M_R is presented in Table 4.31. An average seismic modulus value of 61,537 MPa (8925 ksi) with a standard deviation of 5688 MPa (825 ksi) and a coefficient of variance of 9% was obtained for the six selected cores. The E_S values are 6 to 8 times higher than the M_R values at a stress ratio of 0.20, 7 to 9 times higher than the M_R at a stress ratio of 0.35 and 9 to 10 higher than the M_R at a stress ratio of 0.50. No studies, to the author's knowledge, have addressed the difference between the seismic modulus and the laboratory M_R for HMA materials. A study by Nazarian et al. (2003) reported that the seismic modulus of sub-grade materials is approximately 10 times higher than that of laboratory triaxial resilient modulus. The difference between the laboratory M_R and E_S could be attributed to the fact that strain level and strain rate involved in these two tests are different. The seismic modulus is a low strain modulus, measured at a high strain rate, whereas, resilient modulus is comparatively a larger strain modulus (Nazarian et al., 2003).

4.3. Field Non-Destructive Tests

The results of non-destructive field tests namely, Falling Weight Deflectometer (FWD), Spectral Analysis of Surface Waves (SASW) and Ground Penetrating Radar (GPR) are presented and discussed in the following sections.

4.3.1. Falling Weight Deflectometer Test

FWD tests were performed at selected sections in the Davis and the OKC sites and all sections of the Tar Creek site. A commercially available software, *Modulus 5.0*, developed by Liu et al. (2000), was used to determine the back-calculated modulus of HMA layers. The overall FWD back-calculated moduli for the Tar Creek sites are presented in Table 4.32 and graphically illustrated in Figure 4.41 along with the pavement sections. The modulus values vary between 689 MPa (100 ksi) and 2,413 MPa (350 ksi) with an average value of 1,400 MPa (203 ksi) and a standard deviation (SD) of 490 MPa (71 ksi). From Table 4.32, it can be observed that the modulus obtained from FWD data (E_{FWD}) for section TS-1 was approximately 1,751 MPa (254 ksi) (with a SD of approximately 283 MPa i.e., 41 ksi), 1,255 MPa (182 ksi) for section TS-2 (with a SD of approximately 310 MPa i.e., 45 ksi), 841 MPa (122 ksi) for section TS-3 (with a SD of approximately 186 MPa i.e., 27 ksi) and 1,668 MPa (242 ksi) for section TS-4 (with a SD of approximately 538 MPa i.e., 78 ksi).

Table 4.33 presents the E_{FWD} results for the Davis site. The results are also plotted along with the pavement length in Figure 4.42. The values are varying between approximately 2,758 MPa to 4,481 MPa (400 ksi to 650 ksi) with an average value of 3,378 MPa (490 ksi) and a SD of 62 MPa (9 ksi).

The FWD test results for the OKC site is presented in the Table 4.34. Figure 4.43 shows the variation of modulus along the pavement length. The values vary between 552 MPa (80 ksi) and 6,895 MPa (1000 ksi). Inconsistently high values were obtained in three locations at 42.4 m (139 ft), 100.6 m (330 ft) and 122.8 m (403 ft) from the south end. This was possibly due to the surface irregularities and debris at the site due to the construction work. Therefore, these three values were removed. The resulting average was of 3,875 MPa (562 ksi), with a SD of 1,889 MPa (274 ksi).

From the aformentioned results, it is evident that the Tar Creek site show comparatively lower FWD back-calculated modulus than the Davis and the OKC sites. This is consistent with the laboratory indirect tension test. As a result, one can conclude that the Davis mix is expected to perform better than the OKC, followed by the Tar Creek mixes.

4.3.2. Relative Comparison between M_R and E_{FWD}

Field cores were retrieved from locations where FWD tests were performed. Resilient modulus tests were conducted on these cores. Since M_R tests were performed at different stress levels and at different temperatures, it was decided to calculate the M_R values at three stress ratios (0.20, 0.35 and 0.50) from the developed semi-log model by using the model parameters corresponding to the FWD test temperature. The results are summarized in Tables 4.35 through 4.37 for the Davis, the Tar Creek and the OKC sites, respectively. From Table 4.35, the results for the Davis site compare well. The ratio of laboratory M_R at R=0.2 to FWD modulus at a load of 40 kN (9 kip) is approximately one (0.92 to 1.09) with an R-squared value of 0.67, as shown in Figure 4.44. This is consistent with the observation by Hossain et al. (1992) who reported that the average

ratio of laboratory moduli to back-calculated moduli varied between 1.10 and 1.22. The Tar Creek and the OKC sites results, on the other hand, show a scattered behavior. Various factors could lead to such behavior including pavement thickness. The HMA thicknesses for both the Tar Creek and the OKC sites are 100 mm (4 in), while the HMA thickness for the Davis site is 267 mm (10.5 in). It is evident from the study by Teredesai (2005) that a thickness less than 150 mm (6 in) may produce unreliable back-calculated modulus.

4.3.3. Spectral Analysis of Surface Waves (SASW) test

SASW tests were only performed at three selected locations at the Tar Creek site. A summary of the test results is presented in Table 4.38. Results showed that the HMA base layer modulus is higher than the surface layer modulus. This is consistent with the indirect tension M_R test results which show higher modulus values for the base mix. From Table 4.38, it can be observed that the section TS-2 showed a comparatively high E_{SASW} value, approximately 8,618 MPa (1,250 ksi) for the surface mix and 9,308 MPa (1,350 ksi) for the base mix. While section TS-1 and TS-4 showed approximately same SASW modulus, 4,895 MPa (710 ksi) and 4,275 MPa (620 ksi) for the surface mix and 6,412 MPa (930 ksi) and 5,309 MPa (770 ksi) for the base mix, respectively.

A comparison of both FWD and SASW field moduli are presented in Table 4.39. The results show that E_{SASW} is approximately 4 times higher at section TS-4 and 6 times higher at section TS-2 than the E_{FWD}. This is consistent with the study by Nazarian et al. (1988) who reported that the moduli of HMA layer obtained from FWD data exhibit, in general, greater variation than those of SASW test data. Nazarian et al. (1988) also reported that the difference is due to the lack of sensitivity of the FWD test method to the

stiffness of the top thin layer, while the SASW method is quite sensitive in this region. Further, Nazarian et al (1988) reported that the strain level is an important factor in this variation of test results. Moduli from SASW tests are low-strain moduli. On the other hand, moduli back-calculated from FWD deflection basins may contain manifestations of nonlinear behavior induced by the heavy loads imparted to the pavement surface.

4.3.4. Ground Penetrating Radar (GPR) test

Ground Penetrating Radar (GPR) test was performed in the Tar Creek site. This test was performed only to determine the thickness profile of the pavement. The results obtained from both the south and the north lanes are shown graphically in Figure 4.45 and Figure 4.46, respectively. The layer thicknesses calculated from the GPR data depend on the dielectric constant of the medium. For relatively similar mixes, the GPR data does not differentiate the HMA surface and base layers (Roddis et al., 1992). At the Tar Creek site, relatively similar HMA mixes were used for the surface and base course. Therefore, the results shown in these figures represent the combined HMA layer thickness. The thickness profile of the south lane varies between 100 mm (4 in) to 150 mm (6 in), while that of the north lane varies between 100 mm (4 in) to 140 mm (5.5 in). By combining both south and north lanes, the average thicknesses of HMA layers were found to be 11.8 mm (4.7 in), 147.3 mm (5.8 in), 124.5 mm (4.9 in) and 119.4 mm (4.7 in) for sections TS-1, TS-2, TS-3 and TS-4, respectively. The design thickness for section TS-3 was 125 mm (5.0 in), while for the remaining sections (TS-1, TS-2 and TS-4) the design thickness was 100 mm (4 in). From these results, it can be concluded that the thicknesses of the HMA layer obtained from the GPR data were fairly consistent and comparable to the

respective design thicknesses. Only section TS-2 showed a high variation. This may be due to the inconsistencies of thickness profile during construction.

The HMA thickness profile of the Tar Creek site was also obtained from the SASW analysis. The results are included in Table 4.38. From the thicknesses reported in this table, other than the HMA base thickness of section TS-2, the thickness values of each layer in sections TS-2, TS-4 and TS-1 compared favorably with the SASW results.

Table 4.1: Measured M_R for Tar Creek Base Mix Laboratory Specimens

Mix/Core Type	Specimen ID	Temp (°F)	Stress Ratio	Measured M_R (ksi)
Tar Creek Base Mix	TC-B-MR-9	41	0.21	1506
			0.28	1520
			0.36	1432
			0.41	1364
	TC-B-MR-10	41	0.19	1584
			0.26	1611
			0.32	1614
			0.38	1531
			0.42	1488
	TC-B-MR-11	41	0.19	1523
			0.25	1516
			0.32	1483
			0.38	1418
			0.42	1375
	TC-B-MR-6	77	0.21	560
			0.27	514
			0.35	445
	TC-B-MR-7	77	0.21	781
			0.28	690
			0.35	598
	TC-B-MR-8	77	0.21	924
			0.28	874
			0.35	740
	TC-B-MR-13	104	0.25	145
			0.33	142
			0.41	143
			0.49	130
			0.57	108
	TC-B-MR-14	104	0.28	187
			0.38	195
			0.47	174
			0.57	142
	TC-B-MR-15	104	0.20	239
			0.26	230
			0.33	243
			0.39	229
			0.45	186

Table 4.2: Measured M_R for Tar Creek Surface Mix Laboratory Specimens

Mix/Core Type	Specimen ID	Temp (°F)	Stress Ratio	Measured M_R (ksi)
Tar Creek Surface Mix	TC-S-MR-4	41	0.21	1232
			0.28	1225
			0.36	1252
			0.42	1181
	TC-S-MR-5	41	0.20	1302
			0.27	1309
			0.35	1301
			0.41	1207
	TC-S-MR-6	41	0.21	1438
			0.28	1385
			0.36	1423
			0.42	1340
			0.46	1310
	TC-S-MR-1	77	0.23	586
			0.30	569
			0.37	536
			0.45	498
			0.52	453
	TC-S-MR-2	77	0.22	552
			0.29	546
			0.36	522
			0.43	487
			0.50	423
	TC-S-MR-3	77	0.21	477
			0.28	449
			0.35	411
			0.42	381
			0.49	335
	TC-S-MR-7	104	0.23	158
			0.31	146
			0.39	128
			0.46	100
	TC-S-MR-8	104	0.24	170
			0.32	168
			0.39	158
			0.47	136
			0.55	119
	TC-S-MR-9	104	0.23	162
			0.30	162
			0.38	147
			0.45	124
			0.53	102

Table 4.3: Measured M_R for Tar Creek Cores

Mix/Core Type	Specimen ID	Temp (°F)	Stress Ratio	Measured M_R (ksi)
Tar Creek Cores	TC-C-MR-3	41	0.21	1465
			0.29	1403
			0.36	1354
			0.44	1346
			0.50	1464
	TC-C-MR-4	41	0.30	994
			0.40	967
			0.51	902
			0.62	897
	TC-C-MR-1	77	0.23	733
			0.30	679
			0.38	642
			0.45	567
			0.53	439
	TC-C-MR-2	77	0.26	733
			0.34	716
			0.43	694
			0.51	612
			0.60	450
	TC-C-MR-5	104	0.31	156
			0.41	144
			0.51	128
			0.61	99
	TC-C-MR-6	104	0.24	177
			0.33	174
			0.41	159
			0.49	138
			0.57	109

Table 4.4: Measured M_R for Davis Base Mix Laboratory Specimens

Mix/Core Type	Specimen ID	Temp (°F)	Stress Ratio	Measured M_R (ksi)
Davis Base Mix	D-MR-9	41	0.19	3322
			0.26	3093
			0.33	3057
			0.39	2928
			0.43	2828
	D-MR-12	41	0.19	1987
			0.25	1931
			0.32	1863
			0.38	1797
			0.42	1708
	D-MR-14	41	0.20	3253
			0.27	3080
			0.34	3023
			0.41	2896
			0.45	2868
	D-MR-6	77	0.30	1332
			0.41	1290
			0.51	1205
			0.61	1110
			0.71	923
	D-MR-8	77	0.49	1386
			0.65	1186
	D-MR-T2	77	0.30	1029
			0.41	943
			0.52	854
			0.61	692
			0.71	311
	D-MR-15	104	0.25	319
			0.33	283
			0.42	234
			0.50	163
	D-MR-16	104	0.21	530
			0.28	463
			0.36	424
			0.43	350
			0.50	213
	D-MR-17	104	0.20	444
			0.27	403
			0.34	385
			0.41	371
			0.47	304

Table 4.5: Measured M_R for Davis Cores

Mix/Core Type	Specimen ID	Temp (°F)	Stress Ratio	Measured M_R (ksi)
Davis Cores	D-C-MR-3	41	0.23	1604
			0.31	1636
			0.39	1557
			0.47	1538
			0.52	1458
	D-C-MR-4	41	0.29	1801
			0.38	1842
			0.48	1900
			0.59	2020
	D-C-MR-1	77	0.21	1026
			0.28	971
			0.35	901
			0.43	810
			0.50	661
	D-C-MR-2	77	0.22	653
			0.29	633
			0.36	603
			0.44	564
			0.51	525
	D-C-MR-5	104	0.20	257
			0.27	248
			0.34	235
			0.40	216
			0.47	190
	D-C-MR-6	104	0.18	281
			0.24	262
			0.30	250
			0.35	234
			0.41	203

Table 4.6: Measured M_R for OKC Base Mix Laboratory Specimens

Mix/Core Type	Specimen ID	Temp (°F)	Stress Ratio	Measured M_R (ksi)
OKC Base Mix	OKC-MR-5	41	0.24	1718
			0.32	1697
			0.40	1639
			0.47	1781
			0.52	1768
	OKC-MR-6	41	0.25	1577
			0.33	1572
			0.42	1602
			0.49	1752
			0.54	1820
	OKC-MR-1	77	0.20	914
			0.27	869
			0.34	767
			0.40	696
			0.47	554
	OKC-MR-2	77	0.19	777
			0.25	705
			0.31	654
			0.37	570
			0.44	471
	OKC-MR-3	77	0.21	792
			0.28	763
			0.35	690
			0.42	570
			0.49	406
	OKC-MR-7	104	0.27	269
			0.36	201
			0.44	110
	OKC-MR-8	104	0.16	309
			0.21	289
			0.26	276
			0.32	249
			0.37	218
	OKC-MR-9	104	0.12	628
			0.17	565
			0.21	462
			0.25	402
			0.29	356

Table 4.7: Measured M_R for OKC Cores

Mix/Core Type	Specimen ID	Temp (°F)	Stress Ratio	Measured M_R (ksi)
OKC Cores	OKC-C-MR-3	41	0.22	1532.1
			0.29	1476.2
			0.36	1421.9
			0.43	1389.4
	OKC-C-MR-4	41	0.28	2729.2
			0.37	2672.6
			0.47	2606.1
	OKC-C-MR-1	77	0.25	616.2
			0.34	582.2
			0.42	495.5
			0.50	393.4
	OKC-C-MR-2	77	0.25	533.5
			0.34	489.4
			0.43	470.4
			0.51	449.8
	OKC-C-MR-5	104	0.32	127.8
			0.43	99.1
			0.53	55.4
	OKC-C-MR-6	104	0.39	123.0
			0.52	97.0
			0.64	60.6

Table 4.8: Linear Model Parameters for Tar Creek Specimens ($M_R = A + BR$)

Mix/Core Type	Sample ID	Temp (°F)	A	B	R-squared
Tar Creek Base Mix	TC-B-MR-9	41	1694.0	-754.0	0.81
	TC-B-MR-10		1701.6	-433.9	0.54
	TC-B-MR-11		1669.9	-663.9	0.90
	TC-B-MR-6	77	732.1	-818.8	0.99
	TC-B-MR-7		1051.8	-1313.8	1.00
	TC-B-MR-8		1209.5	-1318.0	0.94
	TC-B-MR-13	104	177.8	-107.9	0.77
	TC-B-MR-14		254.4	-166.2	0.74
	TC-B-MR-15		279.7	-167.7	0.55
Tar Creek Surface Mix	TC-S-MR-4	41	1276.1	-166.9	0.26
	TC-S-MR-5		1407.4	-414.1	0.58
	TC-S-MR-6		1533.9	-446.7	0.71
	TC-S-MR-1	77	697.9	-452.3	0.98
	TC-S-MR-2		663.9	-441.0	0.90
	TC-S-MR-3		587.9	-504.3	0.99
	TC-S-MR-7	104	218.6	-246.5	0.96
	TC-S-MR-8		217.9	-171.9	0.92
	TC-S-MR-9		217.6	-208.4	0.92
Tar Creek Cores	TC-C-MR-3	41	1436.2	-83.1	0.03
	TC-C-MR-4		1093.7	-334.6	0.91
	TC-C-MR-1	77	962.6	-928.2	0.94
	TC-C-MR-2		977.2	-786.5	0.83
	TC-C-MR-5	104	215.4	-182.3	0.96
	TC-C-MR-6		237.5	-211.2	0.92

Table 4.9: Linear Model Parameters for Davis Specimens ($M_R = A + BR$)

Mix/Core Type	Sample ID	Temp (°F)	A	B	R-squared
Davis Base Mix	D-MR-9	41	3651.9	-1896.0	0.95
	D-MR-12		2212.9	-1139.5	0.98
	D-MR-14		3532.5	-1521.4	0.97
	D-MR-6	77	1667.0	-969.8	0.93
	D-MR-8		2014.0	-1269.6	1.00
	D-MR-T2		1604.3	-1642.6	0.87
	D-MR-15	104	484.9	-625.2	0.98
	D-MR-16		766.7	-1040.5	0.95
	D-MR-17		535.0	-453.2	0.92
Davis Cores	D-C-MR-3	41	1756.3	-514.7	0.79
	D-C-MR-4		1573.9	729.0	0.95
	D-C-MR-1	77	1317.9	-1249.4	0.96
	D-C-MR-2		757.7	-446.9	0.99
	D-C-MR-5	104	311.9	-247.2	0.96
	D-C-MR-6		338.3	-313.2	0.97

Table 4. 10: Linear Model Parameters for OKC Specimens ($M_R = A + BR$)

Mix/Core Type	Sample ID	Temp (°F)	A	B	R-squared
OKC Base Mix	OKC-MR-5	41	1629.3	234.6	0.22
	OKC-MR-6		1313.2	872.2	0.80
	OKC-MR-1	77	1206.7	-1324.4	0.97
	OKC-MR-2		1009.8	-1204.1	0.99
	OKC-MR-3		1128.8	-1389.1	0.93
	OKC-MR-7	104	515.3	-905.5	0.99
	OKC-MR-8		379.2	-420.9	0.98
	OKC-MR-9		835.2	-1689.8	0.98
OKC Cores	OKC-C-MR-3	41	1664.2	-645.4	0.99
	OKC-C-MR-4		2913.8	-653.1	1.00
	OKC-C-MR-1	77	861.8	-898.5	0.96
	OKC-C-MR-2		607.6	-318.1	0.96
	OKC-C-MR-5	104	241.4	-343.3	0.98
	OKC-C-MR-6		220.1	-245.9	0.99

Table 4.11: Semi-Log Model Parameters for Tar Creek Specimens ($M_R = A\ B^R$)

Mix/Core Type	Sample ID	Temp (°F)	A	B	R-squared
Tar Creek Base Mix	TC-B-MR-9	5	1715.6	0.59	0.81
	TC-B-MR-10		1708.8	0.76	0.55
	TC-B-MR-11		1685.4	0.63	0.89
	TC-B-MR-6	25	791.4	0.19	0.98
	TC-B-MR-7		1163.1	0.15	1.00
	TC-B-MR-8		1306.0	0.20	0.92
	TC-B-MR-13	40	188.0	0.43	0.75
	TC-B-MR-14		265.4	0.37	0.74
	TC-B-MR-15		290.0	0.45	0.55
Tar Creek Surface Mix	TC-S-MR-4	5	1278.1	0.87	0.26
	TC-S-MR-5		1415.9	0.72	0.58
	TC-S-MR-6		1542.8	0.72	0.71
	TC-S-MR-1	25	729.0	0.42	0.97
	TC-S-MR-2		695.2	0.41	0.88
	TC-S-MR-3		631.9	0.29	0.98
	TC-S-MR-7	40	256.1	0.15	0.94
	TC-S-MR-8		237.5	0.31	0.91
	TC-S-MR-9		247.9	0.21	0.90
Tar Creek Cores	TC-C-MR-3	5	1436.2	0.94	0.03
	TC-C-MR-4		1105.5	0.70	0.91
	TC-C-MR-1	25	1102.6	0.20	0.91
	TC-C-MR-2		1114.4	0.26	0.79
	TC-C-MR-5	40	252.1	0.24	0.93
	TC-C-MR-6		272.2	0.23	0.89

Table 4.12: Semi-Log Model Parameters for Davis Specimens ($M_R = A\ B^R$)

Mix/Core Type	Sample ID	Temp (°F)	A	B	R-squared
Davis Base Mix	D-MR-9	5	3706.3	0.54	0.96
	D-MR-12		2247.7	0.54	0.97
	D-MR-14		3569.7	0.61	0.97
	D-MR-6	25	1801.3	0.42	0.90
	D-MR-8		2260.9	0.37	1.00
	D-MR-T2		2698.9	0.07	0.76
	D-MR-15	40	657.6	0.07	0.94
	D-MR-16		1073.8	0.05	0.88
	D-MR-17		572.3	0.30	0.89
Davis Cores	D-C-MR-3	5	1769.9	0.72	0.79
	D-C-MR-4		1599.8	1.47	0.96
	D-C-MR-1	25	1466.0	0.23	0.94
	D-C-MR-2		782.0	0.47	0.98
	D-C-MR-5	40	330.0	0.33	0.94
	D-C-MR-6		358.6	0.27	0.95

Table 4.13: Semi-Log Model Parameters for OKC Specimens ($M_R = A\ B^R$)

Mix/Core Type	Sample ID	Temp (°F)	A	B	R-squared
OKC Base Mix	OKC-MR-5	5	1632.2	1.14	0.21
	OKC-MR-6		1348.7	1.68	0.80
	OKC-MR-1	25	1380.6	0.16	0.95
	OKC-MR-2		1150.6	0.14	0.97
	OKC-MR-3		1419.4	0.10	0.88
	OKC-MR-7	40	1106.2	0.01	0.96
	OKC-MR-8		406.5	0.20	0.96
	OKC-MR-9		985.1	0.03	0.99
OKC Cores	OKC-C-MR-3	5	1681.1	0.64	0.99
	OKC-C-MR-4		2925.1	0.78	1.00
	OKC-C-MR-1	25	1013.7	0.17	0.94
	OKC-C-MR-2		621.7	0.52	0.97
	OKC-C-MR-5	40	484.8	0.02	0.94
	OKC-C-MR-6		376.5	0.06	0.95

Table 4.14: Log-Log Model Parameters for Tar Creek Specimens ($M_R = AR^B$)

Mix/Core Type	Sample ID	Temp (°F)	A	B	R-squared
Tar Creek Base Mix	TC-B-MR-9	41	1219.9	-0.15	0.73
	TC-B-MR-10		1433.2	-0.07	0.44
	TC-B-MR-11		1255.9	-0.13	0.81
	TC-B-MR-6	77	285.2	-0.43	0.96
	TC-B-MR-7		350.1	-0.51	0.99
	TC-B-MR-8		487.4	-0.42	0.88
	TC-B-MR-13	104	99.9	-0.30	0.65
	TC-B-MR-14		123.6	-0.38	0.65
	TC-B-MR-15		173.5	-0.22	0.45
Tar Creek Surface Mix	TC-S-MR-4	41	1169.4	-0.04	0.21
	TC-S-MR-5		1148.5	-0.09	0.49
	TC-S-MR-6		1234.5	-0.10	0.66
	TC-S-MR-1	77	387.3	-0.30	0.91
	TC-S-MR-2		369.7	-0.29	0.79
	TC-S-MR-3		262.0	-0.41	0.94
	TC-S-MR-7	104	66.6	-0.62	0.88
	TC-S-MR-8		98.9	-0.42	0.82
	TC-S-MR-9		79.7	-0.53	0.81
Tar Creek Cores	TC-C-MR-3	41	1365.3	-0.03	0.08
	TC-C-MR-4		825.5	-0.16	0.92
	TC-C-MR-1	77	345.5	-0.55	0.83
	TC-C-MR-2		403.3	-0.50	0.69
	TC-C-MR-5	104	78.9	-0.62	0.87
	TC-C-MR-6		89.6	-0.54	0.81

Table 4.15: Log-Log Model Parameters for Davis Specimens ($M_R = AR^B$)

Mix/Core Type	Sample ID	Temp (°F)	A	B	R-squared
Davis Base Mix	D-MR-9	41	2448.0	-0.18	0.96
	D-MR-12		1501.7	-0.18	0.93
	D-MR-14		2530.5	-0.16	0.98
	D-MR-6	77	876.6	-0.39	0.82
	D-MR-8		932.0	-0.56	1.00
	D-MR-T2		306.0	-1.17	0.67
	D-MR-15	104	94.5	-0.93	0.88
	D-MR-16		137.8	0.94	0.80
	D-MR-17		247.5	-0.38	0.84
Davis Cores	D-C-MR-3	41	1392.4	-0.11	0.70
	D-C-MR-4		2162.8	0.16	0.90
	D-C-MR-1	77	513.2	-0.48	0.87
	D-C-MR-2		453.9	-0.25	0.93
	D-C-MR-5	104	155.3	-0.34	0.87
	D-C-MR-6		156.9	-0.35	0.90

Table 4.16: Log-Log Model Parameters for OKC Specimens ($M_R = AR^B$)

Mix/Core Type	Sample ID	Temp (°F)	A	B	R-squared
OKC Base Mix	OKC-MR-5	41	1790.9	0.04	0.15
	OKC-MR-6		1975.3	0.18	0.72
	OKC-MR-1	77	397.6	-0.56	0.88
	OKC-MR-2		317.7	-0.56	0.91
	OKC-MR-3		280.1	-0.73	0.80
	OKC-MR-7	104	29.0	-1.74	0.93
	OKC-MR-8		156.3	-0.39	0.90
	OKC-MR-9		156.1	-0.69	0.98
OKC Cores	OKC-C-MR-3	41	1219.1	-0.15	0.99
	OKC-C-MR-4		2440.5	-0.09	0.99
	OKC-C-MR-1	77	273.0	-0.63	0.88
	OKC-C-MR-2		381.5	-0.24	0.99
	OKC-C-MR-5	104	21.9	-1.62	0.90
	OKC-C-MR-6		35.1	-1.37	0.93

Table 4.17: Average M_R for the Stress Ratios 0.20, 0.35 and 0.50

Mix/Core Type	Temp (°F)	M_R								
		R = 0.20			R = 0.35			R = 0.50		
		Average (ksi)	Stdev (ksi)	CV (%)	Average (ksi)	Stdev (ksi)	CV (%)	Average (ksi)	Stdev (ksi)	CV (%)
TCB	41	1827	11	0.6	1731	8	0.5	1640	6	0.4
	77	869	11	1.3	745	7	1.0	639	5	0.7
	104	218	16	7.4	160	10	6.1	117	6	4.9
TCS	41	1610	0	0.0	1540	0	0.0	1474	0	0.0
	77	372	19	5.1	340	17	4.9	310	14	4.6
	104	81	26	32.0	61	19	31.0	46	14	30.0
DB	41	2342	81	3.5	2235	58	2.6	2132	37	1.7
	77	1423	48	3.4	1203	20	1.7	1017	2	0.2
	104	627	34	5.4	460	8	1.7	338	9	2.7
OKCB	41	1748	42	2.4	1691	35	2.1	1635	28	1.7
	77	1057	45	4.2	890	26	3.0	750	13	1.7
	104	295	63	21.2	218	37	17.0	161	21	12.9
TCC	41	1311	157	12.0	1294	142	11.0	1277	127	9.9
	77	709	15	2.2	627	12	1.9	555	9	1.7
	104	51	23	44.1	41	18	43.5	33	14	42.8
DC	41	1961	104	5.3	1932	88	4.6	1904	73	3.8
	77	1218	35	2.9	1082	24	2.2	961	16	1.6
	104	656	4	0.6	437	14	3.1	291	16	5.6
OKCC	41	2007	22	1.1	1894	17	0.9	1787	11	0.6
	77	844	37	4.4	746	28	3.8	659	21	3.1
	104	376	7	1.9	225	12	5.3	134	12	8.8

Table 4.18: Materials and Mix Properties

Project Site Site	Mix Type Type	Aggregate					Binder		
		Type	Max. Size (in)	G_{se}	L.A. Abrasion	N_{200} (%)	Type	Content (%)	G_b
Tar Creek	Surface Mix (S5)	Lime Stone with 80% Chat	1/2	2.61	22	6.0	PG 64-22 OK	6.9	1.01
Tar Creek	Base Mix (S3)	Lime Stone with 50% Chat	1	2.60	28	4.9	PG 64-22 OK	5.6	1.02
Davis	Base Mix (S2)	Lime Stone	3/4	2.70	22	5.9	PG 64-22 OK	4.5	1.01
OKC	Base Mix (S2)	Lime Stone	1	2.71	16	4.7	PG 64-22 OK	4.3	1.01

Table 4.19: Percentage Difference in M_R Values of Field Cores with Respect to Laboratory Specimens

Mix Type	Temp (°F)	M_R Difference with respect to Laboratory Specimen (%)		
		R = 0.20	R = 0.35	R = 0.50
Davis	41	16	14	11
	77	14	10	6
	104	-5	5	14
OKC	41	-15	-12	-9
	77	20	16	12
	104	-28	-3	17
Tar Creek	41	28	25	22
	77	18	16	13
	104	76	74	72

Table 4.20: Measured and Predicted Model Parameters

Mix Type	Specimen ID	Temp (°F)	A_v (%)	$A_{Measured}$	$B_{Measured}$	$A_{Pred.}$	$B_{Pred.}$
Tar Creek Base Mix	TC-B-MR-9	41	5.9	1716	0.59	1949	0.70
	TC-B-MR-10	41	5.8	1709	0.76	1964	0.70
	TC-B-MR-11	41	5.7	1685	0.63	1979	0.69
	TC-B-MR-6	77	6.3	791	0.19	1058	0.36
	TC-B-MR-7	77	6.1	1163	0.15	1087	0.35
	TC-B-MR-8	77	6.3	1306	0.20	1058	0.36
	TC-B-MR-13	104	7.2	188	0.43	300	0.14
	TC-B-MR-14	104	6.8	265	0.37	359	0.12
	TC-B-MR-15	104	7.0	290	0.45	329	0.13
Tar Creek Surface Mix	TC-S-MR-4	41	6.7	1278	0.87	1708	0.74
	TC-S-MR-5	41	6.7	1416	0.72	1708	0.74
	TC-S-MR-6	41	6.7	1543	0.72	1708	0.74
	TC-S-MR-1	77	9.8	729	0.42	415	0.55
	TC-S-MR-2	77	9.6	695	0.41	445	0.54
	TC-S-MR-3	77	9.9	632	0.29	401	0.55
	TC-S-MR-7	104	7.9	257	0.15	73	0.18
	TC-S-MR-8	104	7.4	238	0.31	147	0.15
	TC-S-MR-9	104	7.5	248	0.21	132	0.15
Davis Base Mix	D-MR-9	41	5.6	3706	0.54	2622	0.69
	D-MR-12	41	7.1	2247	0.54	2400	0.77
	D-MR-14	41	6.7	3570	0.61	2459	0.74
	D-MR-6	77	5.9	1801	0.42	1746	0.34
	D-MR-8	77	4.9	2261	0.37	1894	0.29
	D-MR-T2	77	6.2	2699	0.07	1701	0.36
	D-MR-15	104	7.8	658	0.07	839	0.17
	D-MR-16	104	6.9	1074	0.05	973	0.12
	D-MR-17	104	6.5	572	0.30	1032	0.10
OKC Base Mix	OKC-MR-5	41	7.5	1632	1.14	1865	0.79
	OKC-MR-6	41	8.0	1349	1.68	1791	0.81
	OKC-MR-1	77	5.1	1381	0.16	1389	0.30
	OKC-MR-2	77	5.3	1151	0.14	1359	0.31
	OKC-MR-3	77	6.1	1419	0.10	1240	0.35
	OKC-MR-7	104	7.2	1106	0.01	453	0.14
	OKC-MR-8	104	8.1	407	0.20	319	0.19
	OKC-MR-9	104	6.5	985	0.03	557	0.10

Table 4.20: Measured and Predicted Model Parameters (Cont'd)

Mix Type	Specimen ID	Temp (°F)	Av (%)	$A_{Measured}$	$B_{Measured}$	$A_{Pred.}$	$B_{Pred.}$
Tar Creek Cores	TC-C-MR-3	41	9.2	1436	0.94	1460	0.88
	TC-C-MR-4	41	10.9	1106	0.70	1207	0.97
	TC-C-MR-1	77	7.7	1103	0.20	850	0.44
	TC-C-MR-2	77	7.9	1114	0.26	820	0.45
	TC-C-MR-5	104	8.6	252	0.24	92	0.21
	TC-C-MR-6	104	8.9	272	0.23	48	0.23
Davis Cores	D-C-MR-3	41	9.2	1770	0.72	2088	0.88
	D-C-MR-4	41	10.4	1600	1.47	1910	0.94
	D-C-MR-1	77	7.8	1466	0.23	1464	0.44
	D-C-MR-2	77	8.3	782	0.47	1389	0.47
	D-C-MR-5	104	5.7	330	0.33	1151	0.06
	D-C-MR-6	104	6.0	359	0.27	1106	0.07
OKC Cores	OKC-C-MR-3	41	5.6	1681	0.6	2147	0.69
	OKC-C-MR-4	41	5.3	2925	1.0	2191	0.67
	OKC-C-MR-1	77	7.5	1014	0.2	1033	0.43
	OKC-C-MR-2	77	8.0	622	0.52	958	0.45
	OKC-C-MR-5	104	5.1	485	0.02	764	0.03
	OKC-C-MR-6	104	5.3	376	0.1	735	0.04

$A_{Pred} = 3048.96 - 23.12\ T - 148.36\ A_v - 280.39\ AC + 443.04\ N_{200}$
$B_{Pred} = 0.803 - 0.010\ T + 0.053\ A_v$

Table 4.21: Sensitivity Check for M_R Model by Changing Each Variable by 20%

Stress Ratio (R)	Temperature T, (°F)	Air Voids (A_V), (%)	Binder Content (AC), (%)	% Passing No. 200 Sieve N_{200}, (%)	M_R (ksi)	Change of M_R (%)
0.20*	77.0*	7.0*	4.0*	5.0*	1104*	-
0.24	77.0	7.0	4.0	5.0	1065	-4
0.20	**92.4**	7.0	4.0	5.0	733	-34
0.20	77.0	**8.4**	4.0	5.0	963	-13
0.20	77.0	7.0	**4.8**	5.0	917	-17
0.20	77.0	7.0	4.0	**6.0**	1474	33

$M_R = (3048.96 - 23.12\ T - 148.36\ A_v - 280.39\ AC + 443.04\ N_{200}) \times (0.803 - 0.010\ T + 0.053\ A_v)^R$

* - Reference Value

Table 4.22: Matrix of APA Rut Results

Sample ID	Air Voids (%)	Rut Depth (mm)
Tar Creek Base Mix		
TC-B-R-1	7.2	3.4
TC-B-R-2	7.5	
TC-B-R-3	7.2	6.1
TC-B-R-4	6.8	
TC-B-R-5	6.7	5.1
TC-B-R-6	6.9	
AVG (STDEV)	*7.0 (0.3)*	*4.9 (1.4)*
Tar Creek Surface Mix		
TC-S-R-1	7.7	7.9
TC-S-R-2	9.5	
TC-S-R-3	7.9	7.7
TC-S-R-4	7.2	
TC-S-R-5	7.9	7.1
TC-S-R-6	7.2	
AVG (STDEV)	*7.9 (0.8)*	*7.6 (0.4)*
Tar Creek Cores		
TC-C-R-1	7.2	8.3
TC-C-R-2	9.6	
TC-C-R-3	7.0	8.5
TC-C-R-4	8.2	
TC-C-R-5	6.9	11.6
TC-C-R-6	8.9	
AVG (STDEV)	*8.0 (1.1)*	*9.5 (1.8)*
Davis Base Mix		
D-B-R-1	7.3	2.9
D-B-R-2	7.6	
D-B-R-3	7.0	2.2
D-B-R-4	7.0	
D-B-R-5	6.3	2.9
D-B-R-6	6.8	
AVG (STDEV)	*7.0 (0.4)*	*2.7 (0.4)*
Davis Cores		
D-C-R-1	8.5	2.4
D-C-R-2	7.8	
D-C-R-3	6.8	3.4
D-C-R-4	6.1	
D-C-R-5	7.8	3.5
D-C-R-6	8.3	
AVG (STDEV)	*7.5 (0.9)*	*3.1 (0.6)*
OKC Base Mix		
OKC-B-R-1	7.3	2.4
OKC-B-R-2	6.9	
OKC-B-R-3	6.9	2.5
OKC-B-R-4	6.6	
OKC-B-R-5	6.5	2.4
OKC-B-R-6	6.4	
AVG (STDEV)	*6.8 (0.3)*	*2.4 (0.05)*
OKC Cores		
OKC-C-R-1	5.8	6.3
OKC-C-R-2	6.6	
OKC-C-R-3	5.0	5.3
OKC-C-R-4	5.3	
OKC-C-R-5	4.5	5.3
OKC-C-R-6	4.4	
AVG (STDEV)	*5.3 (0.8)*	*5.6 (0.6)*

Table 4.23: Predicted Rut Depth from Material and Mix properties

Mix Type	Sample ID	$Rut_{Measured}$ (mm)	Rut_{Pred} (mm)
Tar Creek Base	1	3.4	6.95
	2	6.1	6.95
	3	5.1	6.95
Tar Creek Surface	1	7.9	6.38
	2	7.7	6.38
	3	7.1	6.38
Tar Creek Cores	1	8.3	6.95
	2	8.5	6.95
	3	11.6	6.95
Davis Base	1	2.9	2.70
	2	2.2	2.70
	3	2.9	2.70
Davis Cores	1	2.4	2.70
	2	3.4	2.70
	3	3.5	2.70
OKC Base	1	2.4	4.06
	2	2.5	4.06
	3	2.4	4.06
OKC Cores	1	6.3	4.06
	2	5.3	4.06
	3	5.3	4.06

$$Log\ (Rut_{Pred}) = 0.676 + 0.179\ AC - 0.178\ N_{200} \qquad (R\text{-squared} = 0.56)$$

Table 4.24: Predicted M_R and APA Rut Depth at 2000 and 8000 Loading Cycles

Mix/ Core Type	Rut_{2000} (mm)	Rut_{8000} (mm)	M_R (ksi) at 41°F R			M_R (ksi) at 77°F R			M_R (ksi) at 104°F R		
			0.20	0.35	0.50	0.20	0.35	0.50	0.20	0.35	0.50
TCB	3.1	4.8	1827	1731	1640	869	745	639	217	159	117
TCS	4.6	7.6	1610	1540	1473	372	339	310	81	61	46
TCC	5.5	9.7	1310	1293	1277	708	627	554	51	40	32
DB	1.5	2.7	2342	2234	2132	1422	1202	1017	626	460	338
DC	1.9	3.1	1960	1932	1904	1218	1082	961	655	436	290
OKCB	1.5	2.5	1748	1690	1634	1057	890	749	295	217	161
OKCC	3.9	5.6	2007	1893	1786	844	745	658	376	224	134

Table 4.25: Models for Predicted M_R and Rut Depth at 2000 and 8000 Loading Cycles

M_R Test Temperature (°F)	Stress Ratio	Rut - M_R Model	R-squared
41	0.20	Rut_{2000} (mm) = -0.0036 M_R (ksi) + 9.70	0.54
		Rut_{8000} (mm) = -0.0065 M_R (ksi) + 17.02	0.61
	0.35	Rut_{2000} (mm) = -0.0040 M_R (ksi) + 10.24	0.58
		Rut_{8000} (mm) = -0.0072 M_R (ksi) + 17.62	0.64
	0.50	Rut_{2000} (mm) = -0.0045 M_R (ksi) + 10.70	0.62
		Rut_{8000} (mm) = -0.0079 M_R (ksi) + 18.46	0.66
77	0.20	Rut_{2000} (mm) = -0.0039 M_R (ksi) + 6.75	0.71
		Rut_{8000} (mm) = -0.0063 M_R (ksi) + 11.03	0.65
	0.35	Rut_{2000} (mm) = -0.0046 MR (ksi) + 6.83	0.69
		Rut_{8000} (mm) = -0.0075 M_R (ksi) + 11.17	0.63
	0.50	Rut_{2000} (mm) = -0.0053 M_R (ksi) + 6.87	0.66
		Rut_{8000} (mm) = -0.0087 M_R (ksi) + 11.25	0.60
104	0.20	Rut_{2000} (mm) = -0.0052 M_R (ksi) + 4.85	0.62
		Rut_{8000} (mm) = -0.0089 M_R (ksi) + 8.08	0.63
	0.35	Rut_{2000} (mm) = -0.0079 M_R (ksi) + 4.96	0.68
		Rut_{8000} (mm) = -0.0134 M_R (ksi) + 8.20	0.67
	0.50	Rut_{2000} (mm) = -0.0117 M_R (ksi) + 5.01	0.72
		Rut_{8000} (mm) = -0.0194 M_R (ksi) + 8.25	0.68

Table 4.26: APA Fatigue Results

APA Fatigue					
Sample ID	Air Voids (%)	# of Cycles	Sample ID	Air Voids (%)	# of Cycles
Tar Creek Base Mix			Tar Creek Surface Mix		
TC-B-F-1	9.6	47,440	TC-S-F-1	10.5	48,080
TC-B-F-2	8.9	49,920	TC-S-F-2	10.0	47,520
TC-B-F-3	8.6	49,680	TC-S-F-3	10.8	49,920
Davis Base Mix			OKC Base Mix		
D-B-F-1	10.6	16,240	OKC-B-F-1	8.4	27,040
D-B-F-2	10.7	22,320	OKC-B-F-2	8.2	26,960
D-B-F-3	10.9	16,240	OKC-B-F-3	8.2	26,960

Table 4. 27: Measured and Predicted Fatigue Cycles

Mix Type	Sample ID	$N_{f, Cal}$	N_{200} (%)	$N_{f, Pred}$
Tar Creek Base	1	47,440	6.00	46,852
	2	49,920	6.00	49,211
	3	49,680	6.00	50,222
Tar Creek Surface	1	48,080	4.90	48,493
	2	47,520	4.90	50,178
	3	49,920	4.90	47,481
Davis Base	1	16,240	5.90	18,953
	2	22,320	5.90	18,616
	3	16,240	5.90	17,942
OKC Base	1	27,040	4.70	26,340
	2	26,960	4.70	27,014
	3	26,960	4.70	27,014

$N_{f, Pred} = 826568 - 3370\ A_v - 279230\ G_{se} - 3234\ N_{200}$ *(R-squared = 0.98)*

Table 4.28: Permeability Test Results

Permeability					
Sample ID	Air Voids (%)	Permeability (10^{-6} cm/s)	Sample ID	Air Voids (%)	Permeability (10^{-6} cm/s)
Tar Creek Base Mix			Tar Creek Surface Mix		
TC-B-P-1	6.6	2.315	TC-S-P-1	7.4	13.51
TC-B-P-2	6.5	2.422	TC-S-P-2	6.6	8.10
Davis Base Mix			OKC Base Mix		
D-P-1	6.9	3.385	OKC-P-1	6.8	11.87
D-P-2	7.0	1.993	OKC-P-2	7.7	17.79

Table 4.29: Comparison of Measured and Predicted Permeability Values

Mix Type	Sample ID	k_{Calc} (10^{-6} cm/s)	k_{Pred} (10^{-6} cm/s)
Tar Creek Base	1	2.315	1.352
	2	2.422	0.804
Tar Creek Surface	1	13.510	13.606
	2	8.100	9.221
Davis Base	1	3.385	3.712
	2	1.993	4.260
OKC Base	1	11.870	11.749
	2	17.790	16.682

$k_{Pred} = 8.10 + 5.48\ A_v - 7.15\ N_{200}$ *(R-squared = 0.96)*

Table 4.30: Laboratory Seismic Modulus Test Results for Davis Cores

Core #	Diameter D, (in)	Height H, (in)	H/D Ratio	Weight (lb)	Mass Density ((lb/in3)/(in/s2))	Hit #	Frequency (Hz)	$E_{Seismic}$ (ksi)
1	3.984	10.557	2.6	13.457	0.000265	1	5,677	3,802
1	3.984	10.557		13.457	0.000265	2	7,852	7,274
1	3.984	10.557		13.457	0.000265	3	8,428	8,380
2	3.990	9.909	2.5	12.702	0.000265	1	8,396	7,347
2	3.990	9.909		12.702	0.000265	2	8,651	7,800
2	3.990	9.909		12.702	0.000265	3	8,555	7,628
3	3.989	9.612	2.4	11.902	0.000256	1	8,811	7,356
3	3.989	9.612		11.902	0.000256	2	9,099	7,844
3	3.989	9.612		11.902	0.000256	3	9,867	9,224
4	3.994	9.820	2.5	12.68	0.000267	1	7,468	5,739
4	3.994	9.820		12.68	0.000267	2	6,413	4,232
4	3.994	9.820		12.68	0.000267	3	8,076	6,711
5	5.921	9.940	1.7	28.14	0.000266	1	8,396	7,414
5	5.921	9.940		28.14	0.000266	2	8,971	8,465
5	5.921	9.940		28.14	0.000266	3	7,628	6,120
6	3.992	10.465	2.6	13.306	0.000263	1	9,131	9,604
6	3.992	10.465		13.306	0.000263	2	9,035	9,403
6	3.992	10.465		13.306	0.000263	3	9,451	10,289
7	3.995	10.235	2.6	13.21	0.000267	1	8,300	7,693
7	3.995	10.235		13.21	0.000267	2	8,364	7,813
7	3.995	10.235		13.21	0.000267	3	9,003	9,052
8	3.988	9.860	2.5	12.623	0.000265	1	8,460	7,381
8	3.988	9.860		12.623	0.000265	2	8,524	7,493
8	3.988	9.860		12.623	0.000265	3	8,300	7,105
9	3.988	10.343	2.6	13.319	0.000267	1	9,227	9,720
9	3.988	10.343		13.319	0.000267	2	8,971	9,188
9	3.988	10.343		13.319	0.000267	3	8,619	8,481
10	5.932	10.600	1.8	30.071	0.000266	1	8,875	9,404
10	5.932	10.600		30.071	0.000266	2	9,003	9,677
10	5.932	10.600		30.071	0.000266	3	9,355	10,449
11	5.937	10.083	1.7	28.443	0.000264	1	9,451	9,579
11	5.937	10.083		28.443	0.000264	2	9,067	8,816
11	5.937	10.083		28.443	0.000264	3	7,116	5,430
12	3.990	9.824	2.5	12.68	0.000267	1	8,728	7,858
12	3.990	9.824		12.68	0.000267	2	8,651	7,720
12	3.990	9.824		12.68	0.000267	3	10,314	10,973
13	3.991	10.679	2.7	13.622	0.000264	1	9,195	10,176
13	3.991	10.679		13.622	0.000264	2	9,419	10,678
13	3.991	10.679		13.622	0.000264	3	9,643	11,192
14	3.993	10.137	2.5	13.15	0.000268	1	9,067	9,059
14	3.993	10.137		13.15	0.000268	2	9,131	9,188
14	3.993	10.137		13.15	0.000268	3	9,995	11,009
15	5.938	10.665	1.8	30.058	0.000263	1	8,268	8,192
15	5.938	10.665		30.058	0.000263	2	8,428	8,512
15	5.938	10.665		30.058	0.000263	3	8,108	7,878

Table 4.30: Laboratory Seismic Modulus Test Results for Davis Cores (Cont'd)

16	5.935	9.830	1.7	28.023	0.000267	1	8,332	7,156
16	5.935	9.830		28.023	0.000267	2	9,803	9,906
16	5.935	9.830		28.023	0.000267	3	8,332	7,156
17	5.940	10.050	1.7	28.281	0.000263	1	9,323	9,230
17	5.940	10.050		28.281	0.000263	2	9,163	8,916
17	5.940	10.050		28.281	0.000263	3	8,044	6,871
18	4.001	9.760	2.4	12.776	0.000269	1	9,931	10,126
18	4.001	9.760		12.776	0.000269	2	9,643	9,547
18	4.001	9.760		12.776	0.000269	3	6,573	4,436
19	5.935	10.350	1.7	29.558	0.000267	1	8,460	8,193
19	5.935	10.350		29.558	0.000267	2	8,939	9,147
19	5.935	10.350		29.558	0.000267	3	9,803	11,001

Table 4.31: Seismic Modulus and Predicted M_R for the Davis Cores

Sample ID	Core	E_S (ksi)			Predicted M_R (ksi), (Ratio, E_S/M_R)		
	ID	Avg	SD	CV (%)	R = 0.20	R = 0.35	R = 0.50
D-C-MR-3	1	7827	782	10.0	1100 (7)	996 (8)	901 (9)
D-C-MR-4	3	8141	969	11.9	966 (8)	890 (9)	820 (10)
D-C-MR-1	9	9130	621	6.8	1243 (7)	1099 (8)	972 (9)
D-C-MR-2	6	9765	464	4.8	1194 (8)	1065 (9)	950 (10)
D-C-MR-5	12	8850	1839	20.8	1422 (6)	1205 (7)	1020 (9)
D-C-MR-6	18	9836	409	4.2	1400 (7)	1194 (8)	1018 (10)

Table 4.32: FWD Back-Calculated Moduli for Tar Creek Site

Section ID	Dist. From East End (ft)	E_{FWD} of HMA Layer (ksi)				Average (ksi)	Std. Dev. (ksi)
		East Bound		West Bound			
		10 kip	18 kip	10 kip	18 kip		
Section TS-2	50	252	220	157	165	182	45
	100	171	159	-	-		
	150	145	148	140	128		
	200	132	138	-	-		
	250	198	221	190*	191*		
	300	185	185	-	-		
	350	-	-	311	259		
	400	186	157	-	-		
	450	-	-	161	157		
Section TS-4	550	-	-	314	302	242	78
	600	353*	323*	-	-		
	650	-	-	261	338		
	700	251	243	-	-		
	750	-	-	180*	161*		
	800	177	234	-	-		
	850	-	-	137	154		
	900	317	324	-	-		
	950	-	-	134	152		
Section TS-1	1125	269	217	-	-	254	41
	1250	-	-	270	238		
	1375	190	202	-	-		
	1500	-	-	230	192		
	1625	217	230	-	-		
	1750	-	-	261	245		
	1875	268	269	-	-		
	2000	-	-	342	295		
	2125	262	277	-	-		
	2250	-	-	242*	227*		
	2375	323*	340*	-	-		
	2500	-	-	251	247		
Section TS-3	2700	-	-	86	94	122	27
	2750	94	100	-	-		
	2800	-	-	119	127		
	2850	138	143	-	-		
	2900	-	-	108	121		
	2950	137	151	-	-		
	3000	-	-	116	124		
	3050	95	97	-	-		
	3100	-	-	165	183		

* - Field cores were retrieved at this locations and preformed laboratory M_R test

Table 4.33: FWD Back-Calculated Moduli for Davis Site

Dist. From East End (ft)	E_{FWD} of HMA Layer (ksi) Load		
	9 kip	12 kip	15 kip
50*	554	543	526
100	387	400	421
150*	634	620	628
200	464	468	534
250*	580	602	579
300	414	417	420
350*	528	487	497
400	386	372	438
450*	460	464	467
500	499	482	531
550*	448	447	459

Average = 490 ksi
Std. Dev. = 9 ksi
* - Field cores were retrieved at this locations and preformed laboratory M_R test

Table 4.34: FWD Back-Calculated Moduli for OKC Site

Dist. From South End (ft)	E_{FWD} of HMA Layer Load		
	9 kip	12 kip	18 kip
0	890	684	674
52	221	322	384
139	1726	1686	1714
330*	1892	3004	3296
403*	1747	1777	1740
475	618	931	1053
540	400	288	246
630*	325	288	287
701	810	760	811
810*	928	888	845
881*	932	853	942
957	492	425	448
1026	84	91	94
1105	804	687	699
1174	432	404	450
1266	537	436	463

Average = 562 ksi
Std. Dev. = 274 ksi
* - Field cores were retrieved at this locations and preformed laboratory M_R test

Table 4.35: Comparison of Modulus from FWD Test and M_R by Semi-Log Model (Davis Site)

Modulus from FWD Test			M_R at FWD Test Temperature		
9 kip	12 kip	15 kip	R = 0.20	R = 0.35	R = 0.50
554	543	526	604	524	446
528	487	497	521	447	377
580	602	579	536	462	390
460	464	467	476	407	340
448	447	459	449	382	318

Table 4.36: Comparison of Modulus from FWD Test and M_R by Semi-Log Model (Tar Creek Site)

Modulus from FWD Test		M_R at FWD Test Temperature		
10 kip	18 kip	R = 0.20	R = 0.35	R = 0.50
323	340	399	354	293
190	191	504	453	384
353	323	399	354	293
180	161	504	453	384
242	227	475	426	359

Table 4.37: Comparison of Modulus from FWD Test and M_R by Semi-Log Model (OKC Site)

Modulus from FWD Test			M_R at FWD Test Temperature		
9 kip	12 kip	15 kip	R = 0.20	R = 0.35	R = 0.50
325	288	287	461	375	306
1892	3004	3296	445	360	291
928	888	845	461	375	306
932	853	942	445	360	291
1747	1777	1740	461	375	306

Table 4.38: Moduli and HMA Thicknesses from SASW Test for Tar Creek Site

Layer	Modulus, E_{SASW} (ksi)			Depth (in)		
Profile	TS-2	TS-4	TS-1	TS-2	TS-4	TS-1
HMA Surface	1257.5	617.5	707.5	1.44	1.44	1.44
HMA Base	1350.0	772.5	930.0	4.8	2.4	2.4

Table 4.39: Comparison of FWD and SASW Moduli for Tar Creek Site

Location	E_{FWD} (ksi)			E_{SASW} (ksi)		
ID	Load		Avg	Surface	Base	Avg
	10 kip	18 kip				
8 (TS-4)	180	161	171	618	773	695
38 (TS-2)	198	221	210	1258	1350	1304

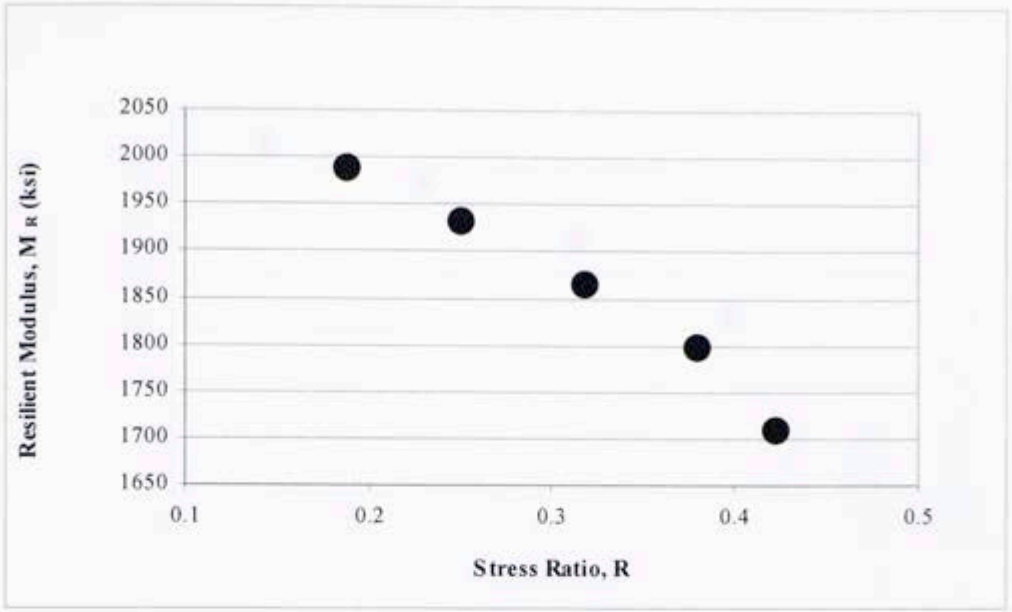


Figure 4.1: Variation of M_R with Stress Ratio (Davis specimen at 41°F)

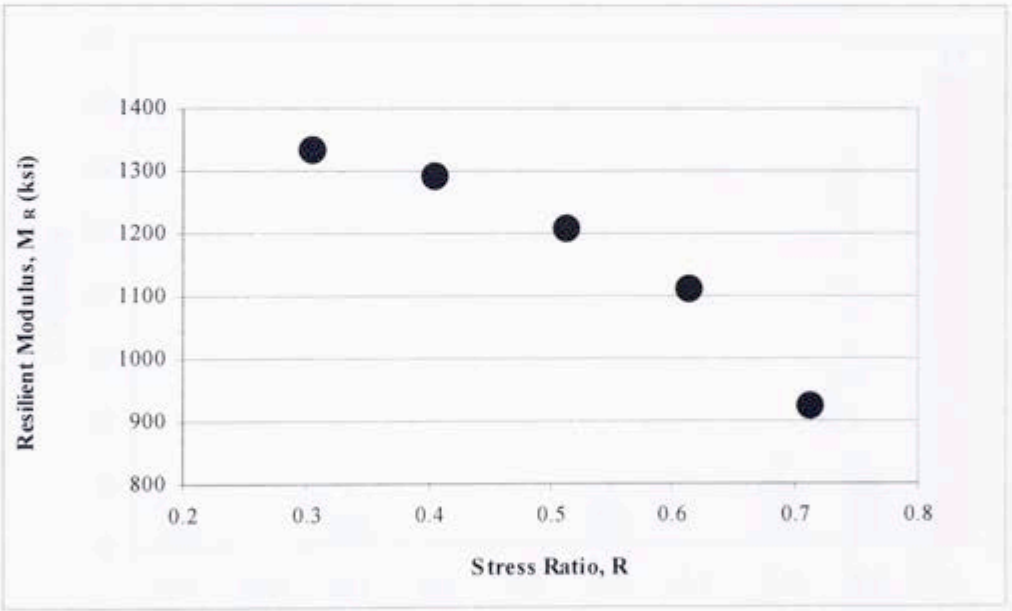


Figure 4.2: Variation of M_R with Stress Ratio (Davis specimen at 77°F)

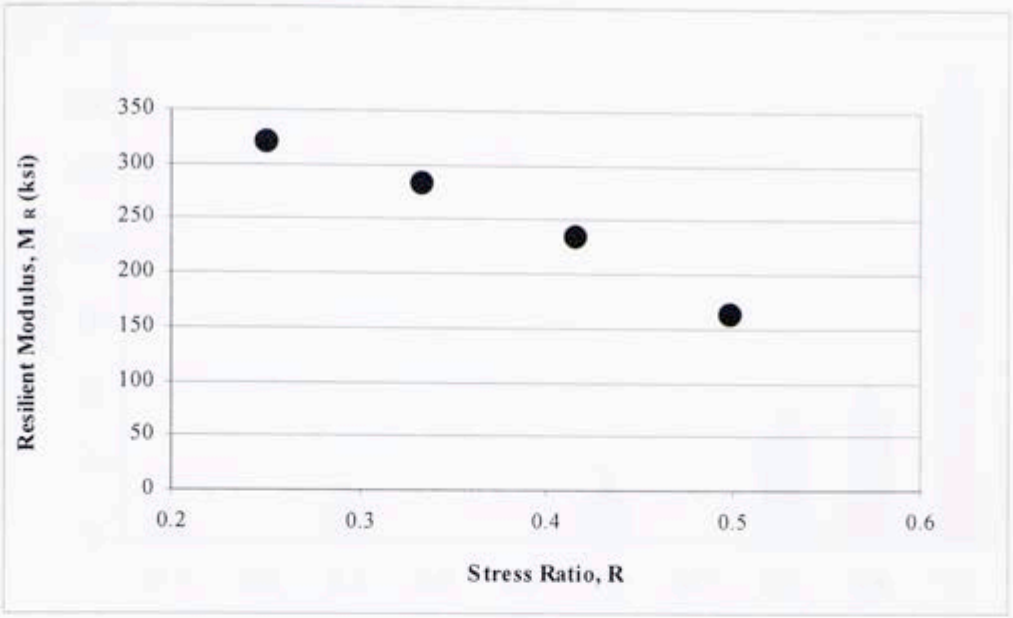


Figure 4.3: Variation of M_R with Stress Ratio (Davis specimen at 104°F)

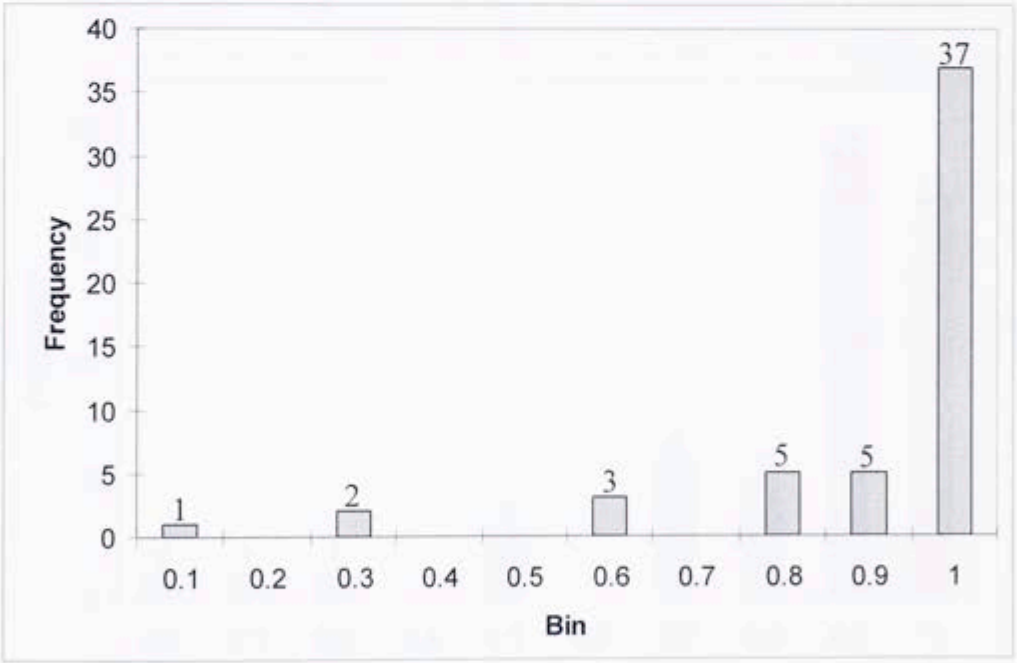


Figure 4.4: Frequency Diagram for Linear Model from 53 Observations

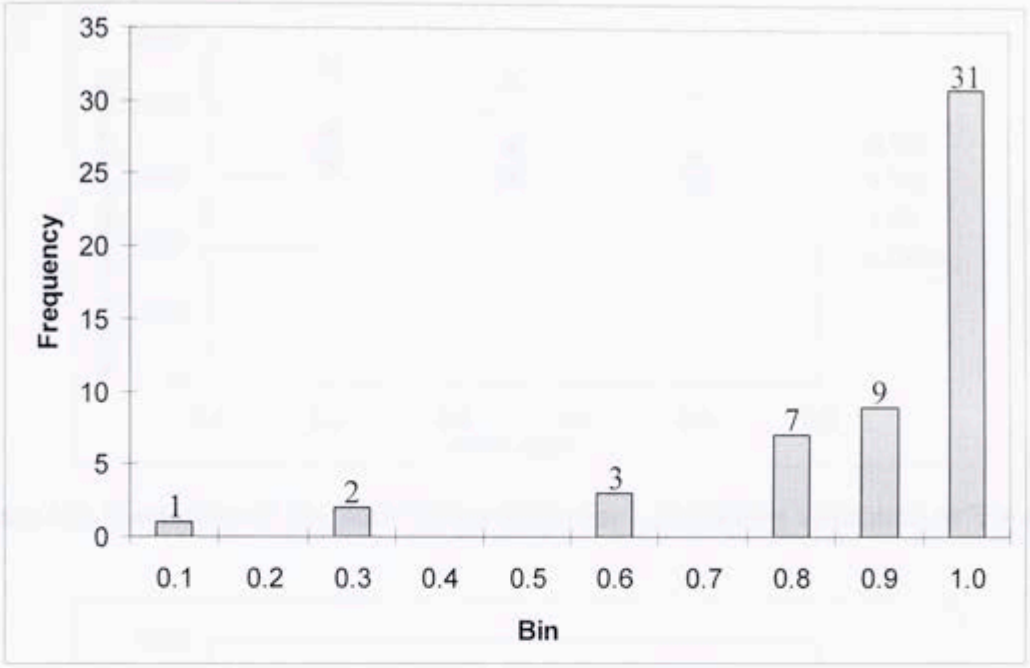


Figure 4.5: Frequency Diagram for Semi-Log Model from 53 Observations

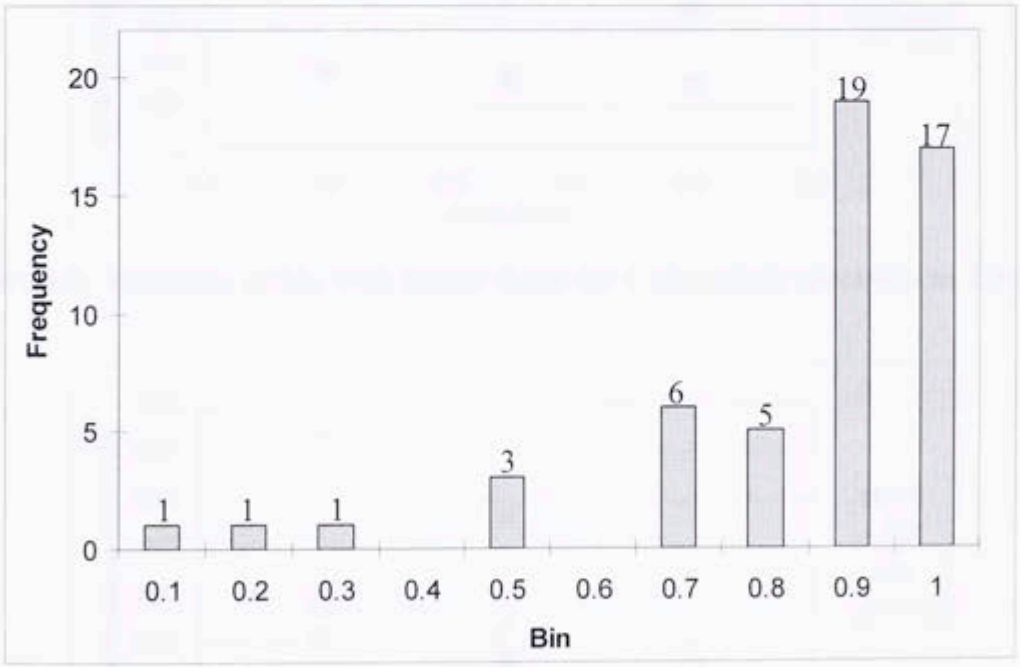


Figure 4.6: Frequency Diagram for Log-Log Model from 53 Observations

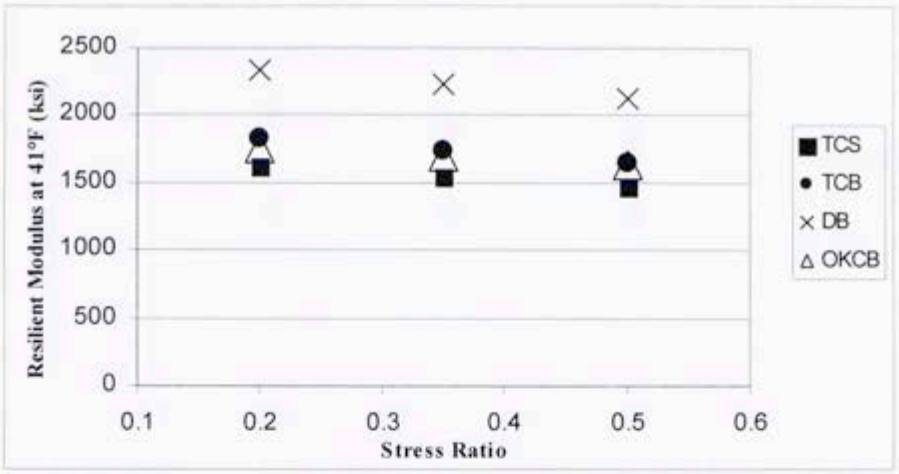


Figure 4.7: Variation of M_R with Stress Ratio for Laboratory specimen at T = 41°F

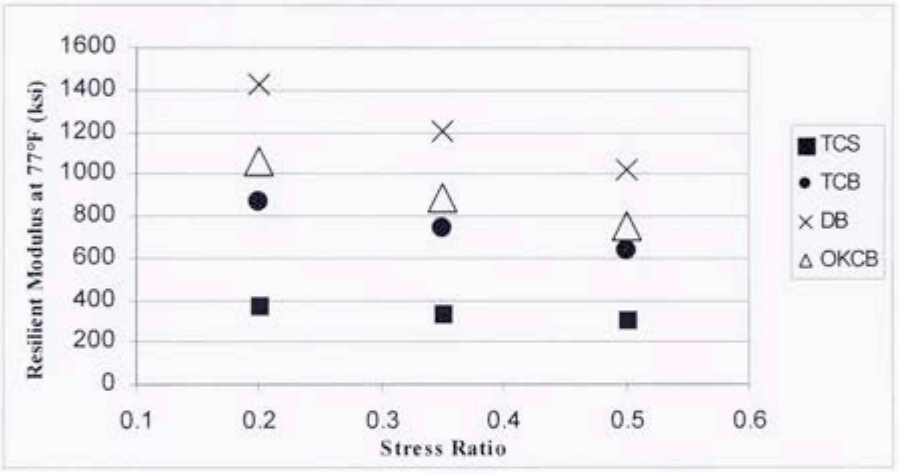


Figure 4.8: Variation of M_R with Stress Ratio for Laboratory specimen at T = 77°F

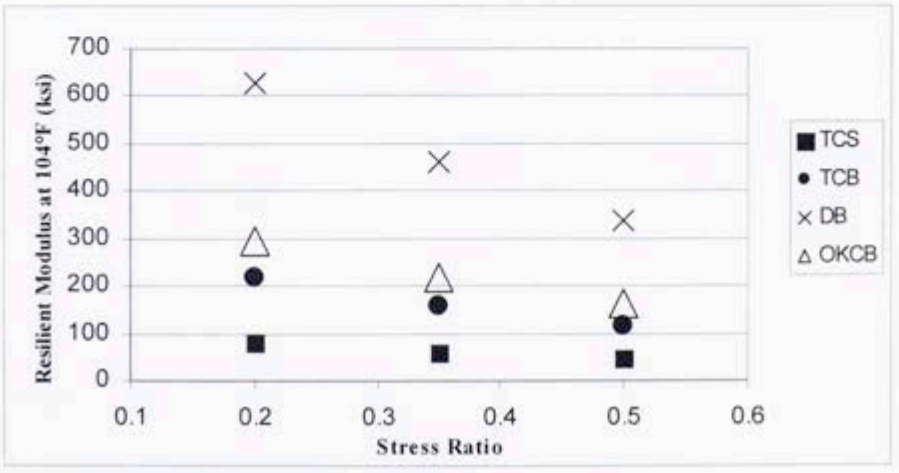


Figure 4.9: Variation of M_R with Stress Ratio for Laboratory specimen at T = 104°F

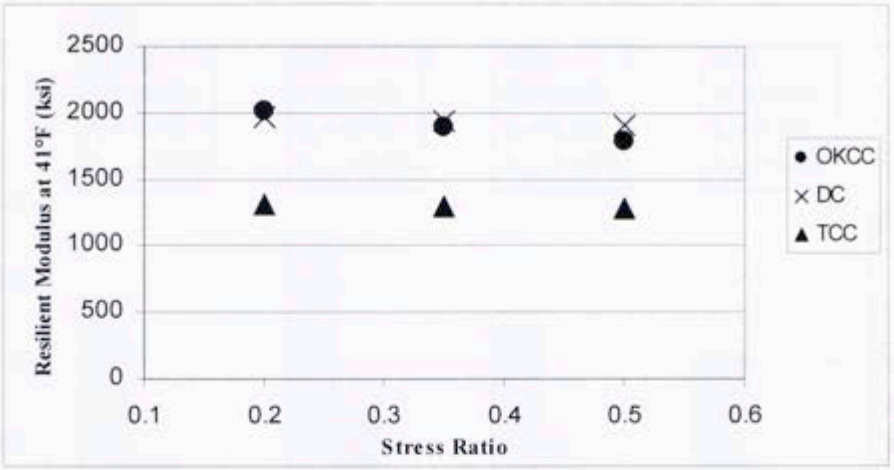


Figure 4.10: Variation of M_R with Stress Ratio for Field Cores at T = 41°F

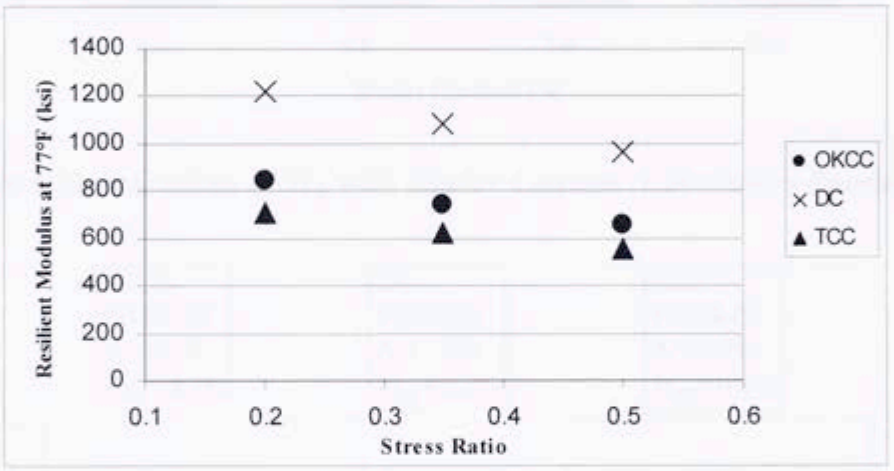


Figure 4.11: Variation of M_R with Stress Ratio for Field Cores at T = 77°F

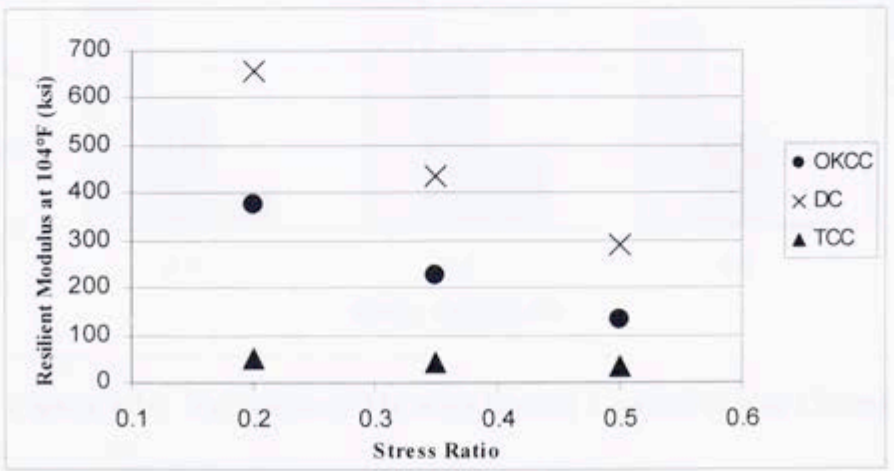


Figure 4.12: Variation of M_R with Stress Ratio for Field Cores at T = 104°F

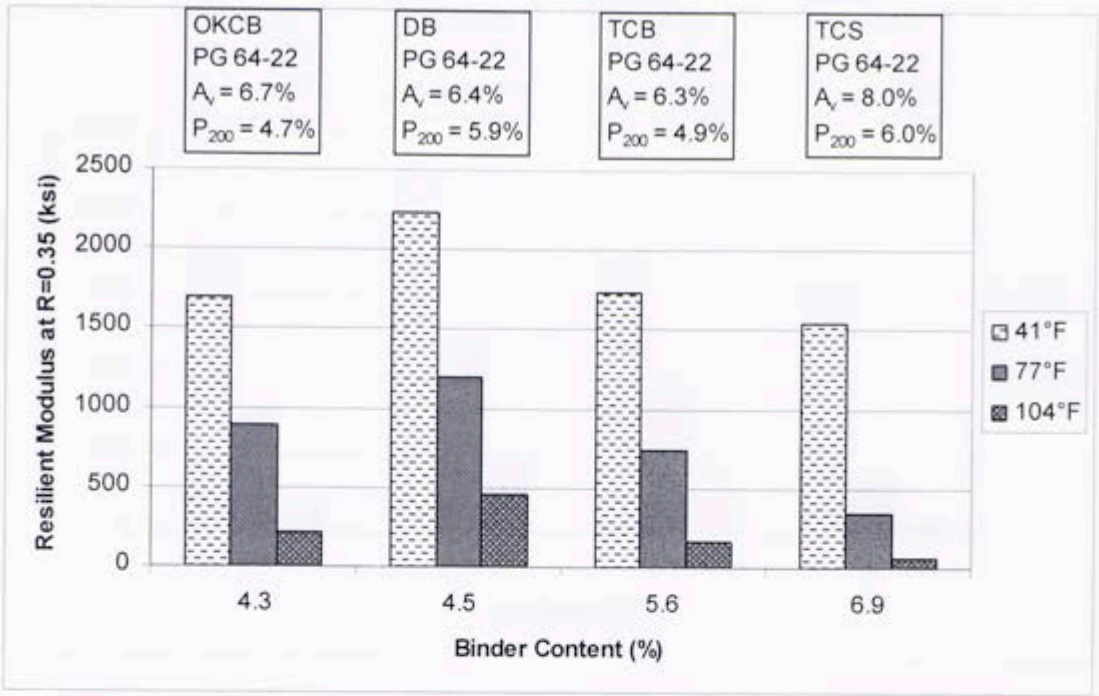


Figure 4.13: Variation of M_R with Binder Content (Laboratory Specimens)

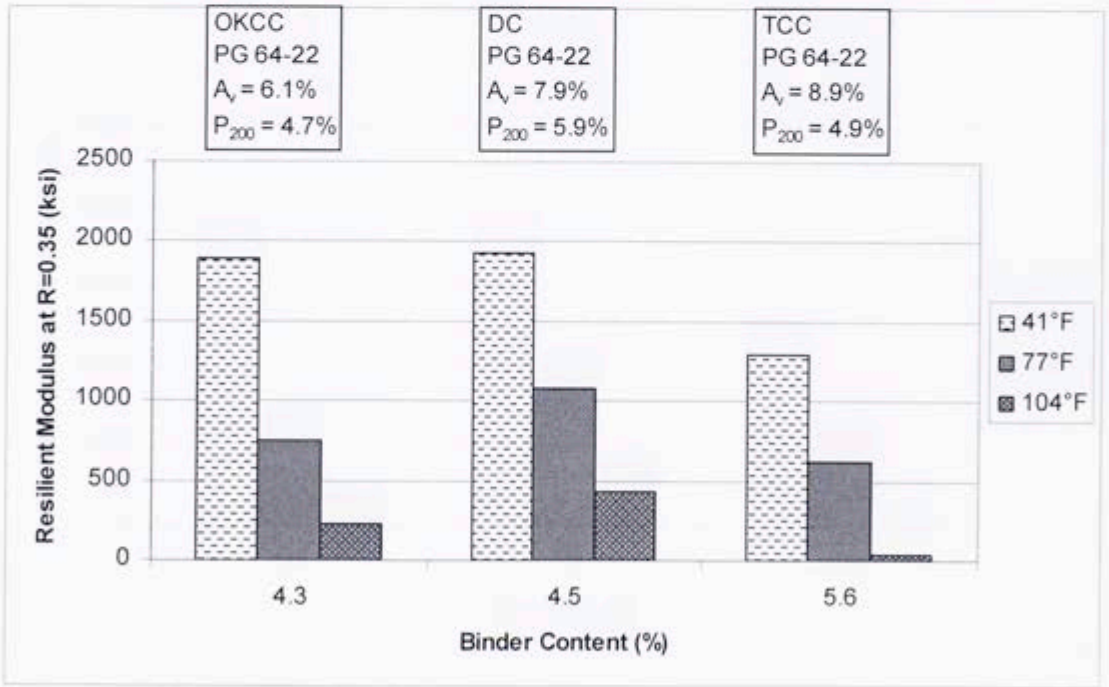


Figure 4.14: Variation of M_R with Binder Content (Field Cores)

(TCB-Tar Creek base mix, TCS-Tar Creek surface Mix, TCC-Tar Creek core, DB-Davis base Mix, DC-Davis core, OKCB-OKC base mix, OKCC-OKC core)

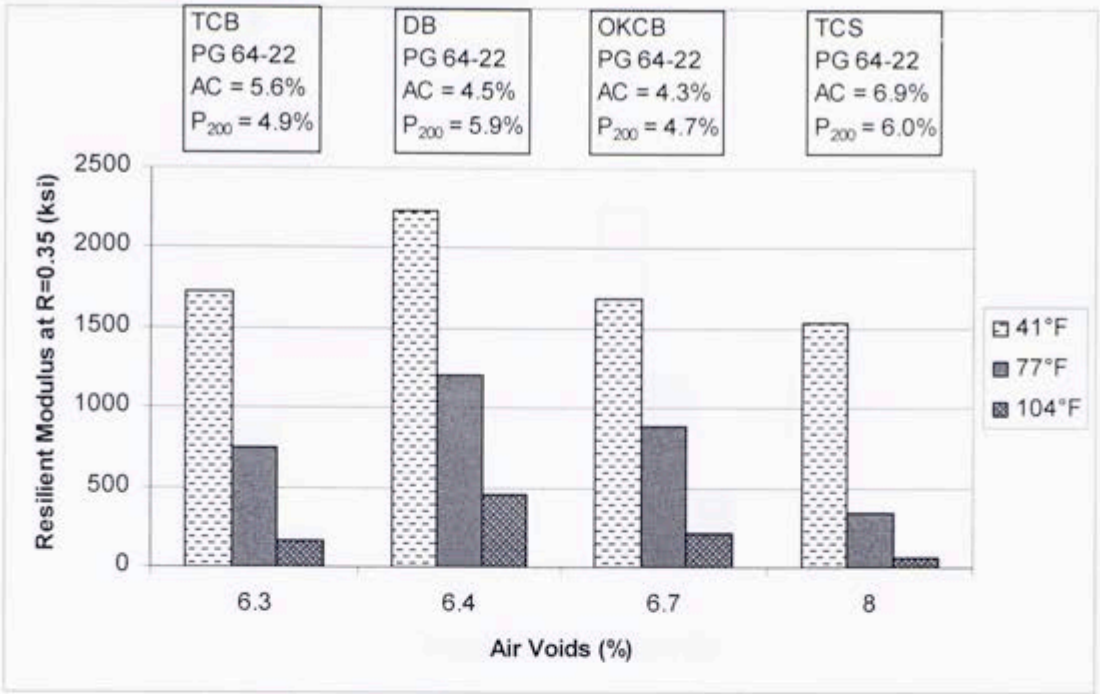


Figure 4.15: Variation of M_R with Air Voids (Laboratory Specimens)

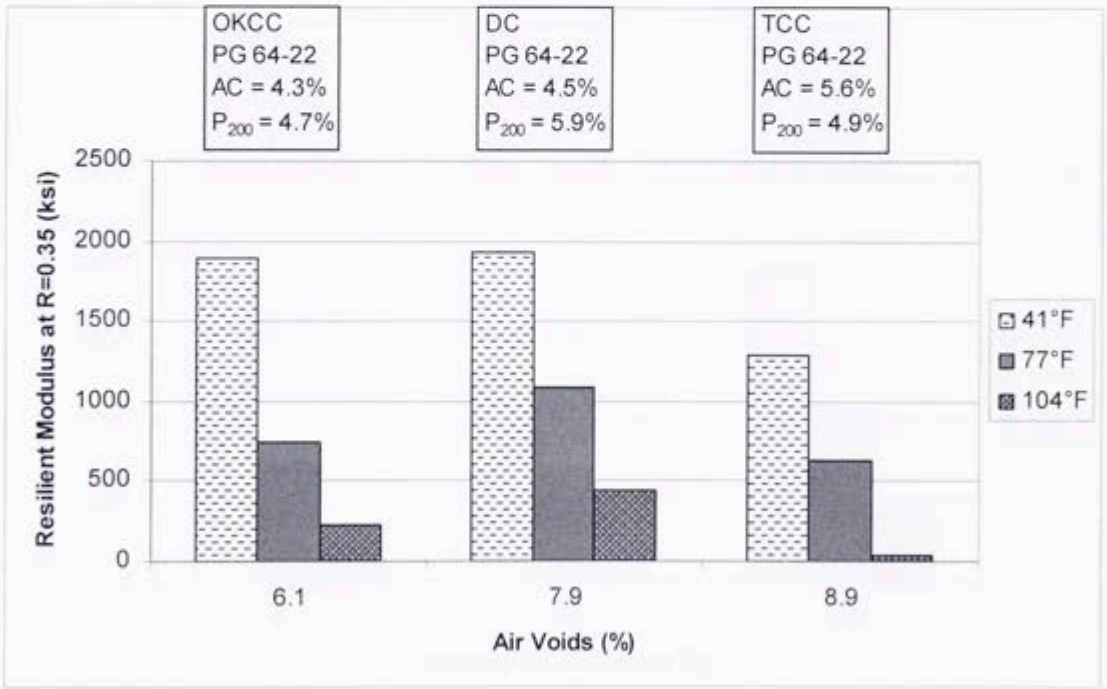


Figure 4.16: Variation of M_R with Air Voids (Field Cores)

(TCB-Tar Creek base mix, TCS-Tar Creek surface Mix, TCC-Tar Creek core, DB-Davis base Mix, DC-Davis core, OKCB-OKC base mix, OKCC-OKC core)

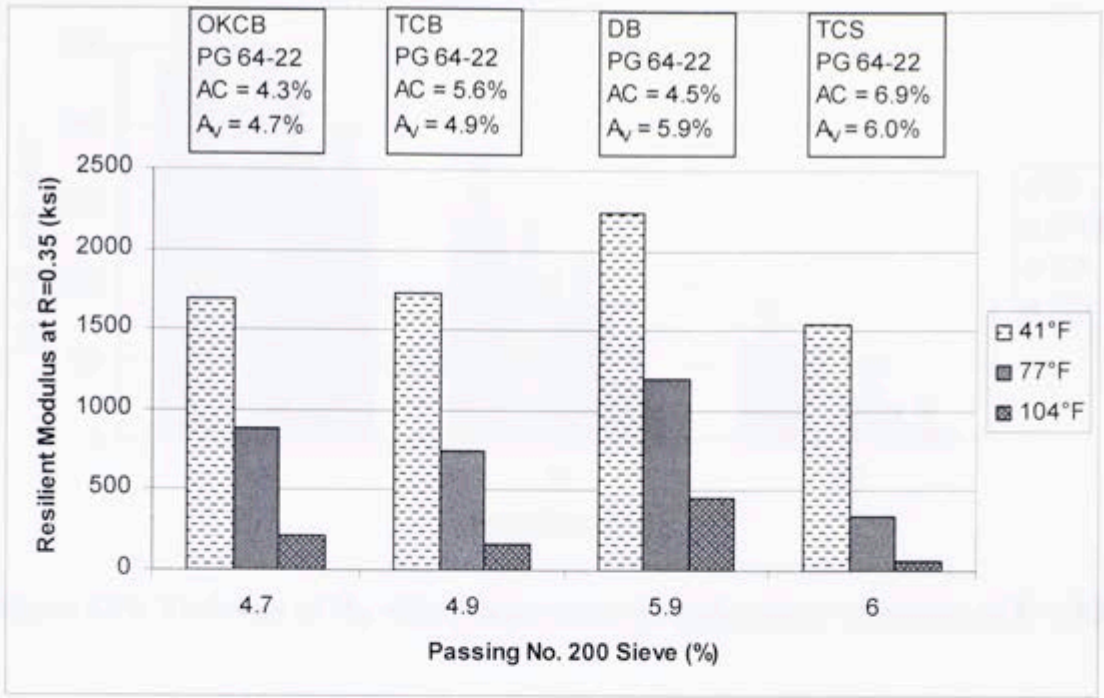


Figure 4.17: Variation of M_R with Percentage Passing No. 200 Sieve (Laboratory Specimens)

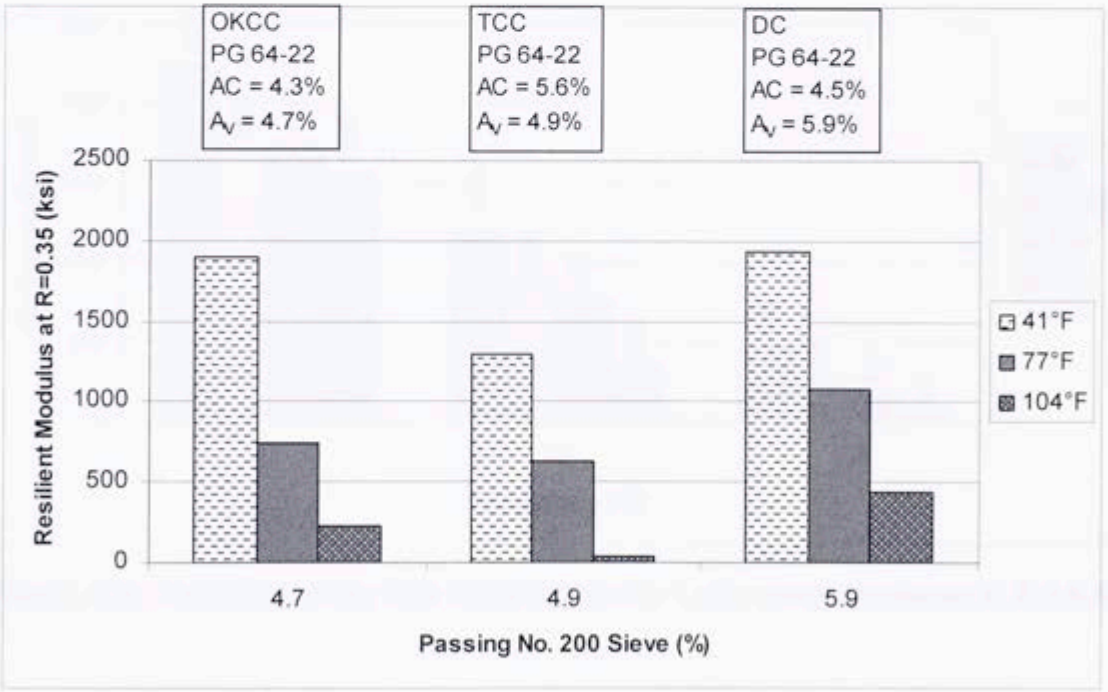


Figure 4.18: Variation of M_R with Percentage Passing No. 200 Sieve (Field Cores)

(TCB-Tar Creek base mix, TCS-Tar Creek surface Mix, TCC-Tar Creek core, DB-Davis base Mix, DC-Davis core, OKCB-OKC base mix, OKCC-OKC core)

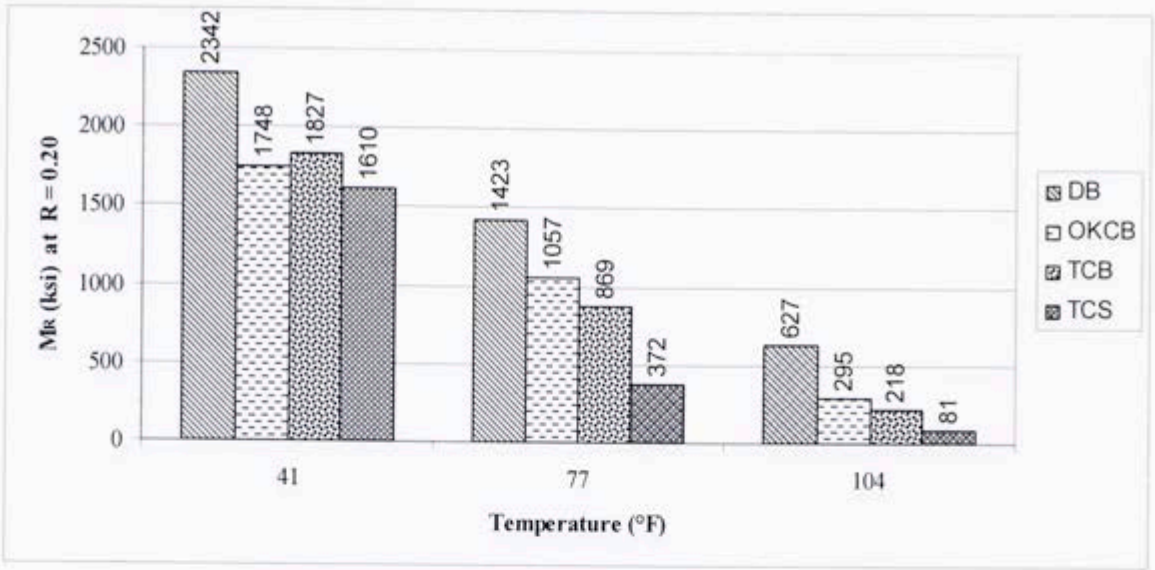


Figure 4.19: Variation of M_R with Temperature for Laboratory specimens at R = 0.20

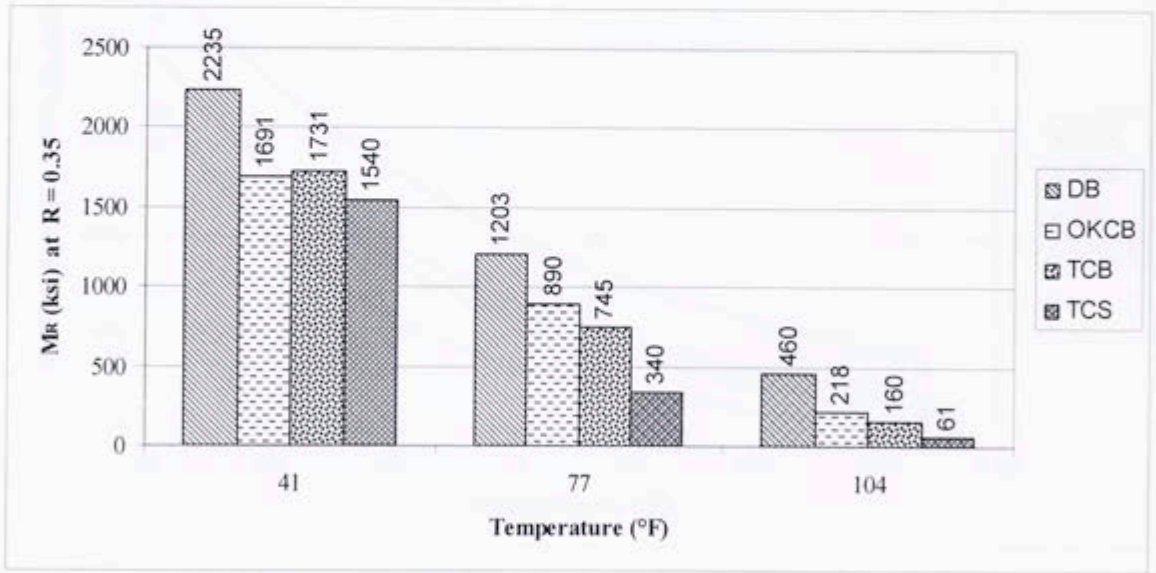


Figure 4.20: Variation of M_R with Temperature for Laboratory specimens at R = 0.35

(TCB-Tar Creek base mix, TCS-Tar Creek surface mix, DB-Davis base mix, OKCB-OKC base mix)

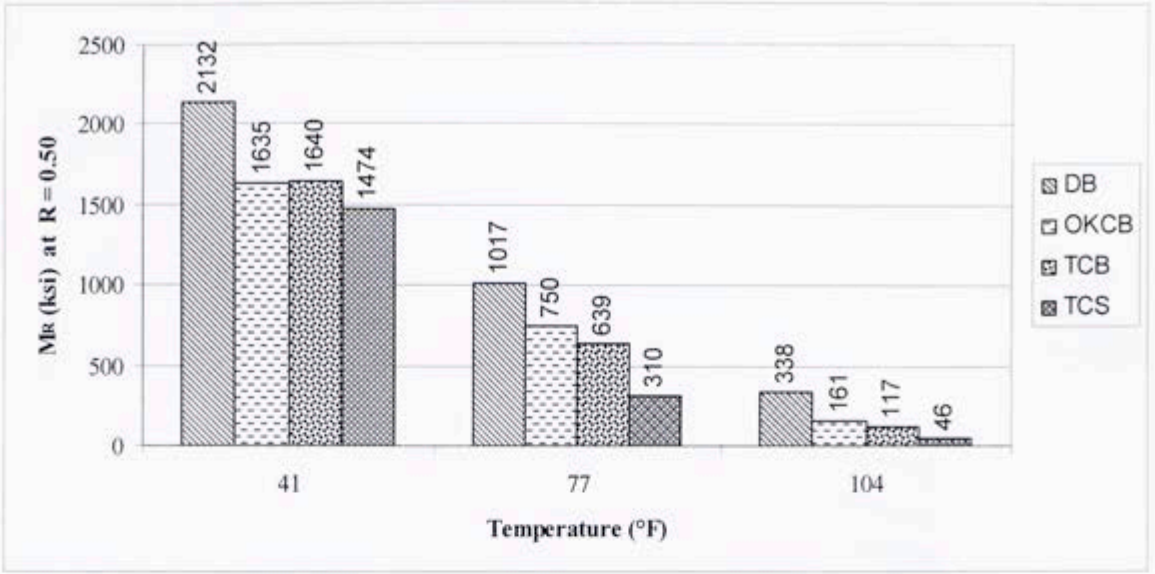


Figure 4.21: Variation of M_R with Temperature for Laboratory specimens at R = 0.50

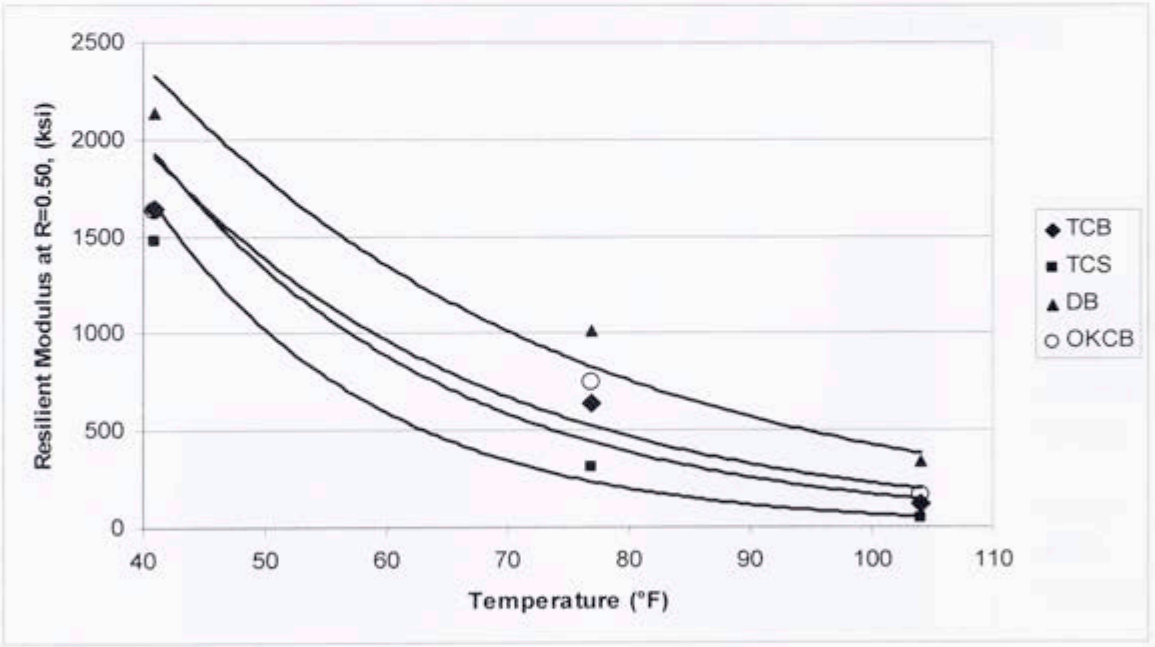


Figure 4.22: Variation of M_R with Temperature at R = 0.35 (Laboratory Specimens)

(TCB-Tar Creek base mix, TCS-Tar Creek surface Mix, TCC-Tar Creek core, DB-Davis base Mix, DC-Davis core, OKCB-OKC base mix, OKCC-OKC core)

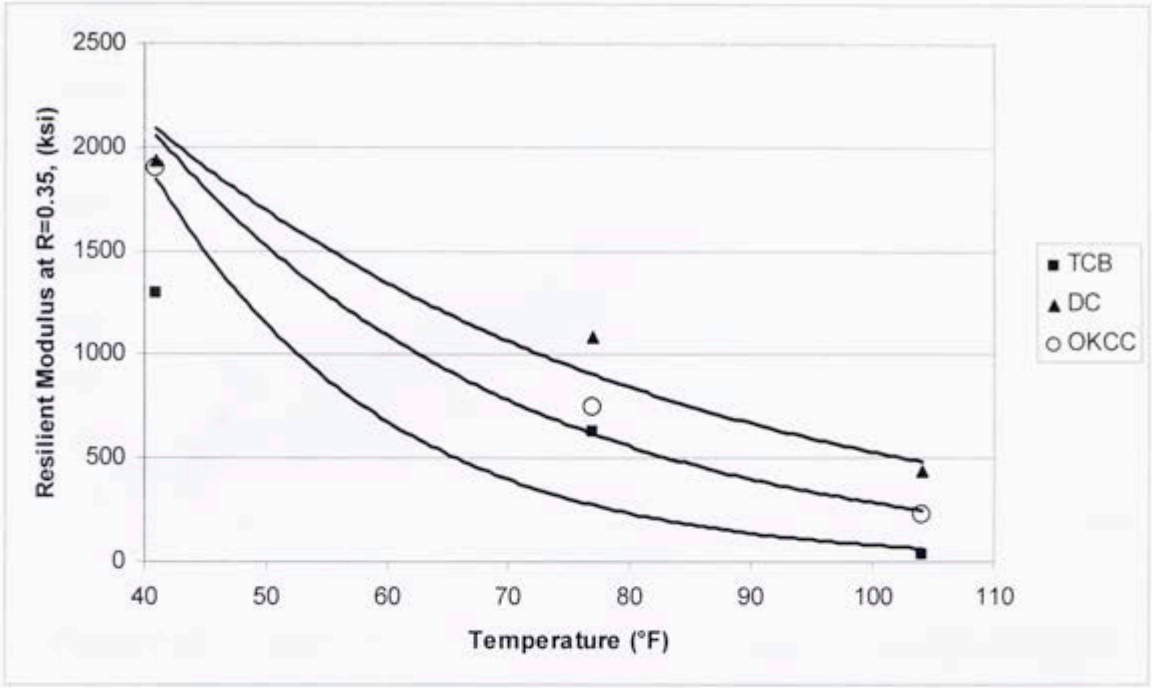


Figure 4.23: Variation of M_R with Temperature at R = 0.35 (Field Cores)

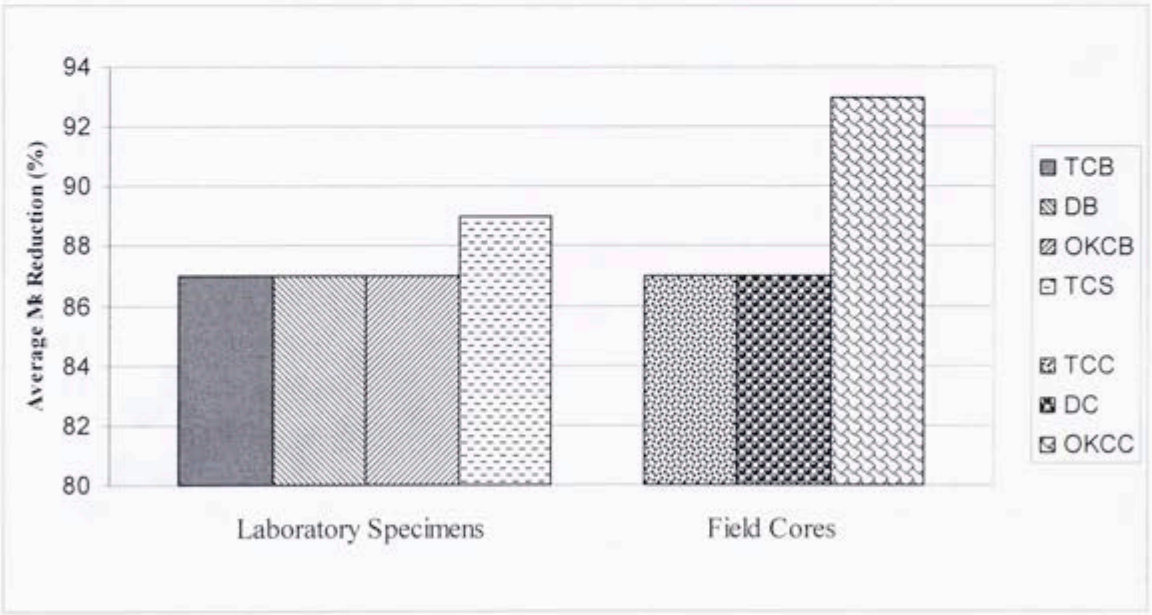


Figure 4.24: Average Decrease of M_R when Temperature increases from 41°F to 104°F

(TCB-Tar Creek base mix, TCS-Tar Creek surface Mix, TCC-Tar Creek core, DB-Davis base Mix, DC-Davis core, OKCB-OKC base mix, OKCC-OKC core)

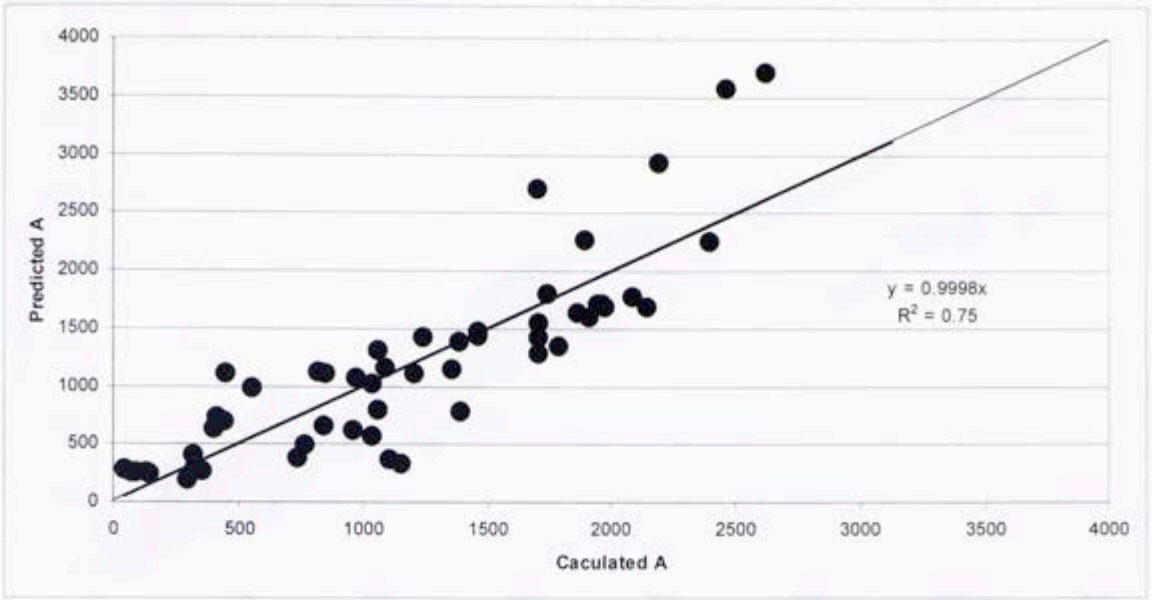


Figure 4.25: Calculated and Predicted Model Parameter A for Power Model

$[A_{pred} = 3048.96 - 23.12\ T - 148.36\ A_V - 280.39\ AC + 443.04\ N_{200}$ *(R-squared = 0.75)*$]$

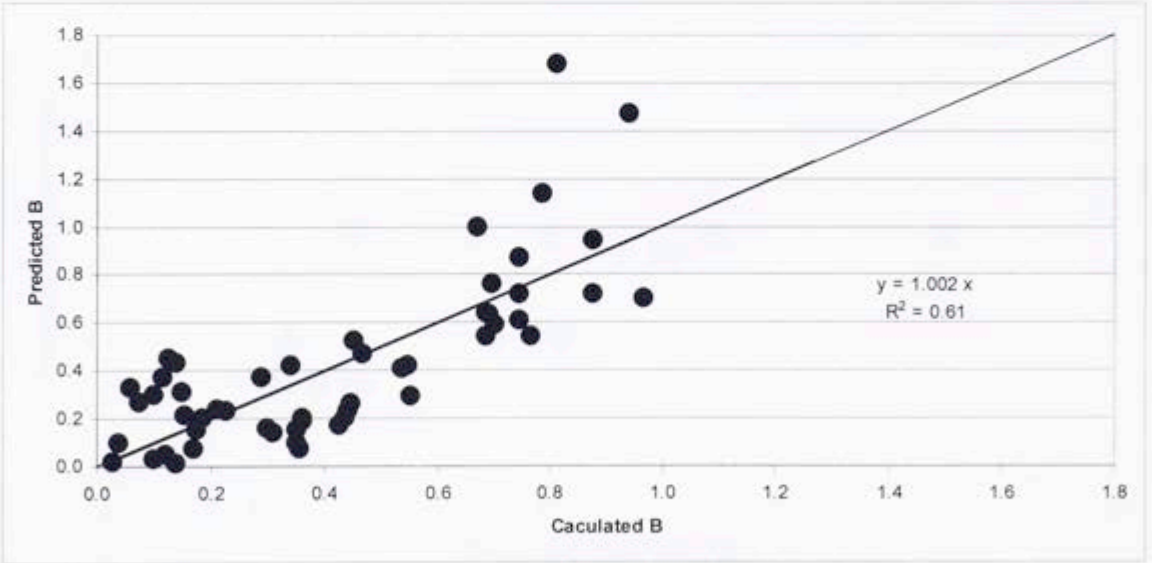


Figure 4.26: Calculated and Predicted Model Parameter B for Power Model

$[B_{pred} = 0.803 - 0.010\ T + 0.053\ A_V$ *(R-squared = 0.61)*$]$

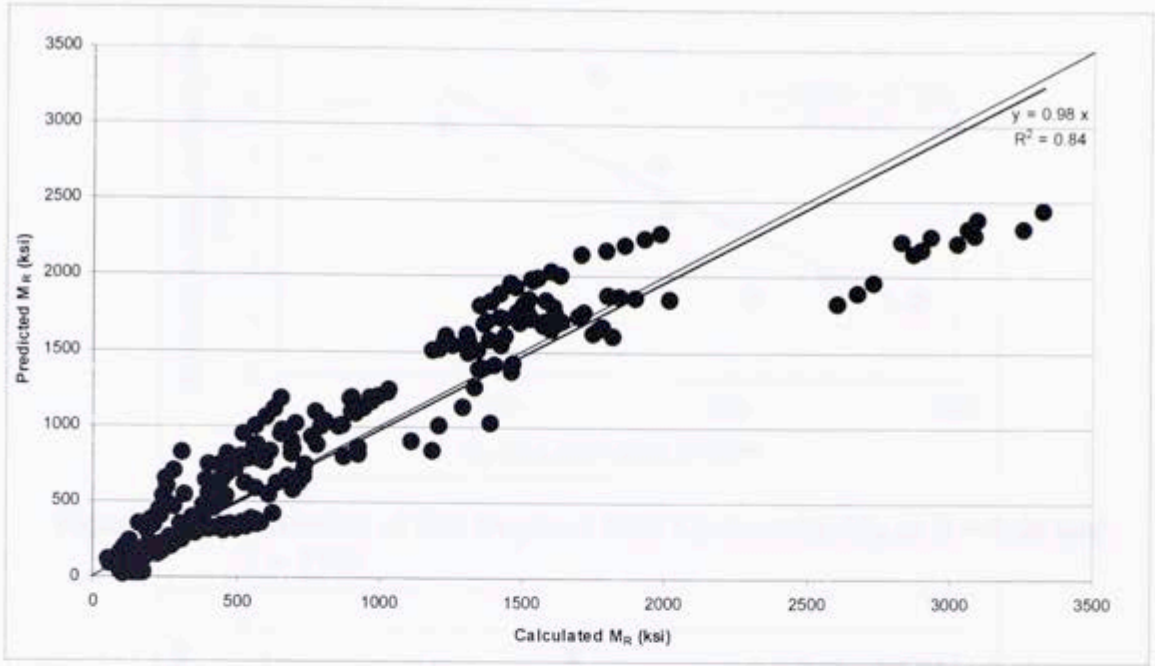


Figure 4.27: Calculated and Predicted M_R from Power Model ($M_R = A\ B^R$)

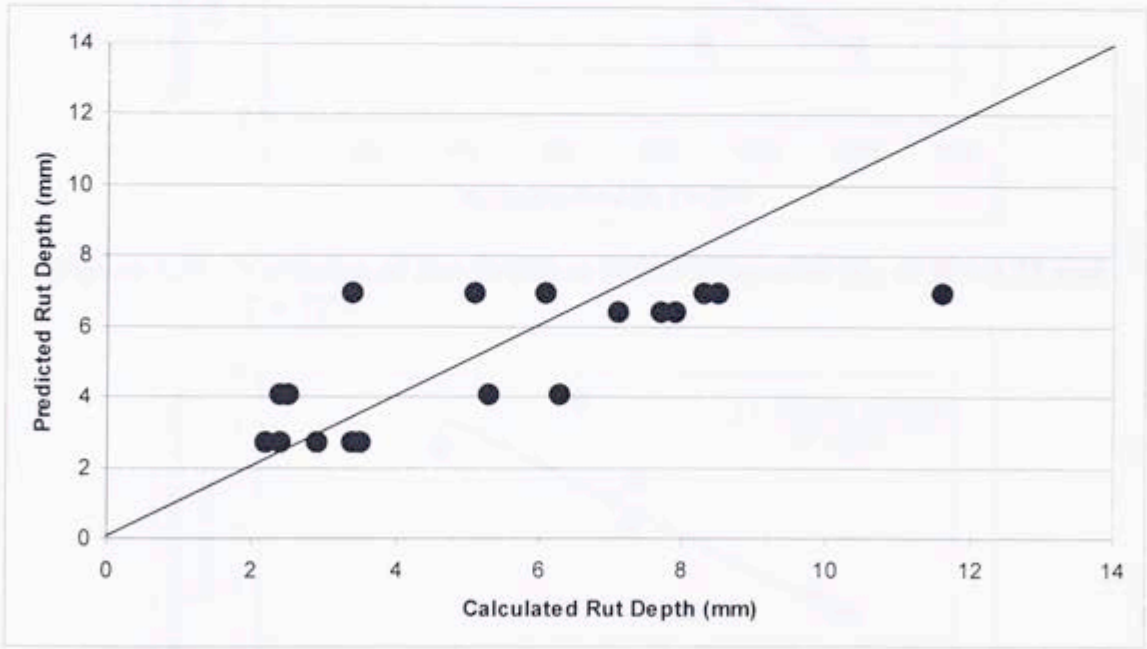


Figure 4.28: Calculated and Predicted Rut Depths

[$\text{Log}\ (\text{Rut}_{\text{Pred}}) = 0.676 + 0.179\ \text{AC} - 0.178\ N_{200}$ *(R-squared = 0.56)*]

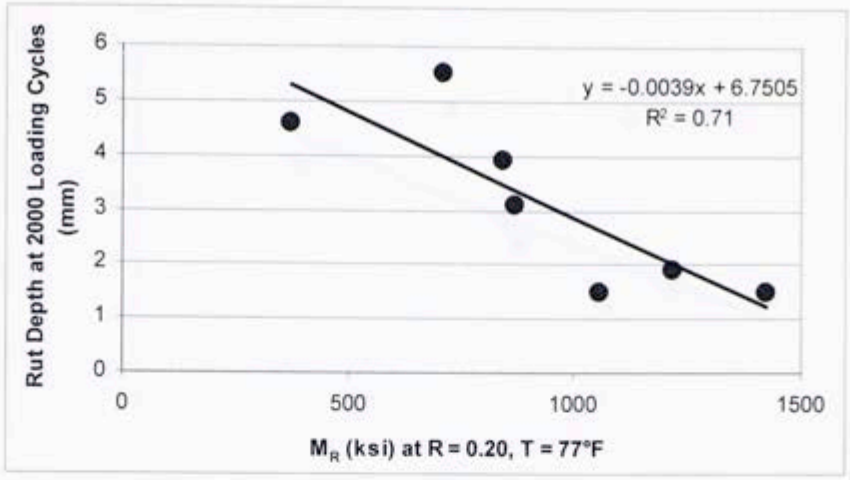


Figure 4.29: Variation of Rut Depth at 2000 Cycles with M_R at R = 0.20 and T = 77°F

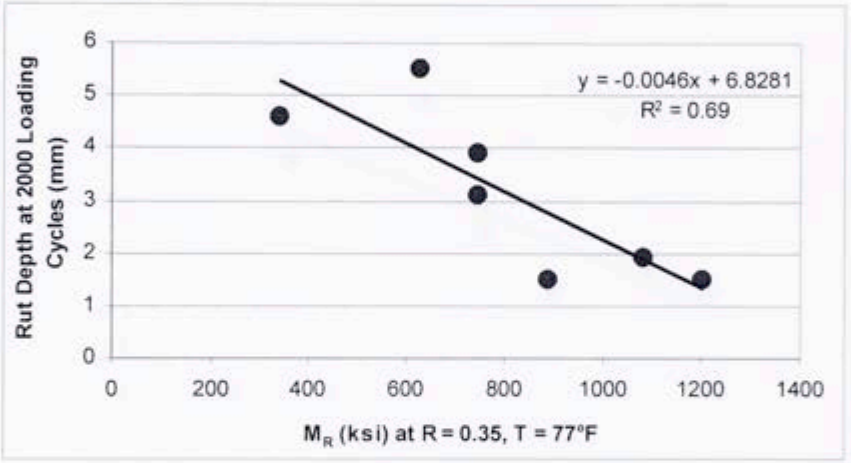


Figure 4.30: Variation of Rut Depth at 2000 Cycles with M_R at R = 0.35 and T = 77°F

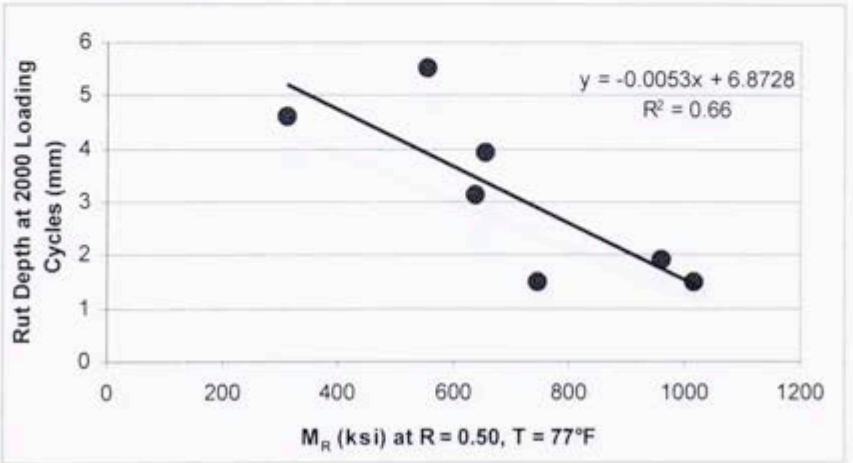


Figure 4.31: Variation of Rut Depth at 2000 Cycles with M_R at R = 0.50 and T = 77°F

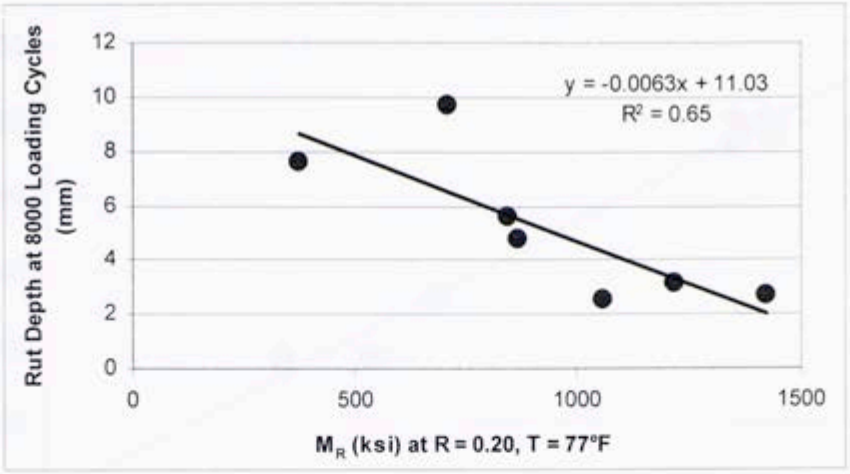


Figure 4.32: Variation of Rut Depth at 8000 Cycles with M_R at R = 0.20 and T = 77°F

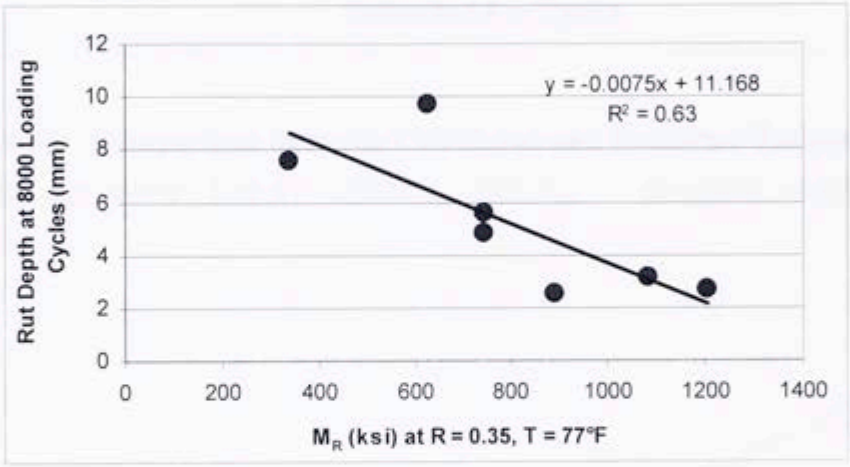


Figure 4.33: Variation of Rut Depth at 8000 Cycles with M_R at R = 0.35 and T = 77°F

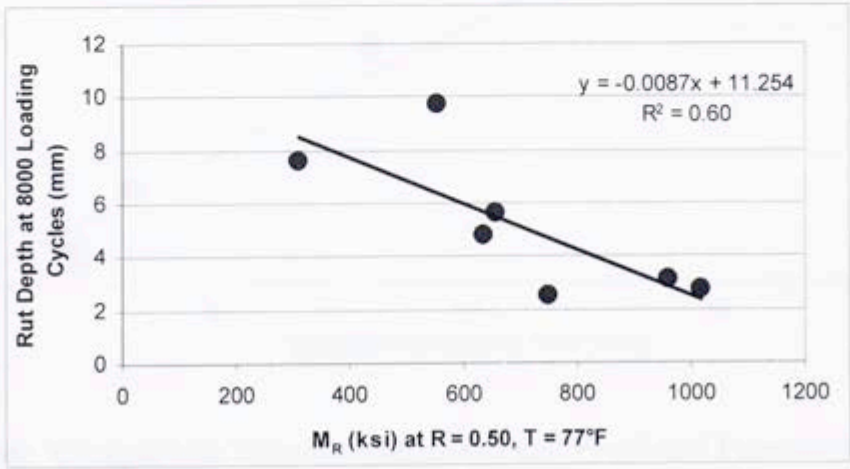


Figure 4.34: Variation of Rut Depth at 8000 Cycles with M_R at R = 0.50 and T = 77°F

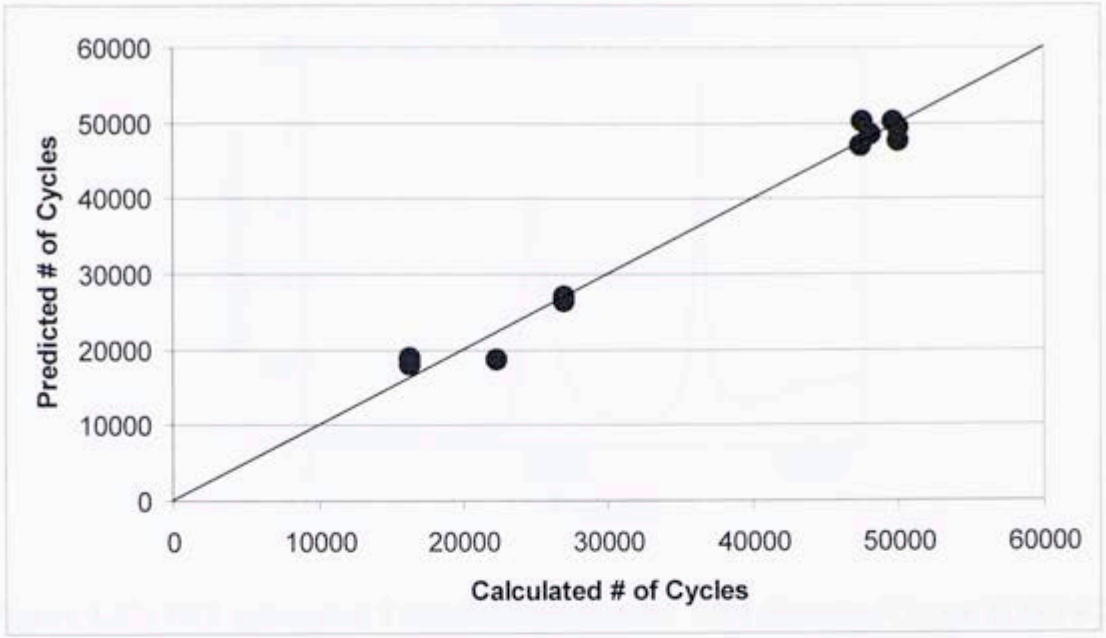


Figure 4.35: Comparison Between Calculated and Predicted Fatigue Cycles

[$N_{f,\,Pred}$ = 826568 - 3370 AV - 279230 G_{se} - 3234 N_{200} *(R-squared = 0.98)*]

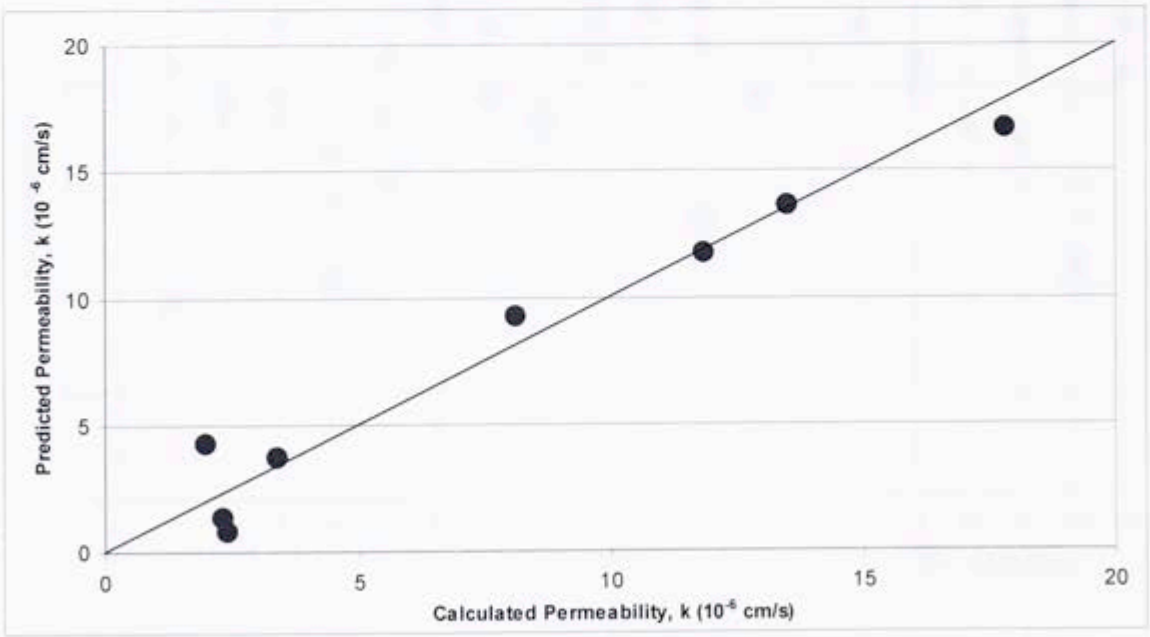


Figure 4.36: Comparison Between Calculated and Predicted Permeability Values

[k_{Pred} = 8.10 + 5.48 AV - 7.15 N_{200} *(R-squared = 0.96)*]

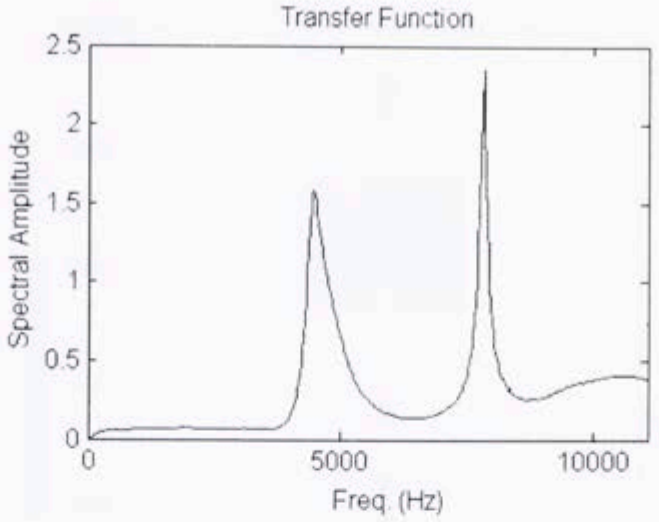


Figure 4.37: FFT generated Transfer Function for NDT Results (Core # 1; Hit # 2)

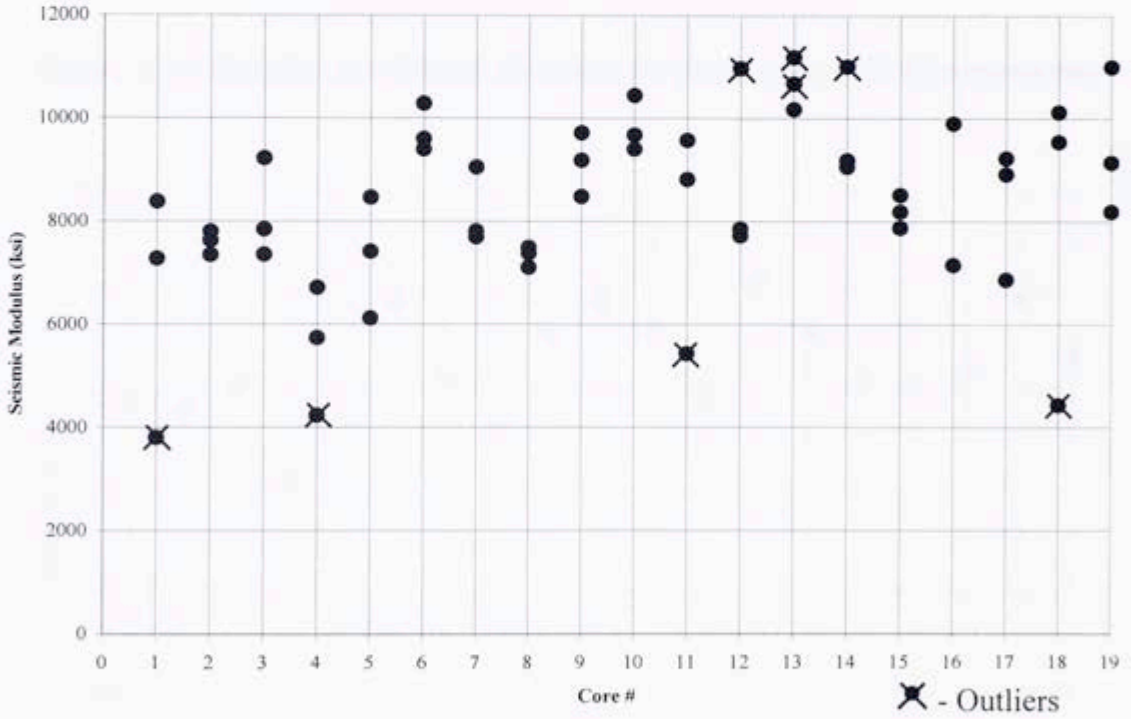


Figure 4.38: Laboratory Seismic Modulus for Davis Cores

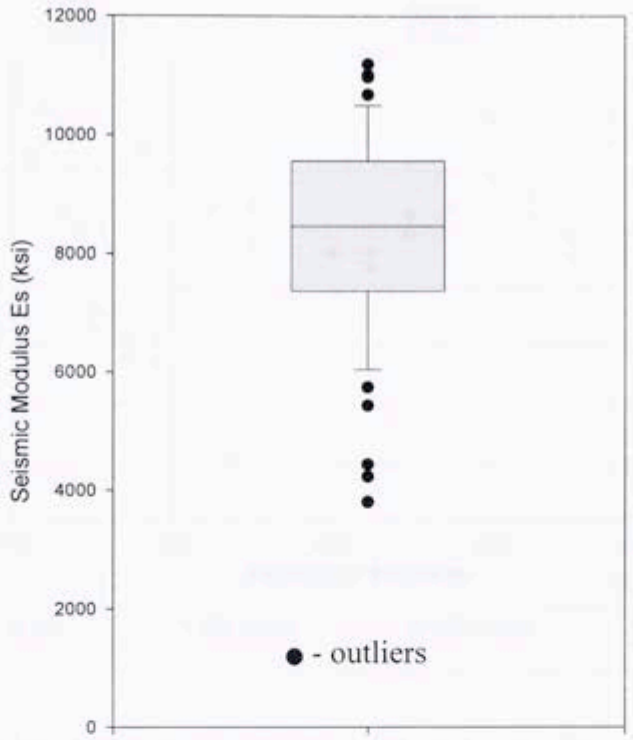


Figure 4.39: Box Plot for Seismic Modulus for Davis Cores (57 Observations)

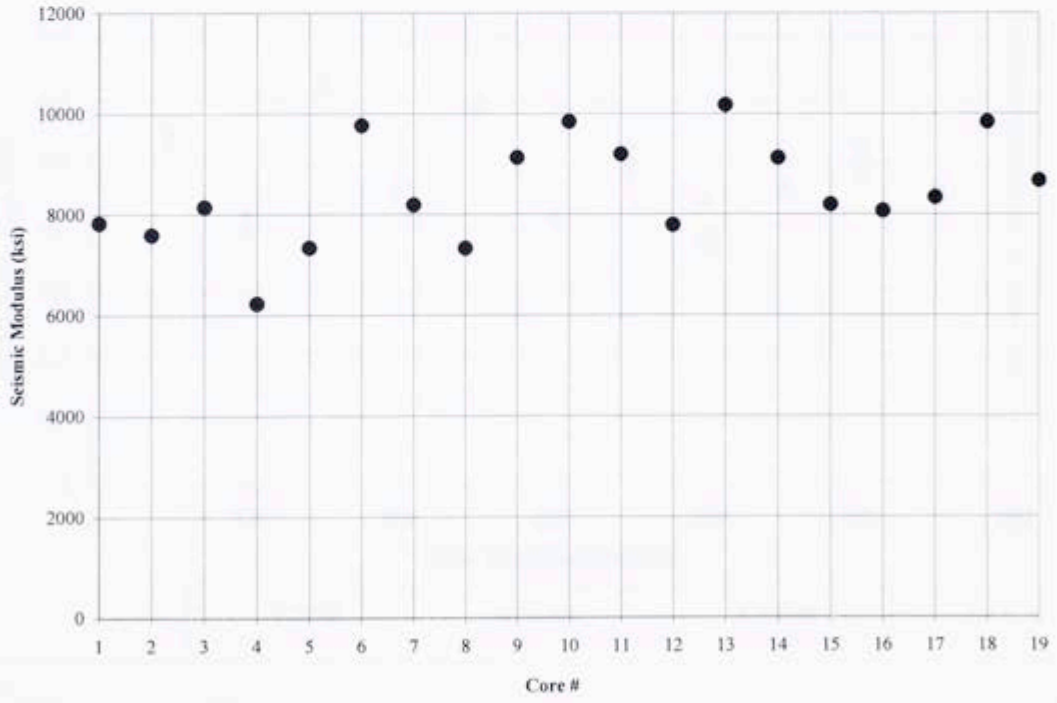


Figure 4.40: Average Laboratory Seismic Modulus for Davis Cores (After Outlier Removed)

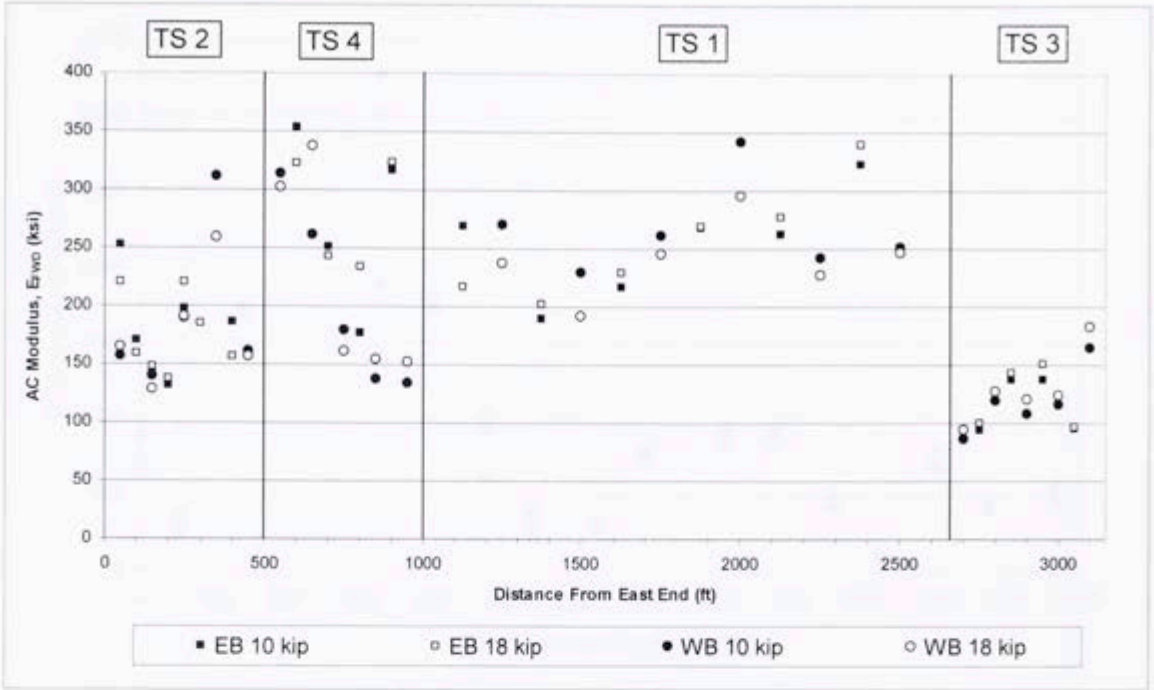


Figure 4.41: FWD Back-calculated Modulus for Tar Creek Site

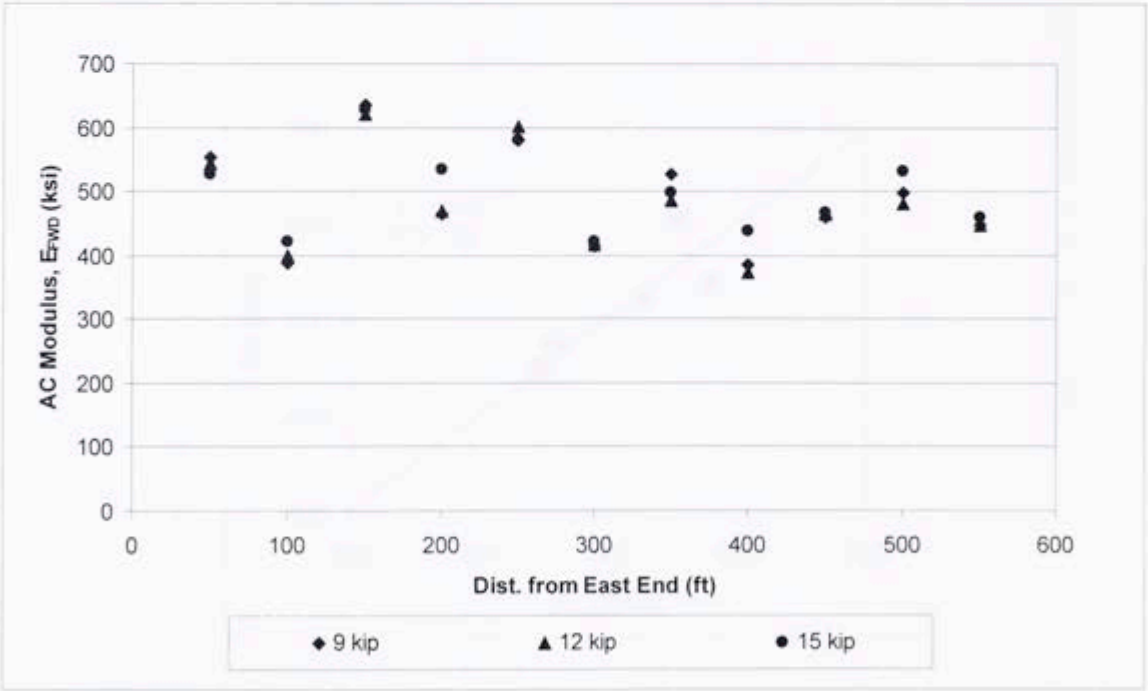


Figure 4.42: FWD Back-calculated Modulus for Davis Site

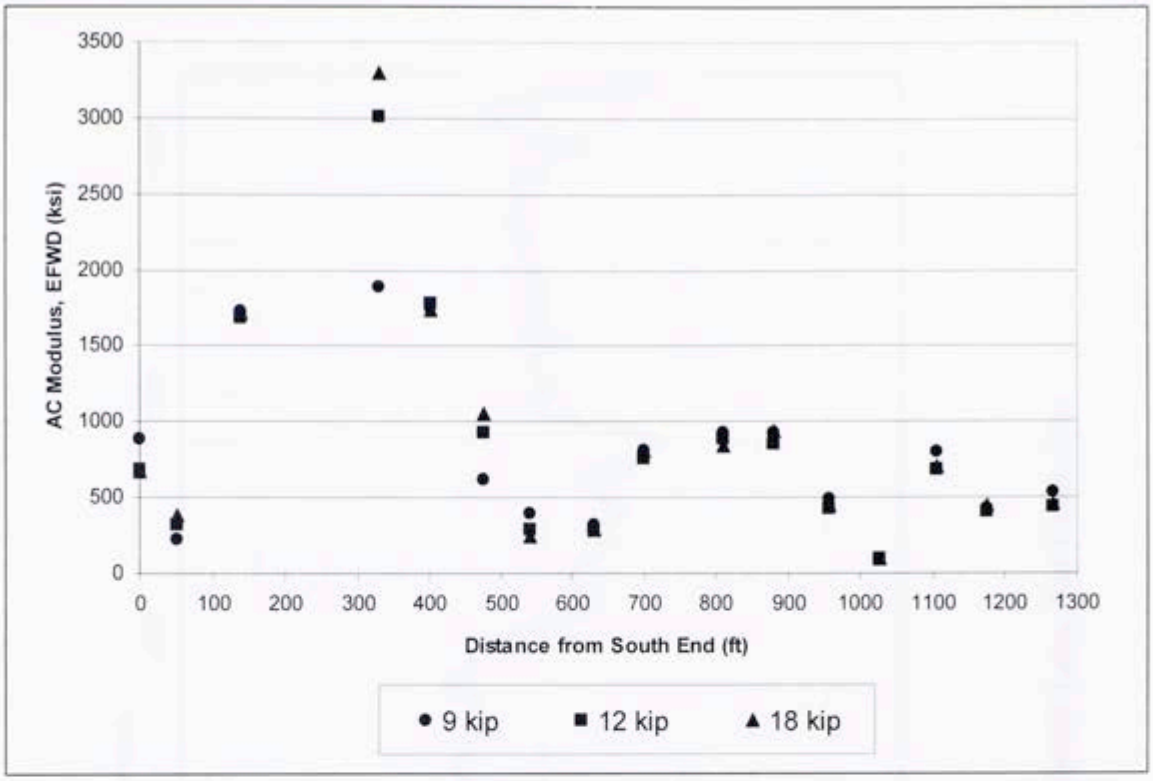


Figure 4.43: FWD Back-calculated Modulus for OKC Site

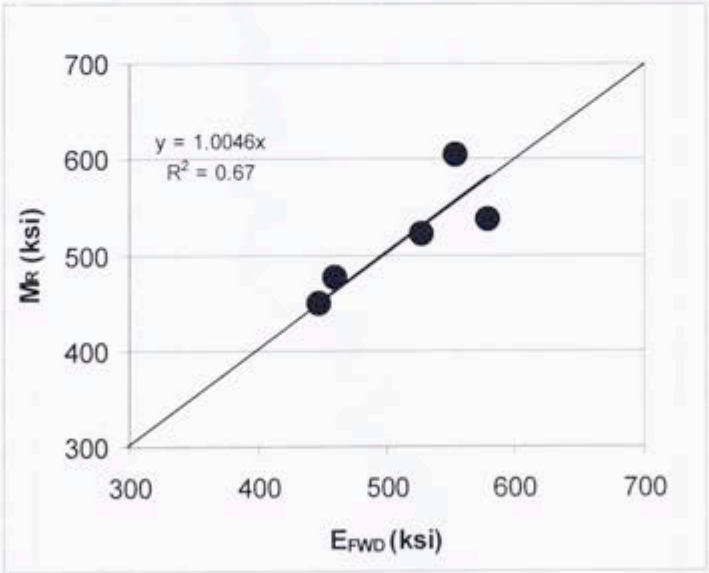


Figure 4.44: Comparison of Laboratory M_R at R = 0.20, E_{FWD} at 9 kip Load for Davis Site

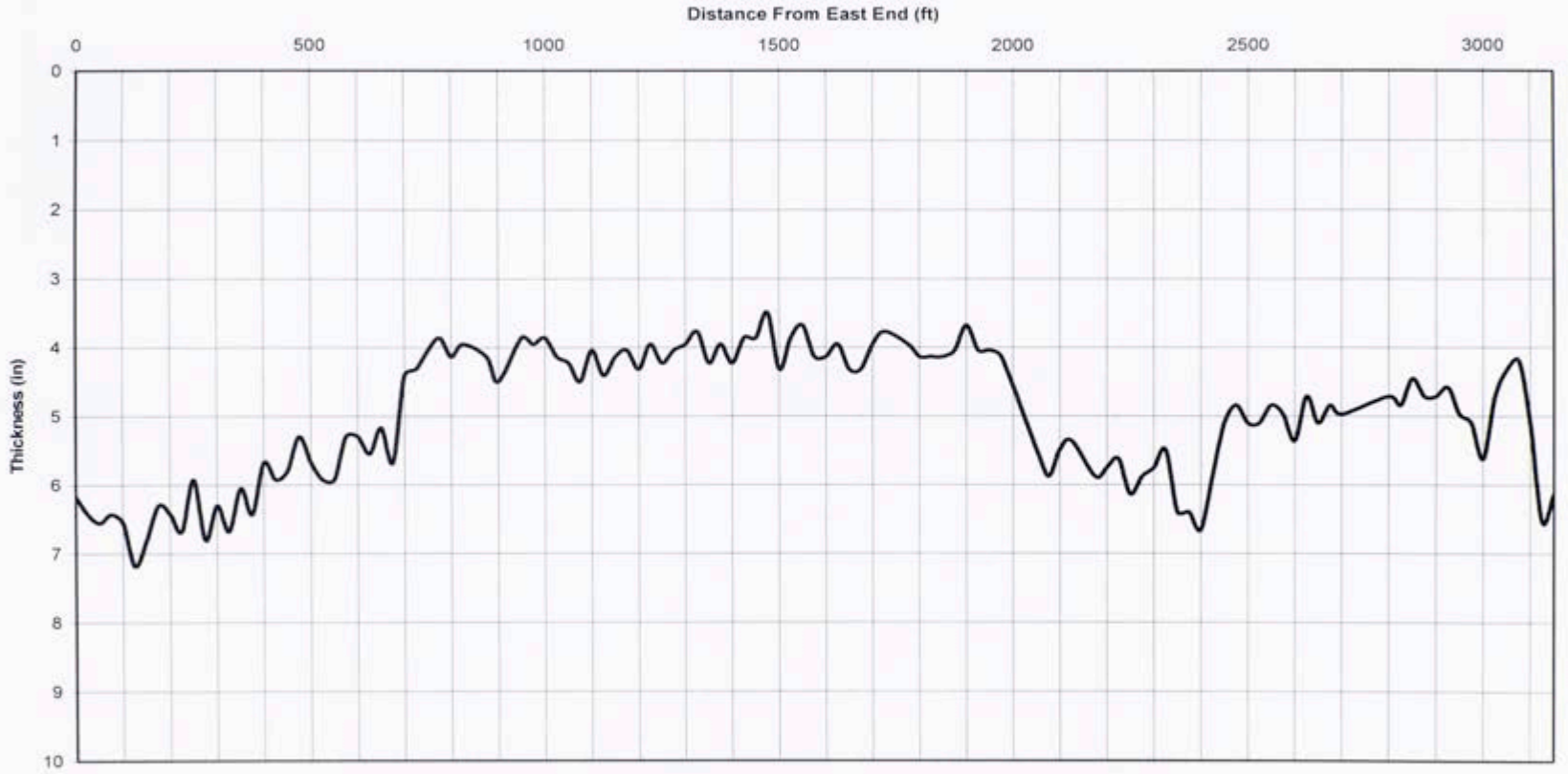


Figure 4.45: GPR Thickness Profile for South Lane, Tar Creek Site

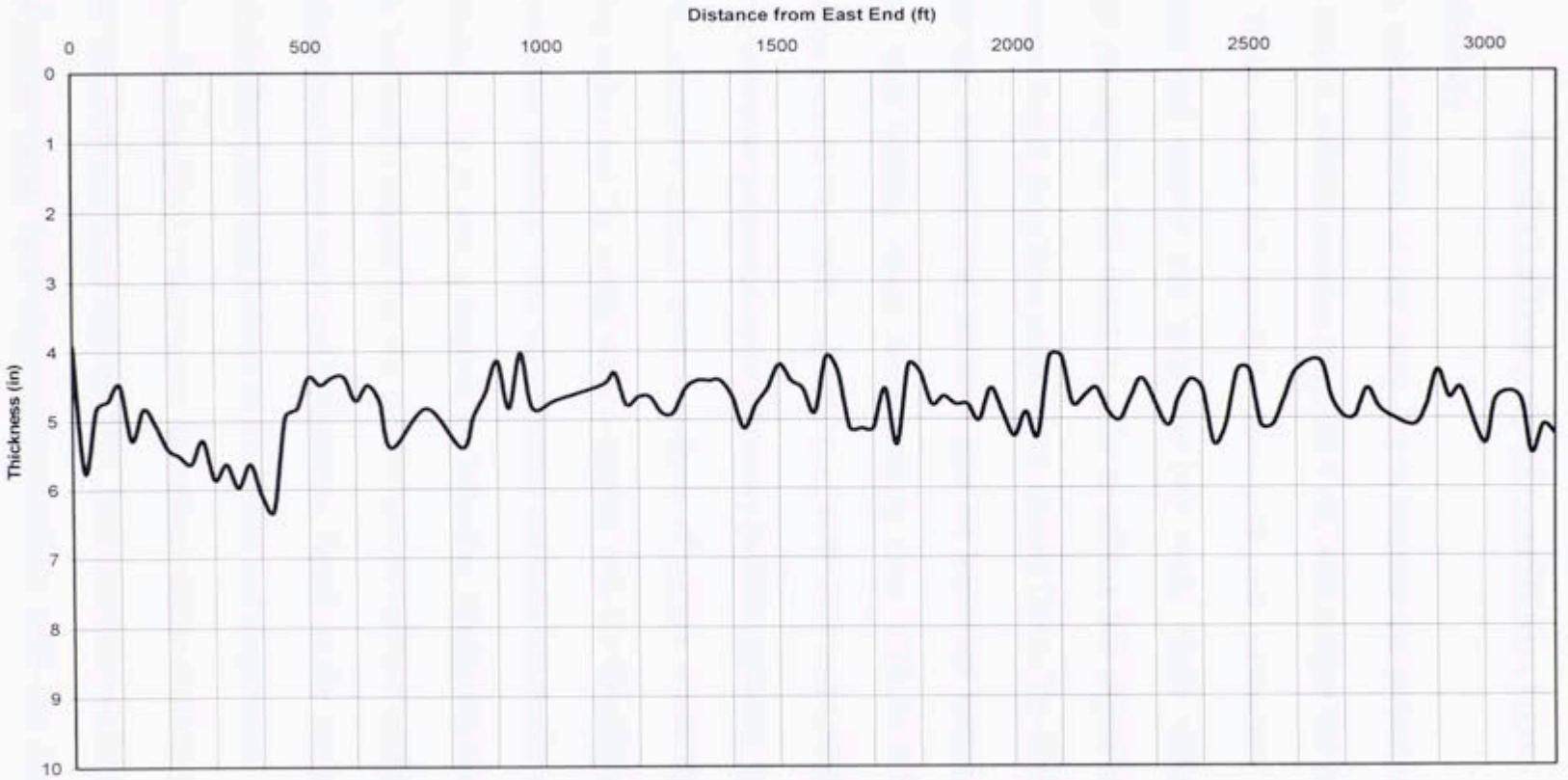


Figure 4.46: GPR Thickness Profile for North Lane, Tar Creek Site

CHAPTER 5

CONCLUSIONS AND RECOMMENDATIONS

5.1. Conclusions

The main objective of this study was to evaluate the performance characteristics (indirect tension resilient modulus (M_R), APA rut, APA fatigue and permeability) of the selected HMA mixes and correlate them with test parameters (stress ratio and temperature) and specific mix properties (air voids, binder content and aggregate percentage passing No. 200 sieve). In order to achieve this objective, four loose HMA mixes were collected from three project sites, namely Davis, Tar Creek and OKC. Field cores were also retrieved from the three sites for laboratory testing. The M_R test was performed with varying stress ratios ranging from 0.15 to 0.70 and three test temperatures, namely 5°C, 25°C and 40°C (i.e., 41°F, 77°F and 104°F). In addition, non-destructive tests were performed in the laboratory (seismic modulus, E_S) and field (falling weight deflectometer (E_{FWD}), spectral analysis of surface waves (E_{SASW}) and ground penetrating radar) and the results were compared with the laboratory resilient modulus results, whenever possible. From the laboratory and field test results, and the analysis of data presented in the preceding chapters, the following conclusions can be drawn:

1. The test results suggest that the indirect tension resilient modulus depends on the applied load (stress ratio) and temperature. Based on the test results, the resilient modulus decreases with increase in stress level and temperature.
2. From the four HMA mixes tested for indirect tensile resilient modulus, the Davis base mix performs better than the OKC base mix followed by the Tar Creek base and surface mixes. An average resilient modulus value at a stress ratio 0.20 and a

test temperature of 25°C (77°F) are 9,811 MPa (1423 ksi) for the Davis base, 7,288 MPa (1057 ksi) for the OKC base, 5,992 MPa (869 ksi) for the Tar Creek base and 2,565 MPa (372 ksi) for the Tar Creek surface specimens. Based on the results of four mixes used in this study, the specific mix properties, namely air voids, binder content, specific gravity of aggregates and sizes of aggregates were identified as the affective factors in the test results.

3. A statistically significant model for resilient modulus with test parameters (stress ratio and temperature), specific mix properties (air voids, binder content and aggregate percentage passing No. 200 sieve) was developed. The resilient modulus correlates well with stress ratio and the model parameters "A" and "B" in the semi-log model. The parameter "A" depends on temperature, air voids, binder content and aggregate percentage passing No. 200 sieve, while the parameter "B" depends on temperature and air voids only.

4. The APA rut results suggest that the Tar Creek mixes are more susceptible to rutting. An average rut depth of the Tar Creek surface mix is 7.6 mm (0.3 in) and that of the base mix is 4.9 mm (0.2 in). The Davis and the OKC base mixes exhibit a lower rutting potential among the mixes. An average rut depth of the Davis base mix is 2.7 mm (0.1 in) and that of the OKC base mix is 2.4 mm (0.1 in). The APA test results for field cores also suggest that the Tar Creek mixes are more susceptible to rutting. The average rut depths are 9.5 mm (0.4 in), 5.6 mm (0.2 in) and 3.1 mm (0.1 in), respectively, for the Tar Creek, the OKC and the Davis cores. The correlations based on the limited results show that the rut depth are functions of binder content and aggregate percentage passing No. 200 sieve.

5. Test Results from this limited study show that resilient modulus may be correlated with APA rut depths. A comparatively high R-squared value of 0.72 was obtained for rut at 2000 loading cycles and laboratory M_R at 40°C (104°F) and a stress ratio of 0.50. However, this correlation may not be applicable to other mixes because it depends on associated test parameters and mechanisms.

6. The APA fatigue results indicate that the Tar Creek specimens have a greater fatigue resistance than the Davis and the OKC mixes. The fatigue cycles for the Tar Creek base and surface mixes are approximately 49,000. On the other hand, the fatigue cycles for the Davis and the OKC mixes are 20,000 and 27,000, respectively. The difference in number of fatigue cycles for different HMA mixes suggest that the fatigue resistance for HMA mixes depends on specific mix properties. Based on the four different HMA mixes tested in this study, the number of fatigue cycles can be correlated with air voids, specific gravity of aggregates and aggregate percentage passing No. 200 sieve.

7. Among the different types of mixes, the Tar Creek surface mix and the OKC base mix have higher permeability values. The average permeability value for the Tar Creek surface mix is 10.8×10^{-6} cm/s (4.3×10^{-6} in/s) and that of the OKC base mix is 14.8×10^{-6} cm/s (5.8×10^{-6} in/s). The Tar Creek base and the Davis base mixes show lower permeability values of approximately 2.4×10^{-6} cm/s (0.9×10^{-6} in/s) and 3.0×10^{-6} cm/s (1.2×10^{-6} in/s), respectively. Based on the permeability values of four HMA mixes tested in this study, there is a strong correlation of permeability with air voids and aggregate percentage passing No. 200 sieve.

8. Laboratory seismic modulus (E_S) of the Davis cores ranges between 41,368 MPa (6,000 ksi) and 68,947 MPa (10,000 ksi) with an average value of 58,336 MPa (8,461 ksi) and a standard deviation of 7,177 MPa (1,041 ksi). Six of the Davis cores tested for both resilient modulus and seismic modulus at room temperature of approximately 25°C (77°F) suggest that the E_S values are 6 to 8 times higher than the M_R values at a stress ratio of 0.20, 7 to 9 times higher than the M_R at a stress ratio of 0.35, and 9 to 10 higher than the M_R at a stress ratio of 0.50.

9. The average FWD back-calculated modulus for the Tar Creek site is approximately 1,751 MPa (254 ksi) for section TS-1, 1,255 MPa (182 ksi) for section TS-2, 841 MPa (122 ksi) for section TS-3, and 1,668 MPa (242 ksi) for section TS-4. The average E_{FWD} values for the Davis and the OKC sites are approximately 3,378 MPa (490 ksi) and 3,875 MPa (562 ksi), respectively. The test results suggest that the laboratory M_R at a stress ratio of 0.20 and E_{FWD} at a load of 40 kN (9 kip) are almost equal for the Davis site. On the other hand, the Tar Creek and the OKC sites show a scattered behavior with compared to laboratory M_R values.

10. The SASW modulus for section TS-2 of the Tar Creek site is approximately 8,618 MPa (1,250 ksi) for the surface layer and 9,308 MPa (1,350 ksi) for the base layer. The corresponding values for sections TS-1 and TS-4 are 4,895 MPa (710 ksi) and 4,275 MPa (620 ksi) for the surface layer and 6,412 MPa (930 ksi) and 5,309 MPa (770 ksi) for the base layer, respectively. Overall, the results show that E_{SASW} is approximately 4 times higher at section TS-4 and 6 times higher at section TS-2 than the corresponding E_{FWD} values.

11. The HMA layer thicknesses obtained from the GPR data are fairly consistent and close to the respective design thicknesses. Only the section TS-2 show a high variation.

5.2. Recommendations

Based on this study, the following recommendations are made for future studies:

1. Since the 2002 AASHTO design guide use dynamic modulus to characterize the HMA mixes. A study correlating dynamic modulus with stress ratio, temperature and mix properties is recommended. Such a study will be useful for the implementation of the 2002 AASHTO Pavement Design Guide.
2. A correlation between resilient modulus and dynamic modulus will also be useful for the HMA mixes used in this study. It is recommended that such a study be undertaken.
3. The number of HMA mixes should be increased to get a better data base. Also, a systematic study with changing mix properties will be more useful to identify the factors affecting the performance characteristics of HMA mixes.
4. The resilient modulus test should be performed at higher temperatures (for example, 64°C, i.e., 147°F, equivalent to rut test temperature) to establish correlations between M_R and APA rut.
5. FWD tests could be performed on pavements with layer thicknesses over 150 mm (6 in) in order to get a better correlation between resilient moduli of laboratory specimens and field cores.

REFERENCES

AASHTO 1993, "*AASHTO Guide for Design of Pavement Structures*," American Association of State Highway and Transportation Officials (AASHTO), Washington, D.C., 1993.

AASHTO T 166 "*Standard Method of Test for Bulk Specific Gravity of Compacted Bituminous Mixtures Using Saturated Surface Dry Specimens*," American Association of State Highway and Transportation Officials (AASHTO), 1993.

AASHTO T 209 "*Standard Method of Test for Theoretical Maximum Specific Gravity and Density of Bituminous Paving Mixtures*," American Association of State Highway and Transportation Officials (AASHTO), 2004.

Abdallah, I., Yuan, D., and Nazarian, S., "*Integrating Seismic and Deflection Methods to Estimate Pavement Moduli*," Transportation Research Record 1755, pp. 43-50, Washington, D.C., 2001.

AI , "*Thickness Design – Asphalt Pavements for Highways and Streets*," Manual Series No. 1, Asphalt Institute, 1981.

Ali, H., and Lobez, A., "*Statistical Analyses of Temperature and Moisture Effects on Pavement Structural Properties Based on Seasonal Monitoring Data*," Transportation Research Record 1540, Washington, D.C., 1996.

Almudaiheem, J.A., and Al-Sugair, F.H., "*Effect of Loading Magnitude on Measured Resilient Modulus of Asphaltic Concrete Mixes*," Transportation Research Record 1317, pp. 139-144, Washington, D.C., 1991.

Anderson, R.M., Turner, P.A., Peterson, R.L., and Mallick, R.B., "*Relationship of Superpave Gyratory Compaction Properties to HMA Rutting Behavior*," NCHRP Report 478, Transportation Research Board, Washington, D.C., 2002.

Ashworth, L., "F*actors Affecting Rutting Potential of Superpave Asphalt Mixtures in New Brunswick*," M.S. Thesis, The University of New Brunswick, USA, August, 2003.

ASTM D 3497, "*Dynamic Modulus of Asphalt Mixtures*," American Society of Testing Materials, Vol. 04.03, 1995.

ASTM D 4123, "*Indirect Tension Test for Resilient Modulus of Bituminous Mixtures*," American Society of Testing Materials, Vol. 04.03, 1995.

ASTM D 4694, "*Standard Test Method for Deflections with a Falling-Weight-Type Pulse Load Device*," American Society of Testing Materials, Vol. 04.03, 2003.

Bai, X., "*Assessment of Relationship between Dynamic and Seismic Moduli of Asphalt Concrete Mixtures,*" M.S. Thesis, the University of Texas at El Paso, December 2004.

Bandara, N., and Briggs, R.C., "*Non-destructive Testing of Pavement Structures,*" American Society for Non-destructive Testing, Inc., Vol. 62, No. 7, pp. 733-740, July, 2004.

Barksdale, R.D., Khosla, P., Kim, R., Lambe, P., and Rehman, M., "*Laboratory Determination of Resilient Modulus for Flexible Pavement Design,*" Final Report, NCHRP Project 1-28, USA, 1997.

Bhasin, A., Button, J.W., and Chowdhury, A., "*Evaluation of Simple Performance Tests on HMA Mixtures,*" Project summary report 9-558-S, Texas Transportation Institute, The Texas A&M University System, August, 2005.

Blakey, F.A., and Beresford, F.D., "*Tensile Strain in Concrete*," Part II, Report No. C2. 2-2, Division of Building Research, Melbourne, 1955.

Bonnaure, F.B., Huibers, A.H.J.J., and Boonders, A., "*A Laboratory Investigation of the Influence of Rest Periods on the Fatigue Characteristics of Bituminous Mixes,*" Proceedings, Association of Asphalt Paving Technologists, Vol. 51, Missouri, 1982.

Boudreau, R.L., Hicks, R.G., and Furber, A.M., "*Effects of Test Parameters on Resilient Modulus of Laboratory-Compacted Asphalt Concrete Specimens,*" Transportation Research Record No. 1353, pp. 46-52, Washington, D.C., 1992.

Brandon, J.M., Jared, D.M., Wu, P.Y., and Geary, G.M., "*Field and Laboratory Investigation of Permeable Asphalt Mixes on Georgia Highways,*" Transportation Research Record 1891, pp. 32-39, Washington, D.C., 2004.

Brown, E.R., and Cross, S.A., "*A Study of In-Place Rutting of Asphalt Pavements,*" NCAT Report 89-02, National Centre for Asphalt Technology, Auburn, AL, April, 1989.

Brown, E.R., and Foo, K.Y., "*Evaluation of Variability in Resilient Modulus Test Results (ASTM D 4123),*" NCAT Report, No 91-6, USA, 1989.

Brown, E.R., Prowel, B., Cooley, A., Zhang, J., and Powell, R.B., "*Evaluation of Rutting Performance on the 2000 NCAT Test Track,*" Asphalt Paving Technology: v 73, Association of Asphalt Paving Technology 2004, pp. 287-336, 2004.

Buchanan, M., "*Evaluation of the Effect of Flat and Elongated Particles on the Performance of Hot Mix Asphalt Mixtures,*" NCAT Report 00-03, National Centre for Asphalt Technology, May, 2000.

Chehab, G.R., O'Quinn, E., and Kim, R., "*Specimen Geometry Study for Direct Tension Test Based on Mechanical Tests and Air Void Variation in Asphalt Concrete Specimens Compacted by Superpave Gyratory Compactor*," Transport Research Record 1723, pp. 125-132, Washington, D.C., 2000.

Choubane, B., Page G.C., and Musselman J.A., "*Investigation of Water Permeability of Coarse graded Superpave Pavements*," Journal of the Association of Asphalt Paving Technologists, Vol. 67, pp. 254-276, 1998.

Choubane, B., Page, G.C., and Musselman, J.A., "*Suitability of Asphalt Pavement Analyzer for Predicting Pavement Rutting*," Transportation Research Record 1723, pp. 107-115, Washington, D.C., 2000.

Christensen, W. D., Bonaquist, R., and Jack, D.P., "*Evaluation of Triaxial Strength as a Simple Test for Asphalt Concrete Rut Resistance*," Final Report, Pennsylvania Department of Transportation, 2000.

Christopher, W.R., and Prowell, B.D., "*Comparison of Laboratory Wheel Tracking Test Results with WesTrack Performance*," Transportation Research Record 1681, Washington, D.C., 1999.

Collins, R., Watson, D.E., and Cambell, B., "*Development and Use of Georgia Loaded Wheel Tester*," Transportation Research Record 1492, Washington, D.C., 1995.

Collins, R., Johnson, A., Wu, Y., and Lai, J., "*Evaluation of Moisture Susceptibility of Compacted Asphalt Mixtures by the Asphalt Pavement Analyzer*," Transportation Research Board, Washington, D.C., January, 1997.

Cooley, L.A., and Brown, E.R., "*Selection an Evaluation of a Field Permeability Device for Asphalt Pavements*," Presented at the 79th Annual Meeting of the Transportation Research Board, Washington, DC, 2000.

Cooley L.A., Brown, E.R., and Maghsoodloo, S., "*Developing Critical Field Permeability and Pavement Density Values for Coarse-graded Superpave Pavements*," Transportation Research Record 1761, pp. 41-49, Washington, D.C., 2001.

Crovetti, J., Hall, K.T., and Williams, C., "*Wisconsin Highway Research Program #0092-03-14 Development of Modulus to Temperature Relations for HMA Mixtures Used in Wisconsin*," Final Report, Wisconsin Department of Transportation, September 2005.

Cruz, J. "*Permeability of Hot-Mix Asphalt Concrete*," M.S. Thesis, University of Arkansas, Fayetteville, May 2000.

Epps. J.A., and Monismith, C.L., "*Fatigue of Asphalt Concrete Mixtures – Summary of Existing Information*," STP 508, pp. 19-45, 1972.

Finn, F., and Epps, J., "*Compaction of Hot Mix Asphalt Concrete*," Research Report 214-21, Texas Transportation Institute, August 1980.

Gandara, J.A., "Characterization of Texas Bases Through Permanent Deformation Testing," M.S. Thesis, the University of Texas at El Paso, December 2004.

Geovision, "*Geovision Geophysical Services*," Corona, CA 928882.
URL: http://www.geovision.com/seismic.htm

Hall, K.D., "*Comparison of Falling –Head and Constant Head Techniques*," Transportation Research Record 1891, pp. 23-31, Washington, D.C., 2004.

Harvey, J., Eriksen, K., Sousa, J., and Monismith, C.L., "*Effects of Laboratory Sample Preparation on Aggregate-Asphalt Structure, Air Void Content Measurement and Repetitive Simple Shear Test Results*," Transportation Research Record 1454, pp. 113-122, Washington, D.C., 1994.

Healow, S.P., "*Analysis and Development of Performance Models for WesTrack*," M.S. Thesis, University of Nevada, Reno, May 1998.

Hondros, G., "*The Evaluation of Poisson's Ratio and the Modulus of Materials of a Low Tensile Resistancy by the Brazilian (Indirect Tensile) Test with Particular Reference to Concrete*," Australian Journal of Applied Science, Vol. 10, No. 3, pp. 243-268, 1959.

Hossain, M., and Scofield, L.A., "*Correlation between Back Calculated and Laboratory-Determined Asphalt Concrete Moduli*," Transportation Research Record 1377, pp. 67-76, Washington, D.C., 1992.

Huang, B., Mohammad, L., Raghavendra, A., and Abadie C., "*Fundamentals of Permeability in Asphalt Mixtures*," Journal of the Association of Asphalt Paving Technologists, Vol. 68, pp. 479-500, 1999.

Huang, Y.H., "*Pavement Analysis and Design*," 2nd Edition, Prentice Hall Inc, NJ, USA, 2004.

Huber, G., and Heiman, G., "*Effects of Asphalt Concrete Parameters on Rutting Performance: A Field Investigation*," Proceedings of the Association of Asphalt Paving Technologists, Vol. 56, 1987.

Hughes, M., "*Sub-grade Stabilization Using Unwashed Mine Tailings From The Tar Creek Superfund Site*," A Report Submitted to Oklahoma Department of Transportation, Oklahoma State University, Stillwater, OK, 2002.

Joh, S.H., "*Advances in Interpretation and Analysis Techniques for Spectral-Analysis-of-Surface-Waves (SASW) Measurements*," Ph.D. Dissertation, University of Texas at Austin, Austin, TX, 1996.

Katicha, S.W., "*Development of Laboratory to Field Shift Factors for Hot Mix Aspahlt Resilient Modulus*," M.S. Thesis, Virginia Polytechnic Institute and State University, November 2003.

Kandhal, P.S., and Cooley, L.A., "*Evaluation of Permanent Deformation of Asphalt Mixtures using Loaded Wheel Tester*," Asphalt Paving Technology: Association of Asphalt Paving Technologists-Proceedings of the Technical Sessions, v 71, pp. 739-753, 2002.

Kandhal, P.S., and Mallick, R.B., "*Evaluation of Asphalt Pavement Analyzers for HMA Mix Design*," National Center for Asphalt Technology, NCAT Report No. 99-4, pp. 34, Auburn, AL, 1999.

Kanitpong, K., Bahia, H.U., Benson, C.H., and Wang, X., "*Effect of Lift Thickness and Flow Direction on Hydraulic Conductivity (Permeability) of Laboratory Compacted Asphalt Mixtures*," Presented at the 81st Annual Meeting of the Transportation Research Board, Washington, D.C., 2002.

Kanitpong, K., Bahia, H.U, Benson, C., and Wang, X., "*Measuring and Predicting Hydraulic Conductivity (Permeability) of Compacted Asphalt Mixtures in the Laboratory*," 82nd Annual Meeting of the Transportation Research Board. Washington, D.C., 2003.

Kennedy, T.W., and Hudson, W.R., "*Application of the Indirect Tensile Test to Stabilized Materials*," Highway Research Record 235, Highway Research Board, Washington, D. C., 1968.

Khanna, V., "Advancing Pavement Management with SASW and IR." Ph.D. Dissertation, University of Oklahoma, Norman, OK, 2006 (expected).

Kim, Y.R., Allen, D.H., and Little, D.N., "*A Computational Model to Predict Fatigue Damage Behavior of Asphalt Mixtures Under Cyclic Loading*," Transportation Research Board, TRB 2006 Annual Meeting, Washington, D.C., 2006.

Kim, Y.R., Seo, Y., King, M., and Momen, M., "*Dynamic Modulus Testing of Asphalt Concrete in Indirect Tension Mode*," Transportation Research Record 1891, pp. 163-173, Washington, D.C., 2004.

Kruger, J., and Horak, E., "*The Appropriateness of Accelerated Pavement Testing to Asses the Rut Prediction Capability of Laboratory Asphalt Tests*," Transport Challenge for 2010, 24th Annual Southern African Transport Conference, pp. 380-390, 2005.

Liu, W., and Scullion, T., "*MODULUS 5.0 for Windows*," Software Program, Texas Transportation Institute, Texas Department of Transportation, Austin, TX, 2000.

Loulizi, A., Flintsch, G.W., Al-Qadi, I.A., and Mokarem, D., "*Comparison between Resilient Modulus and Dynamic Modulus of Hot-Mix Asphalt as Material Properties for Flexible Pavement Design*," Transportation Research Board, 85th Annual Meeting, Washington, D.C., Jan, 2006.

Mallick, R.B., Cooley, Jr., L.A., Teto, M.R., Bradbury, R.L., and Peabody, D., "*An Evaluation of Factors Affecting Permeability of Superpave Designed Pavements,*" NCAT Report 03-02, National Center for Asphalt Technology, June, 2003.

Maupin, Jr., G.W., "*Asphalt Permeability Testing in Virginia*," Presented at the 79th Annual Meeting of the Transportation Research Board, Washington, DC, 2000.

McClave, J., Benson, G., and Sincich, T., "*Statistics for Business and Economics,*" Prentice Hall, Upper saddle River, NJ, 2001.

McWilliams, C.E., "*Air and Water Permeability related to Asphalt Mix Characteristics*," M.S. Thesis, University of Arkansas, Fayetteville, 1986.

Mindess, S., Young, J.F., and Darwin, D., "*Concrete*," 2nd Edition, Prentice Hall Inc., Englewood Cliffs, NJ, 2002.

Mohammad, L. N., Herath, A., and Huang, B., "*Evaluation of Permeability of Superpave Asphalt Mixtures*," Transportation Research Record 1832, pp. 50–58, Washington, D.C., 2003.

Mohammad, L.N., Wu, Z., Zhang, C., Khattak, M.J., Abadie, C., and Hewitt, J.W., "*Variability of Air Voids and Mechanistic Properties of Plant Produced Asphalt Mixture*," Transportation Research Record 1891, pp. 85-102, Washington, D.C., 2004.

MTS "*User Information and Software References,*" MTS System Corporation, 100-077-223 J, Eden Prairie, MN, 2005.

National Cooperative Highway Research Program, "*Development of the 2002 Guide for the Design of New and Rehabilitated Pavement Structures*," NCHRP Project, No. 1-37 A, Washington, D.C., 2004.

Nazarian, S., Abdallah, I., Meshkani, A., and Ke, L., "*Use of Resilient Modulus Test Results in Flexible Pavement Design*," ASTM Special Technical Publication, No. 1437, pp. 3-15, 2002.

Nazarian, S., Abdallah, I., and Yuan, D., "*Neural Networks for Rapid Reduction Interpretation of Spectral Analysis of Surface Waves Results*," Transportation Research Record 1868, pp. 150-155, Washington, D.C., 2004.

Nazarian, S., Yuan, D., Smith, K., Ansari, F., and Gonzalez, C., "*Acceptance Criteria of Airfield Concrete Pavement Using Seismic and Maturity Concepts: Appendices*," Innovative Pavement Research Foundation, Report IPRF 01-G-002-02-2, May, 2006.

Nazarian, S., Stokoe, K.H., Briggs, R.C, and Rogers, R., "*Determination of Pavement Layer Thicknesses and Moduli by SASW Method*," Transportation Research Record 1196, pp. 133-150, Washington, D.C., 1988.

Nazarian, S., Yuan, D., and Williams, R. R., "*A Simple Method for Determining Modulus of Base and Subgrade Materials*," Resilient Modulus of Testing for Pavement Components, ASTM STP 1437, West Conshohocken, PA, 2003.

OHD L-43, "*Method of Test for Determining Rutting Susceptibility Using the Asphalt Pavement Analyzer*," Department Test Methods, Oklahoma Department of Transportation, 2003.

OHD L-44, "*Method of Test for Measurement of Water Permeability of Compacted Paving Mixtures*," Department Test Methods, Oklahoma Department of Transportation, 2003.

OHD L-45, "*Method of Test for Determining the Specific Gravity and Unit Weight of Compacted Bituminous Mixtures Using the CORELOK Apparatus*," Department Test Methods, Oklahoma Department of Transportation, 2003.

Prowell, B.D., and Dudley, M.C., "*Evaluation of Measurement Techniques for Asphalt Pavement Density and Permeability*," Transportation Research Record 1789, pp. 36-45, Washington, D.C., 2002.

Roberts, F.L., Kandhal, P.S., Brown, E.R., Lee, D.Y., and Kennedy, T.W., "*Hot mix asphalt materials, mixture design and construction*," 2nd ed. Lanham, MD: NAPA Research and Education Foundation, 1996.

Roddis, W.M.K., Maser, K., and Gisi, A.J., "*Radar Pavement Thickness Evaluation for Varying Base Conditions,*" Transportation Research Record 1355, pp. 90-98, Washington, D.C., 1992.

Roque, R., and Buttlar, W.G., "*The Development of a Measurement and Analysis System to Accurately Determine Asphalt Concrete Properties Using the Indirect Tensile Mode*," Draft for Association of Asphalt Paving Technologists, Annual Meeting, Charleston, South Carolina, 1992.

Salem, H.M., "*Quantification of Environmental Impacts on the Performance of Asphalt Pavements*," Ph.D. Dissertation, University of Idaho, June 2004.

Salem, H.M., Bayomy, F.M., Al-Taher, M.G., and Genc, I.H., "*Using Long-term Pavement Performance Data to Predict Seasonal Variation in Asphalt Concrete Modulus*" Transportation Research Record 1896, pp. 119-128, 2004.

Schmidt, R.J., "*A Practical Method for Measuring the Resilient Modulus of Asphalt Treated Mixes*," Highway Research Record 404, National Research Council, Washington, D.C., 1972.

Shalaby, A., Liske, T., and Kavussi, A., "*Comparing Back Calculated and Laboratory Resilient Moduli of Bituminous Paving Mixtures*," Canadian Journal of Civil Engineering, v 31, No. 6, pp. 988-996, December, 2004.

SHRP Protocol P07, "*Resilient Modulus of Asphalt Concrete*," Long Term Pavement Performance (LTPP) Program Directive M-1, November 1992.

Srinivasan, G., "*Evaluation of Indirect Tensile Strength to Identify Asphalt Concrete Rutting Potential*," M.S. Thesis, West Virginia University, Morgantown, West Virginia, 2004.

Tangella, S.C.S.R., Craus, J., Deacon, J.A., and Monismith, C.L., "*Summary Report on Fatigue Response of Asphalt Mixtures*," TM-UCB-A-003A-89-3, Prepared for Strategig Highway Research Program, Project A-003-A, February, 1990.

Tarefder, R.A., "*Laboratory and Model Prediction of Rutting in Asphalt Concrete*," Ph.D. Dissertation, University of Oklahoma, December 2003.

Tarefder, R.A. and Zaman, M., "*Correlating Asphalt Concrete Modulus with Rut Potential,*" Proc. Third International Symp. on Maintenance and Rehabilitation of Pavements and Technological Control, held on July 7-10, 2003 in Portugal, Vol. 1, pp. 207-217, 2003.

Tarefder, R.A., and Zaman, M., "*Resilient Modulus Testing and Density Gradient Analysis of Selected Asphalt Mixes*," Final Report, Planning and Research Division, Oklahoma Department of Transportation, USA, July 2004.

Tarefder, R.A., Zaman, M., and Hobson, K., "*A laboratory and Statistical Evaluation of Factors Affecting Rutting.*" The International Journal of Pavement Engineering, Vol. 4 (1), pp. 59-68, March, 2003.

Teng, T.P., "*Performance of Coarse-Graded Mixes at WesTrack Premature Rutting*," Federal Highway Administration, Final Report, June, 1998.

Teredesai, R.V., "*Stabilization of Pile Run Chat for Roadway Base Application*," M.S. Thesis, University of Oklahoma, Norman, December 2005.

Teredesai, R.V., Zaman, M., Miller, G., and Nairn, R., "*A Study to Optimize Use of Raw Chat in Stabilized Base Construction,*" A Report Prepared for Oklahoma Department of Environmental Quality, Oklahoma City, OK, 2005.

Timoshenko, S., and Goodier, J., "*Theory of Elasticity*," McGraw Hill Book Company, September 1970.

U.S. Department of Transportation, "*Ground Penetrating Radar for Measuring Pavement Layer Thickness*," U.S. Department of Transportation-Federal Highway Administration, Pub. No. FHWA-HIF-00-015, 2005(a).

U.S. Department of Transportation, "*Ground Penetrating Radar (GPR)*," Federal Lands Highway Program, U.S. Department of Transportation- Federal Highway Administration, 2005(b).

Wahnee, K., Coursey, K., Norton, A., Jefferson, M., Cogburn, M., Kimbro, M., Lipe, S., Rhoney, K., BilesT., Pankop, A., Sprowl, M., Suiter, J., Tsai, S., Gillespie, C., Athay, D., Wolfard, T., Alcazar, A., Stearns, C., and Pham, V., "*Development of Holistic Remediation Alternatives for the Catholic 40 and Beaver Creek*," Environmental Capstone Project, Civil Engineering and Environmental Science, University of Oklahoma, Norman, OK, 2000.

Wallace, K., and Monismith, C.L., "*Diametral Modulus Testing on Nonlinear Pavement Materials*," Proceedings, Association of Asphalt Paving Technologists, Vol. 49, Louisville, Kentucky, 1986.

Wasiuddin, N., Zaman, M., and Nairn, R., "*A Laboratory Study to Optimize the Use of Raw Chat in Hot Mix Asphalt for Pavement Application*," A Report Prepared for Oklahoma Department of Environmental Quality, Oklahoma City, OK, 2005.

Wasiuddin, N., Zaman, M., Nairn, R., and Kolothody, N., "*Characteristics of Chat-Asphalt for Road Base Application,*" Submitted for Possible Publication in the Journal of Solid Waste Technology and Management, January, 2006.

Williams, C.R., and Prowell, B.D., "*Comparison of Laboratory Wheel-Tracking Test Results to WesTrack Performance*," Transportation Research Record No. 1681, pp. 121-128, Washington, D.C., 1999.

Witczak, M.W., "*Harmonized Test Methods for Laboratory Determination of Resilient Modulus for Flexible Pavement Design*," Transportation Research Board, NCHRP 1-28A, Vol. I, June, 2000.

Wright, P.J.F., "*Comments on an Indirect Tensile Test for Concrete Cylinders*," Magazine of Concrete Research, Vol. 7, No. 20, pp. 87-96, 1955.

Zhou, H., Huddleston, J., and Lundy, J., "*Implementation of Back-calculation in Pavement Evaluation and Overlay Design in Oregon*," Transportation Research Record 1377, pp. 150-158, Washington, D.C., 1992.

APPENDIX A: Mix Design Sheets

Sheet A.1: Mix Design Sheet for Tar Creek Base Mix

STATE OF OKLAHOMA
DEPARTMENT OF TRANSPORTATION
MATERIALS DIVISION

Prj. No. 125- S3 **Design No.** 3073-OU-RBM50
Project No. Chat-Asphalt Road **Hwy.** County Road **ESAL** 0.3M+
Contractor Glover Const. Co. **Producer** Glover Const. Co.

MATERIAL	SOURCE	%USED
1-1/4" Limestone	Midwest Minerals @ Miami, OK (5801)	15
9/16" Limestone	Midwest Minerals @ Miami, OK (5801)	28
Screenings (CS-2)	Midwest Minerals @ Miami, OK (5801)	7
Raw Chat	Tri-State Asphalt @ Miami, OK	50
Asphalt Cement (PG 64-22OK)	Valero @ Ardmore, OK	

Laboratory No.

Aggregate Percent Passing	1-1/4" Limestone	9/16" Limestone	Scrns CS-2	Raw Chat	Combined Aggregate	Job Formula	JMF Tolerance
1"	97				100	100	± 0
3/4"	62	100			94	94	± 7
1/2"	33	99		100	90	90	± 7
3/8"	19	74	100	99	80	80	± 7
No. 4	3	10	93	76	48	48	± 7
No. 8	3	3	75	49	31	31	± 5
No. 16	2	2	61	31	21	21	± 4
No. 30	2	2	46	20	14	14	± 4
No. 50	2	2	30	13	9	9	± 4
No. 100	2	2	20	8	6	6	± 3
No. 200	2.0	2.0	14.0	6.1	4.9	4.9	± 2
%AC (PG64-22OK)						5.6	± 0.4
Mix Temperature @ discharge from Mixer, °F						305	± 20
Optimum Roadway Compaction Temperature, °F						290	

Tests on Asphalt Cement:

	Found	Required
Spec. Grav. @ 77 °F	1.02	

Tests on Compressed Mixtures (at Design AC Content):

	SGC	Dens. % of Gmm	Dens. % of Gmm Req'd
Nini	7	85.0	< 90.5
Ndes	75	96	96
Nmax	115	97.8	< 98

Tests on Aggregates:

	Found	Required
F.A.A. %U	47.0	40 Min.
Sand Equivalent	84	40 Min.
L.A. Abrasion	28.0	40 Max.
Durability (DC)	72.0	40 Min.
IOC	0.50	
Insoluble Residue	62.0	30 Min.
Fractured Faces	100/100	75/75 Min.
Gse	2.603	
Gsb	2.504	
Specimen Wt	4500	

Tests on Compressed Mixtures:

Percent Asphalt	Gmb	Gmm	Dens. % of Gmm	Dens. % of Req'd of Gmm	V.M.A. (%)	V.M.A. (Min.%)	%VFA	%VFA Req'd	%DP	%DP Req'd
5.0	2.293	2.416	94.9		13.0		61.0		1.39	
5.5	2.303	2.398	96.0	95-97	13.1	13	69.6	65-78	1.21	0.6-1.6
6.0	2.324	2.381	97.6		12.8		81.2		1.08	

Mix Layer Depth < 4 in.
Compacted mass 105.4 lbs/sq.yd/1" thickness

Sheet A.2: Mix Design Sheet for Tar Creek Surface Mix

STATE OF OKLAHOMA
DEPARTMENT OF TRANSPORTATION
MATERIALS DIVISION

Prj. No. 125- S5 **Design No.** 3075-OU-RSM80
Project No. Chat-Asphalt Road **Hwy.** County Road **ESAL** 0.3M+
Contractor Glover Const. Co. **Producer** Glover Const. Co.

MATERIAL	SOURCE	%USED
9/16" Limestone	Midwest Minerals @ Miami, OK (5801)	14
Screenings (CS-2)	Midwest Minerals @ Miami, OK (5801)	6
Raw Chat	Tri-State Asphalt @ Miami, OK	80
Asphalt Cement (PG 64-22OK)	Valero @ Ardmore, OK	

Laboratory No.

Aggregate Percent Passing	9/16" Limestone	Scrns CS-2	Raw Chat	Combined Aggregate	Job Formula	JMF Tolerance
1/2"	99		100	100	100	± 7
3/8"	74	100	99	96	96	± 7
No. 4	10	93	76	68	68	± 7
No. 8	3	75	49	44	44	± 5
No. 16	2	61	31	29	29	± 4
No. 30	2	46	20	19	19	± 4
No. 50	2	30	13	12	12	± 4
No. 100	2	20	8	8	8	± 3
No. 200	2.0	14.0	6.1	6.0	6.0	± 2
%AC (PG70-28OK)					6.9	± 0.4
Mix Temperature @ discharge from Mixer, °F					325	± 20
Optimum Roadway Compaction Temperature, °F					305	

Tests on Asphalt Cement:

	Found	Required
Spec. Grav. @ 77 °F	1.01	

Tests on Aggregates:

	Found	Required
F.A.A. %U	47.0	40 Min.
Sand Equivalent	78	40 Min.
L.A. Abrasion	22.0	40 Max.
Durability (DC)	75.0	40 Min.
IOC	0.38	
Insoluble Residue	83.0	30 Min.
Fractured Faces	100/100	75/75 Min.
Gse	2.607	
Gsb	2.465	
Specimen Wt	4500	

Tests on Compressed Mixtures (at Design AC Content):

	SGC	Dens. % of Gmm	Dens. % of Gmm Req'd
Nini	7	86.0	< 90.5
Ndes	75	96	96
Nmax	115	96.6	< 98

Tests on Compressed Mixtures:

Percent Asphalt	Gmb	Gmm	Dens. % of Gmm	Dens. % of Req'd of Gmm	V.M.A. (%)	V.M.A. (Min.%)	%VFA	%VFA Req'd	%DP	%DP Req'd
6.3	2.228	2.373	93.9		15.3		60.1		1.44	
6.8	2.256	2.356	95.8	95-97	14.7	15	71.2	65-78	1.29	0.6-1.6
7.3	2.273	2.339	97.2		14.5		80.5		1.16	

Mix Layer Depth < 4 in.
Compacted mass 103.4 lbs/sq.yd/1" thickness

Sheet A.3: Mix Design Sheet for Davis Base Mix

STATE OF OKLAHOMA
DEPARTMENT OF TRANSPORTATION
MATERIALS DIVISION

A.D. No. 010-024-002 S2 Recycle Design No. 3072-BCC-02140
Project No. BHFY-21N(04) 16231(04) Hwy. SH-7 ESAL 3M+
Contractor Plains Bridge Contracting of OK Producer Broce Construction Co.

MATERIAL	SOURCE	%USED
1-1/2" Rock	Dolese @ Davis, OK(5002)	32
3/8" Chips	Dolese @ Davis, OK(5002)	11
Screenings	Hanson @ Davis, OK(5008)	8
Stone Sand	Dolese @ Davis, OK(5002)	28
M.A.P.	Stockpile @ Plantsite	21
Asphalt Cement (PG64-22OK)	Valero @ Ardmore, OK	

Laboratory No. / Aggregate Percent Passing	1 1/2" Rock	3/8" Chips	Screens	Stone Sand	M.A.P.	Combined Aggregate	Job Formula	JMF Tolerance
1 1/2"	100					100	100	± 0
1"	100				100	100	100	± 7
3/4"	74				93	90	90	± 7
1/2"	36	100			90	77	**88	± 7
3/8"	21	99	100	100	66	72	**82	± 7
No. 4	2	17	83	99	62	54	**61	± 7
No. 8	1	4	56	69	75	40	**41	± 5
No. 16	1	3	39	35	70	28	**24	± 4
No. 30	1	3	28	16	62	20	**16	± 4
No. 50	1	2	21	6	54	15	*11	± 4
No. 100	1	2	16	5	24	8	8	± 3
No. 200	1.1	2.0	12.3	3.9	9.0	4.6	**5.9	± 2
%AC (PG64-22OK)					5.2		**4.5	± 0.4
Mix Temperature @ discharge from Mixer, °F							305	± 20
Optimum Roadway Compaction Temperature, °F							290	

Tests on Asphalt Cement:

	Found
Spec. Grav. @ 77 °F	1.01 Est.

Tests on Aggregates:

	Found	Required
F.A.A. %U	44.2	40 Min.
Sand Equivalent	84	45 Min.
L.A. Abrasion	22.2	40 Max.
Durability (DC)	71	40 Min.
IOC	0.12	
Insoluble Residue	N/A	N/A
Fractured Faces	100/100	75/75 Min.
Gse	2.696	
Gsb	2.641	
Specimen Wt.	4750	

Tests on Compressed Mixtures (at Design AC Content):

	SGC	Dens. % o Gmm	Dens. % of Gmm Req'd
Nini	8	85.5	< 89
Ndes	100	96	96
Nmax	160	97.4	< 98

Tests on Compressed Mixtures:

Percent Asphalt	Gmb	Gmm	Dens. % of Gmm	Dens. % of Req'd of Gmm	V.M.A. (%)	V.M.A. (Min.%)	%VFA	%VFA Req'd	%DP	%DP Req'd
3.8	2.360	2.536	93.1		14.0		50.4		1.49	
4.3	2.380	2.517	94.6	95-97	13.8	12	60.5	65-76	1.28	0.6-1.6
4.9	2.400	2.494	96.2		13.6		72.3		1.09	

Mix Layer Depth: ≥ 4 in. TSR: 0.80 0.80 Min. (0.75 Min. Field) Required
Compacted Wt. 110.7 lbs/sq.yd/1" thickness
Lab Permeability Test(cm/sec) - 0.1×10^{-5} (Required: 125×10^{-5} Max.)
APA Rut Test Depth(mm) - 3.985 (Required: 5 mm Max.)
Recommended **3.4% New Asphalt Cement
*REVISED(GRAD.) per Contractor's request effective 8/25/04.
**REVISED(GRAD. & AC) per Contractor's request effective 8/30/04.

MEETS SPECIFICATION REQUIREMENTS for 708-16(a-g)99 Rev. 10/29/03
708-5(a-b)99 Rev. 9/26/02

Sheet A.4: Mix Design Sheet for OKC Base Mix

STATE OF OKLAHOMA
DEPARTMENT OF TRANSPORTATION
MATERIALS DIVISION

A.D. No. 010-029-003 S2 Recycle Design No. 3072-OAEST-03145
Project No. STP-055B(802)AG 14364(04)C Hwy. City Street ESAL 0.3M+
(tractor Allen Contracting, Inc. Producer PMI, Inc.

MATERIAL	SOURCE	%USED
1 ½" Rock	Hanson Aggregates @ Davis, OK(5008)	42
Screenings	Hanson Aggregates @ Davis, OK(5008)	15
Wash Shot	Dolese @ Davis, OK(5002)	10
Sand	G.M.I. Meridian Pit @ Oklahoma City, OK	8
M.A.P.	Stockpile @ Plantsite	25
Asphalt Cement (PG64-22OK)	Wynnewood Refining @ Wynnewood, OK	

Laboratory No.								
Aggregate Percent Passing	1 1/2" Rock	Scrns	Washed Shot	Sand	M.A.P.	Combined Aggregate	Job Formula	JMF Tolerance
1 1/2"	100					100	100	± 0
1"	98				100	99	99	± 7
3/4"	77				99	90	90	± 7
1/2"	41				95	74	74	± 7
3/8"	27	100	100		92	67	67	± 7
No. 4	8	84	87	100	77	52	52	± 7
No. 8	4	56	10	99	61	34	34	± 5
No. 16	3	37	2	98	48	27	27	± 4
No. 30	3	25	2	90	39	22	22	± 4
No. 50	2	16	1	72	30	17	17	± 4
No. 100	2	12	1	19	16	8	8	± 3
No. 200	1.6	8.4	1.1	2.0	10.0	4.7	4.7	± 2
%AC (PG64-22OK)					4.7		4.3	± 0.4
Mix Temperature @ discharge from Mixer, °F							305	± 20
Optimum Roadway Compaction Temperature, °F							290	

Tests on Asphalt Cement:

	Found	Required
Spec. Grav. @ 77 °F	1.01 Est.	

Tests on Compressed Mixtures (at Design AC Content):

	SGC	Dens. % o Gmm	Dens. % of Gmm Req'd
Nini	7	89.4	85.5 - 90.5
Ndes	75	96	96
Nmax	115	97.4	< 98

Tests on Aggregates:

	Found	Required
F.A.A. %U	46.1	40 Min.
Sand Equivalent	76	40 Min.
L.A. Abrasion	16.3	40 Max.
Durability (DC)	73.0	30 Min.
IOC	0.43	
Insoluble Residue		N/A
Fractured Faces	100/100	65/65 Min.
Gse	2.710	
Gsb	2.678	
Specimen Wt.	4935	

Tests on Compressed Mixtures:

Percent Asphalt	Gmb	Gmm	Dens. % of Gmm	Dens. % of Req'd of Gmm	V.M.A. (%)	V.M.A. (Min.%)	%VFA	%VFA Req'd	%DP	%DP Req'd
4.3	2.428	2.527	96.1	95-97	13.2	12	70.4	65-78	1.21	0.6-1.6

Mix Layer Depth: > 4"
TSR: 1.00 0.80 Min. (0.75 Min. Field) Required
Compacted Wt. 111.2 lbs./sq.yd./1" thickness
Lab Permeability Test(cm/sec) - $2x10^{-5}$ (Required: $12.5x10^{-5}$ Max.)
APA Rut Test Depth(mm) - 4.163 (Required: 6 mm Max.)
Recommended 3.2% New Asphalt Cement (PG 64-22OK)
TIED: STP-055B(803)AG

MEETS SPECIFICATION REQUIREMENTS for 708-3(a-g)99 Rev. 6/3/04
708-5(a-b)99 Rev. 6/3/04

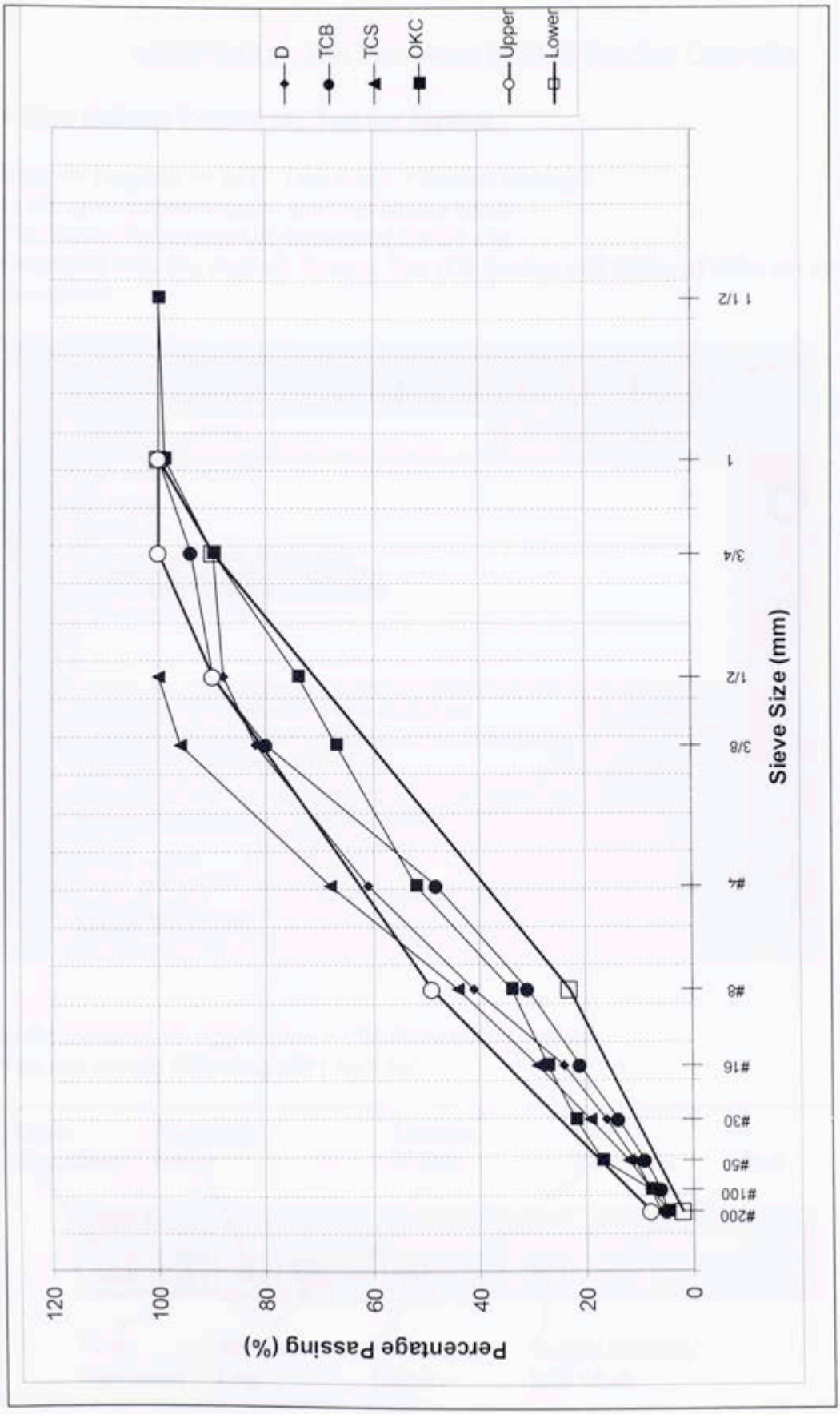
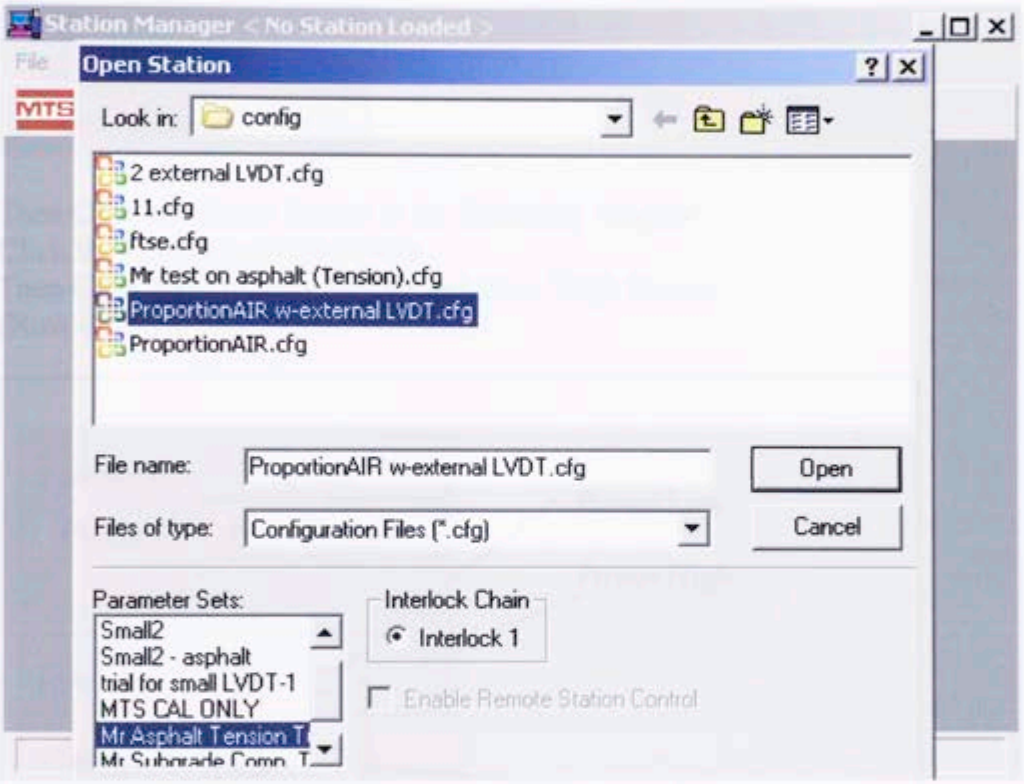


Figure A.1: Gradation Curve for All Four HMA Mixes

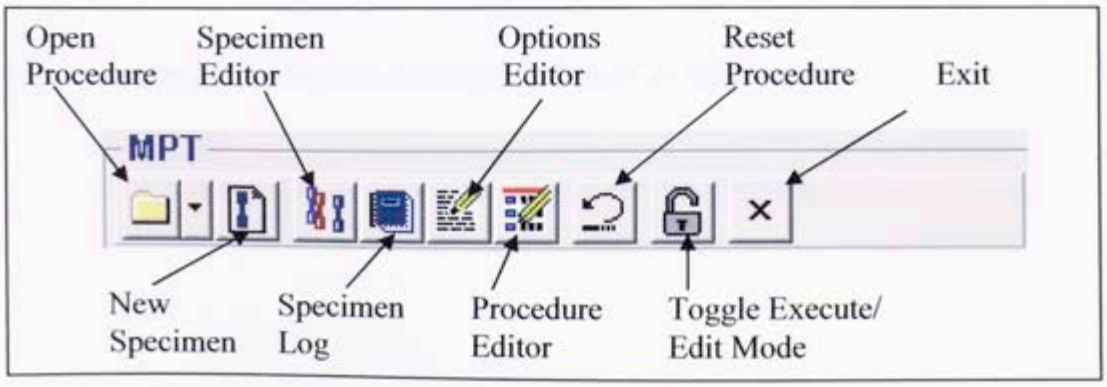
APPENDIX B: Test Procedures by MTS FlexTest Controller

1. Run Indirect Tension M_R Test for Asphalt

Start >> Program >> MTS Flex Test >> Station Manager
In the open station window select as shown below
File Name: ProportionAIR w-external LVDT.cfg
Parameter Sets: M_R Asphalt Tension Test (Calibration and tuning of pulse are sets in this parameter)



In the menu Go to Application >> Multipurpose Testware
You can see the following MPT tool bar



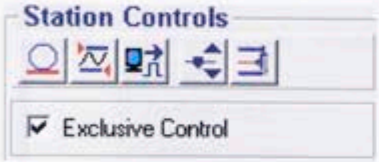
File Name: MR Asphalt Tension.000

Click Specimen Editor >> Set Specimen Directory path: **C:\ftse\mpt\Specimens\MR Asphalt Tension**

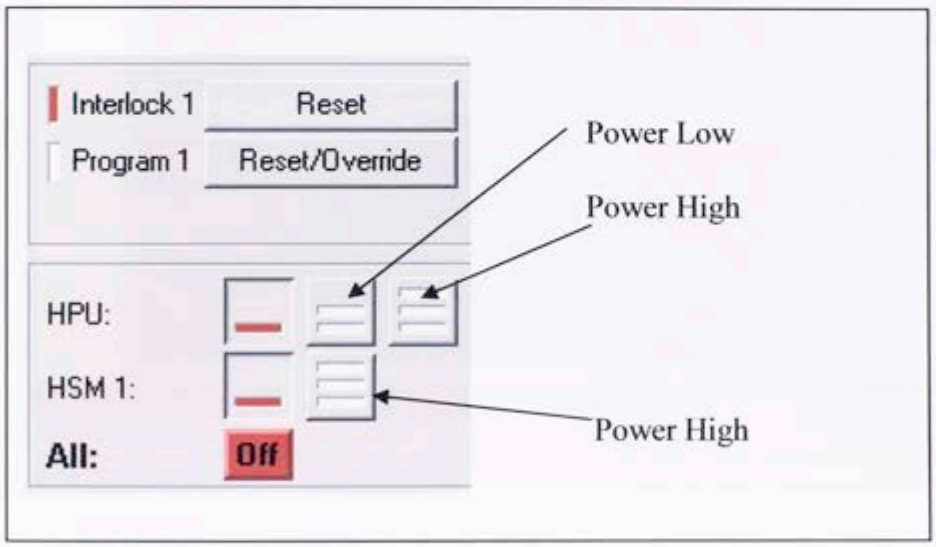
Click New Specimen and give specimen Name: for e.g. **D-MR-2**

Then Click Toggle Execute/Edit Mode and lock it.

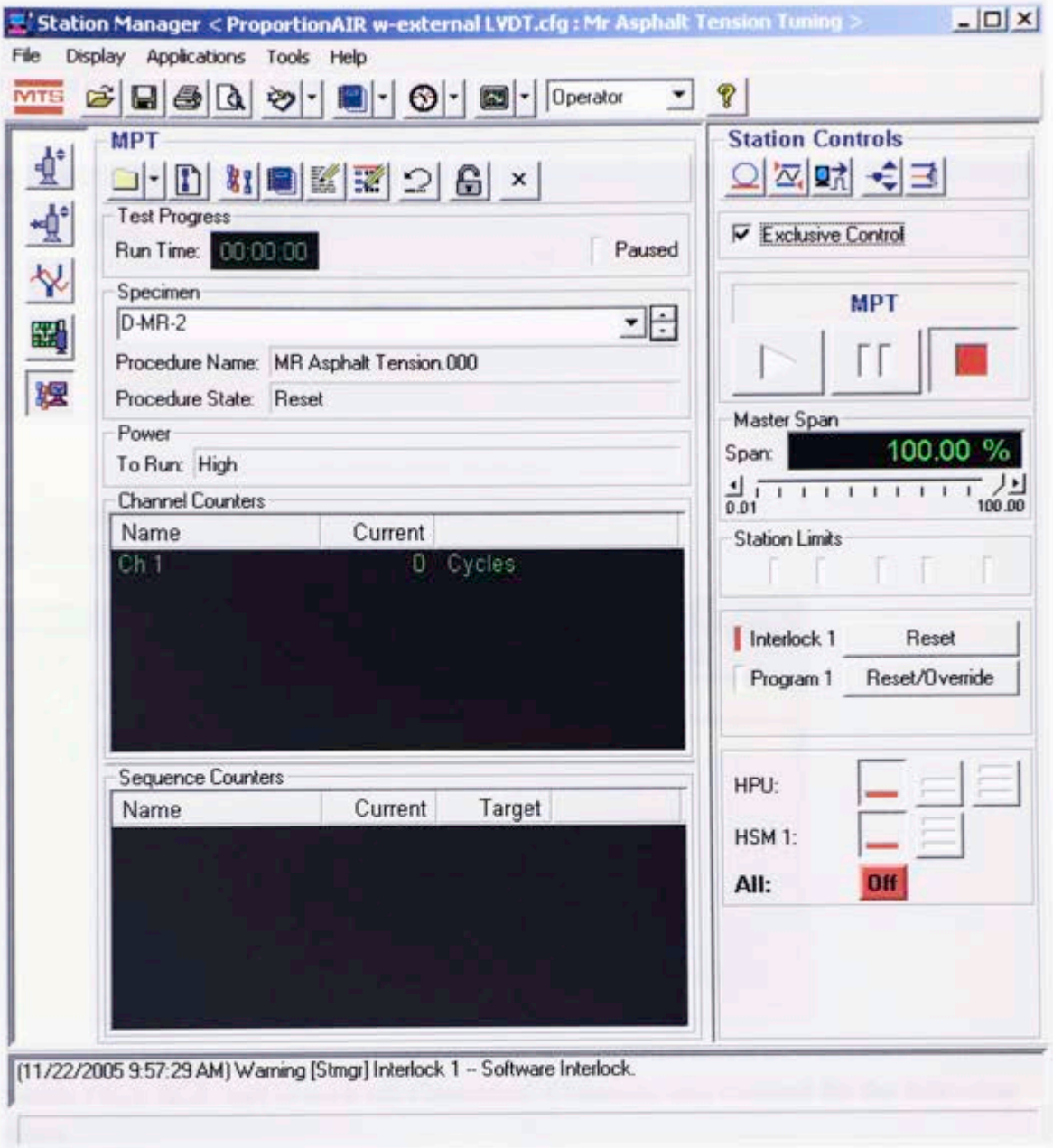
Check Exclusive Control under Stations Controls



Then Click the **Reset** Button in the following window
Click the HSM 1 to **High Power**
Then Click HPU to **Low Power** and Then **High Power**
(Now the Hydraulic system will start)



Now you can see the **Station Manager** Window as follows

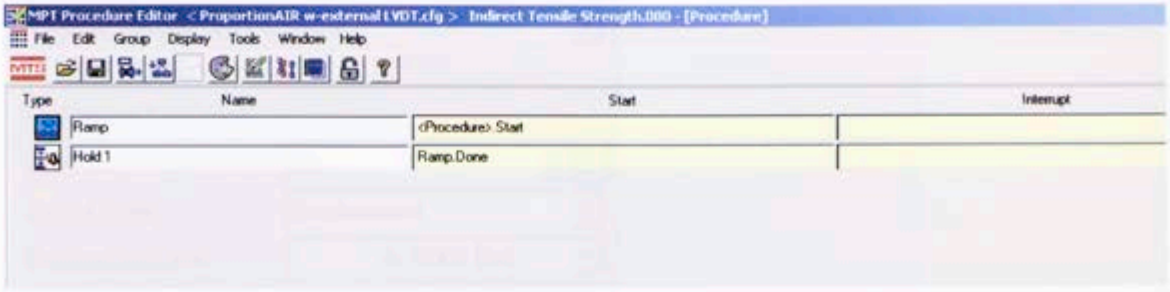


Then Click **Program Run** button  to start the test.

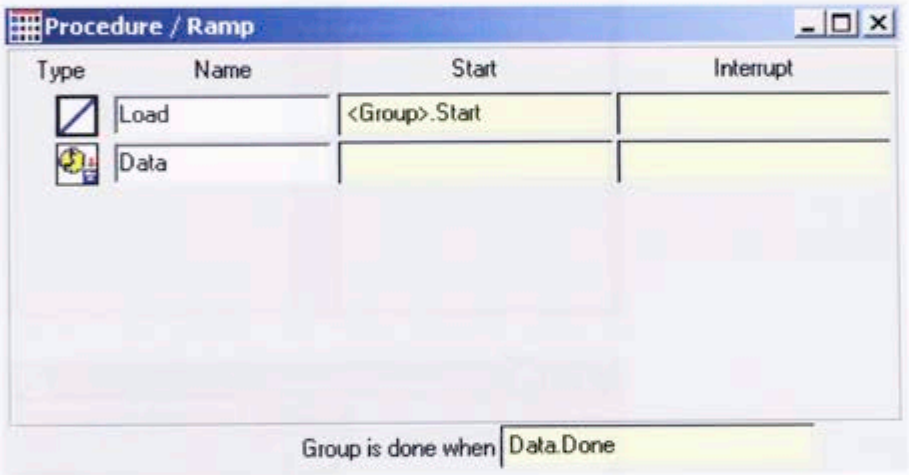
During the test to see the load pulse and deflection curve Click **Scope**  in the main tool bar, a Scope window will open, you can change required setting to see a better wave forms.

2. Indirect Tensile Strength Test

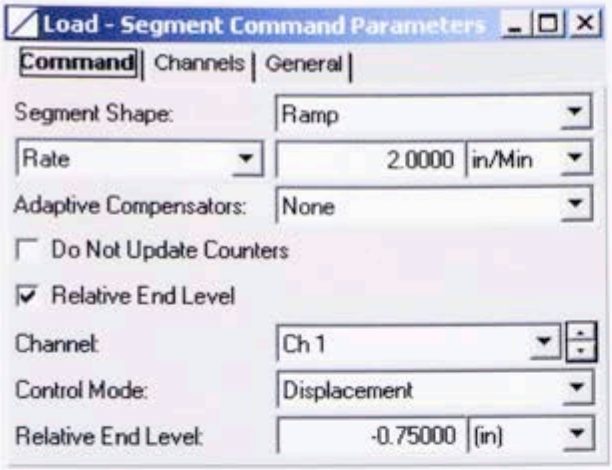
Open MPT Procedure Editor
Then open the file <Indirect Tensile Strength.000>

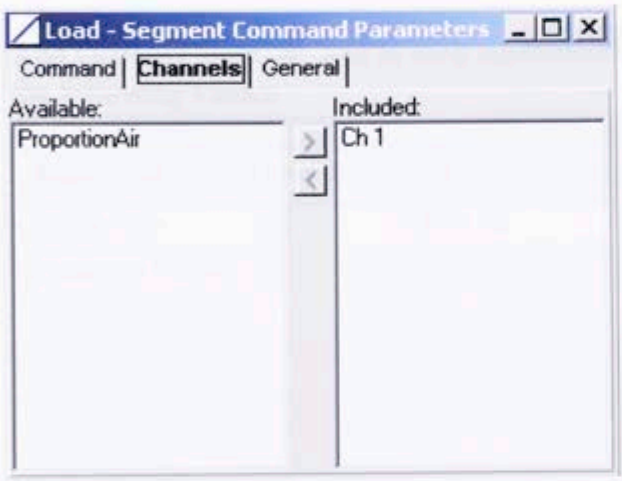


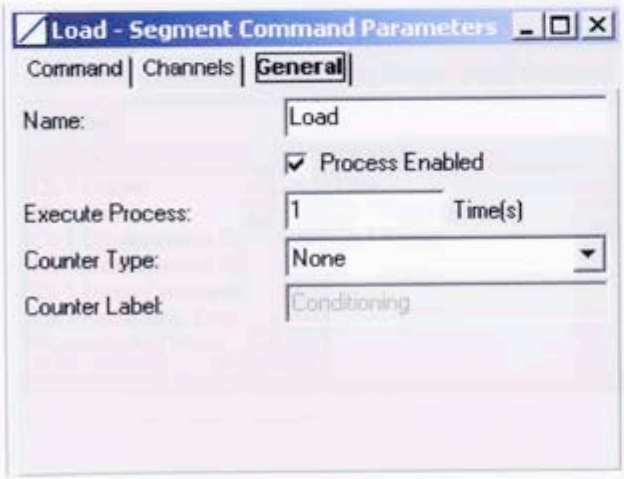
Right click 
Select Open Table



Double Click , and in each tab Command, Channels, and General fill the following values

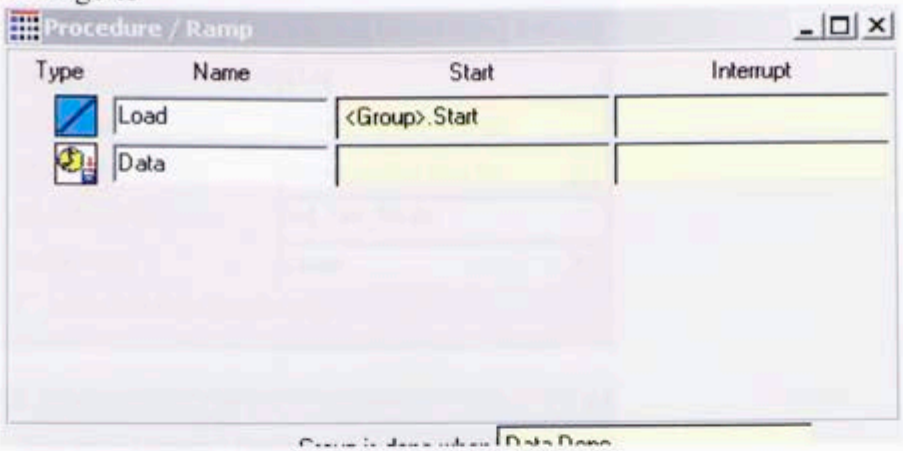

Load - Segment Command Parameters
Command
Channels
General
Segment Shape:
Ramp
Rate
2.0000
in/Min
Adaptive Compensators:
None
Do Not Update Counters
Relative End Level
Channel:
Ch 1
Control Mode:
Displacement
Relative End Level:
-0.75000
(in)


Load - Segment Command Parameters
Command
Channels
General
Available:
ProportionAir
Included:
Ch 1

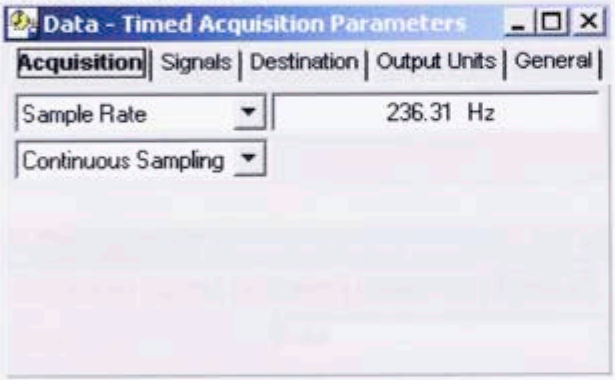

Load - Segment Command Parameters
Command
Channels
General
Name:
Load
Process Enabled
Execute Process:
1
Time(s)
Counter Type:
None
Counter Label:
Conditioning

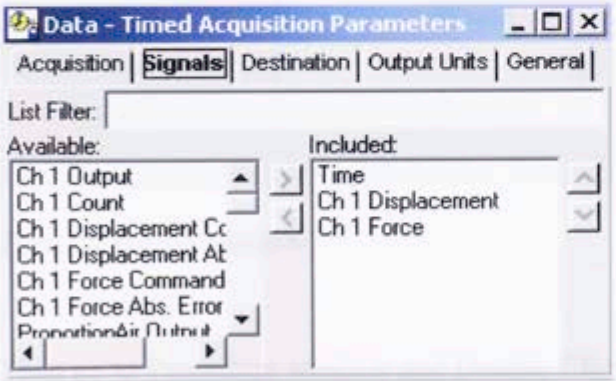
Close this 
Load - Segment Command Parameters

Then go to

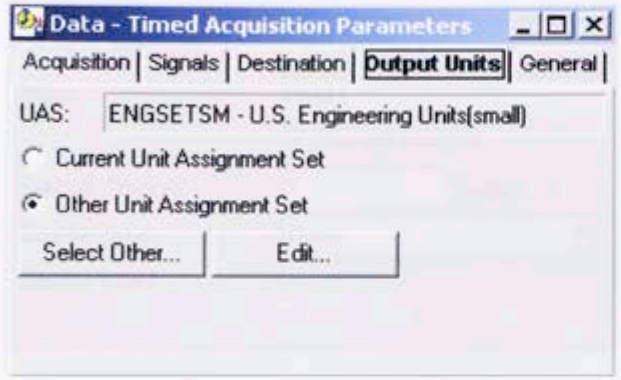


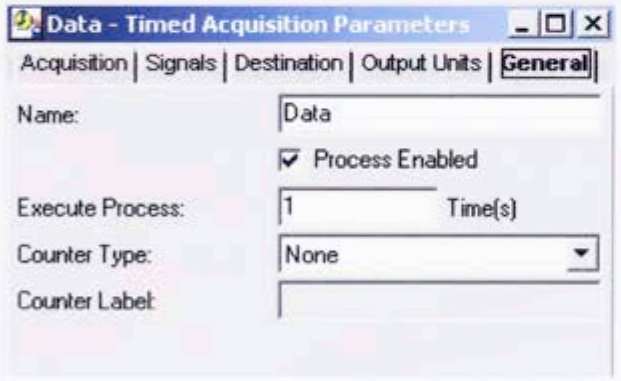
And Double Click , and in each tab Acquisition | Signals | Destination | Output Units | General, fill the following values





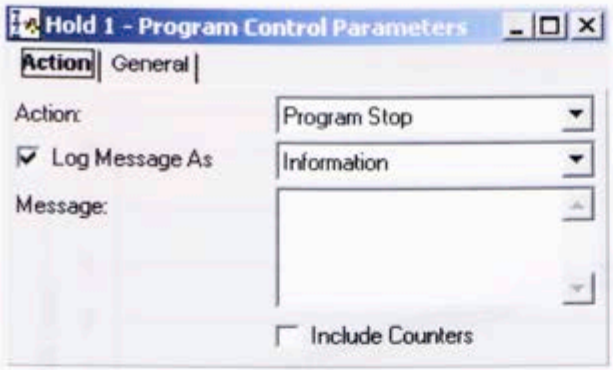


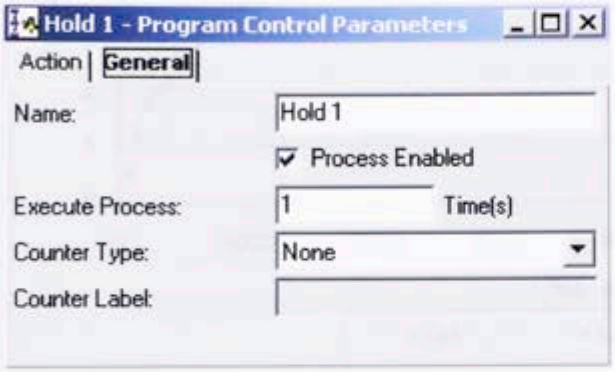




Then close this window

Then go to Procedure window and Double Click , and in each tab Action and General fill the following values





This program for Indirect Tensile Strength test was developed by the author.

APPENDIX C: APA Rut Results

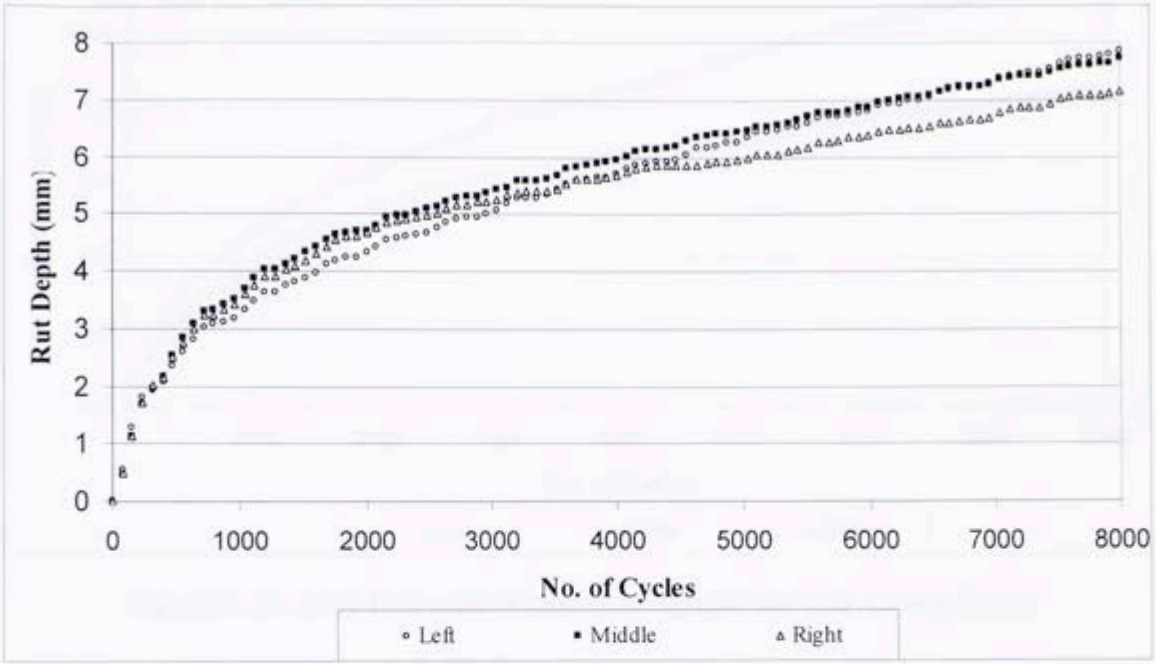


Figure C.1: APA Rut with Number of Cycles for Tar Creek Surface Mix

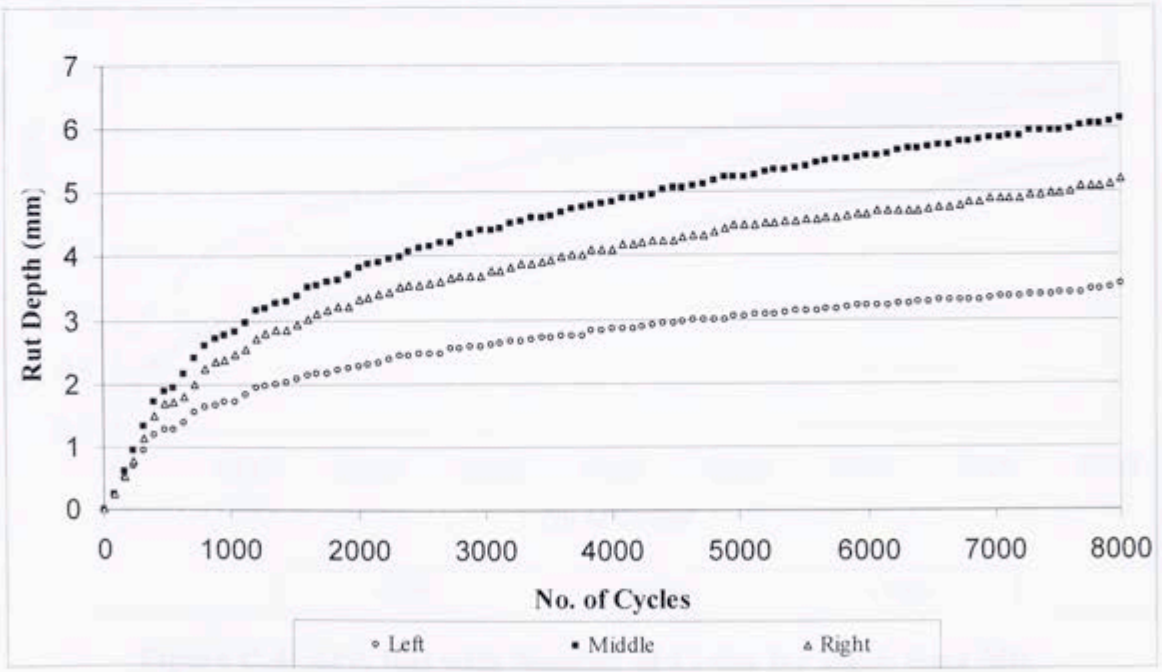


Figure C.2: APA Rut with Number of Cycles for Tar Creek Base Mix

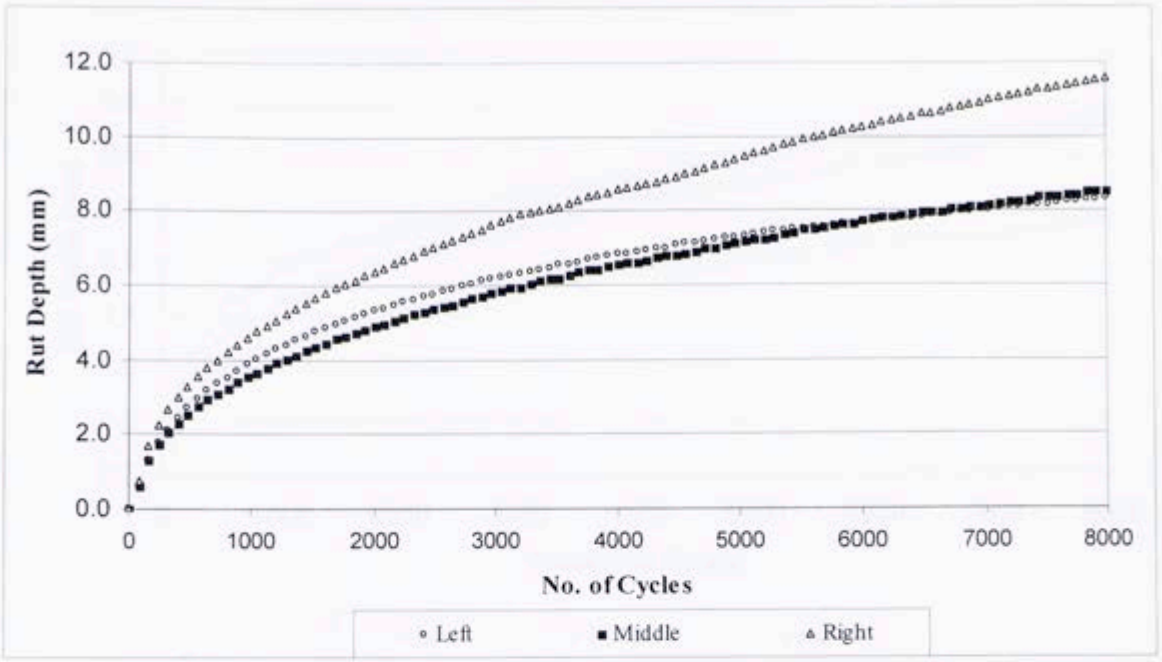


Figure C.3: APA Rut with Number of Cycles for Tar Creek Cores

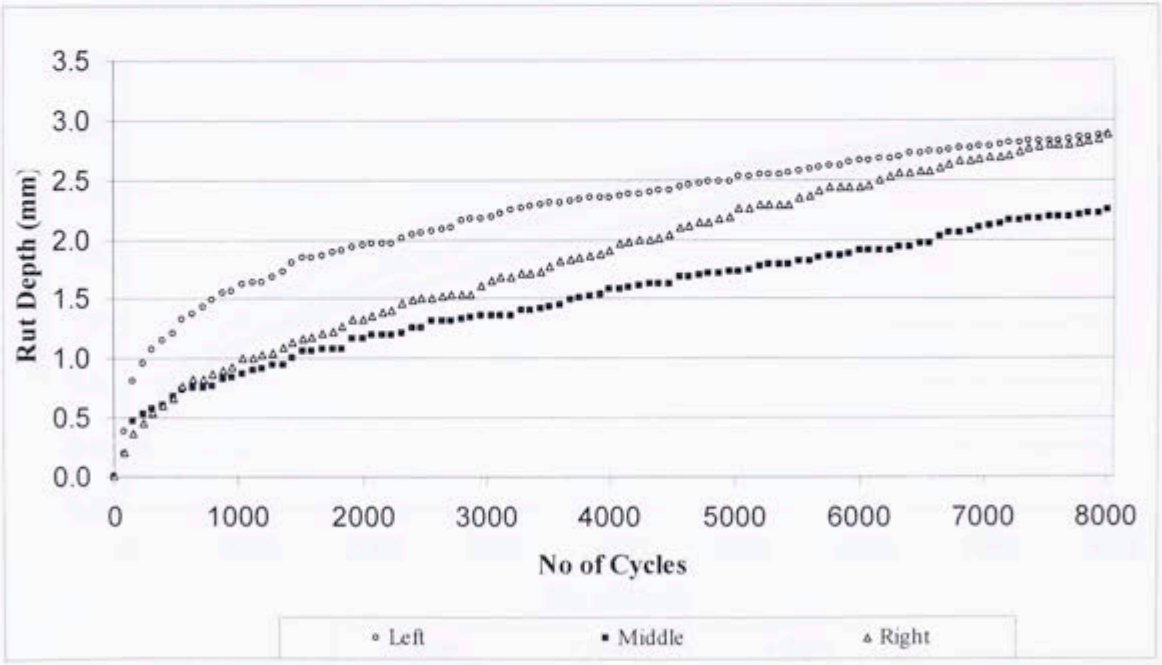


Figure C.4: APA Rut with Number of Cycles for Davis Base Mix

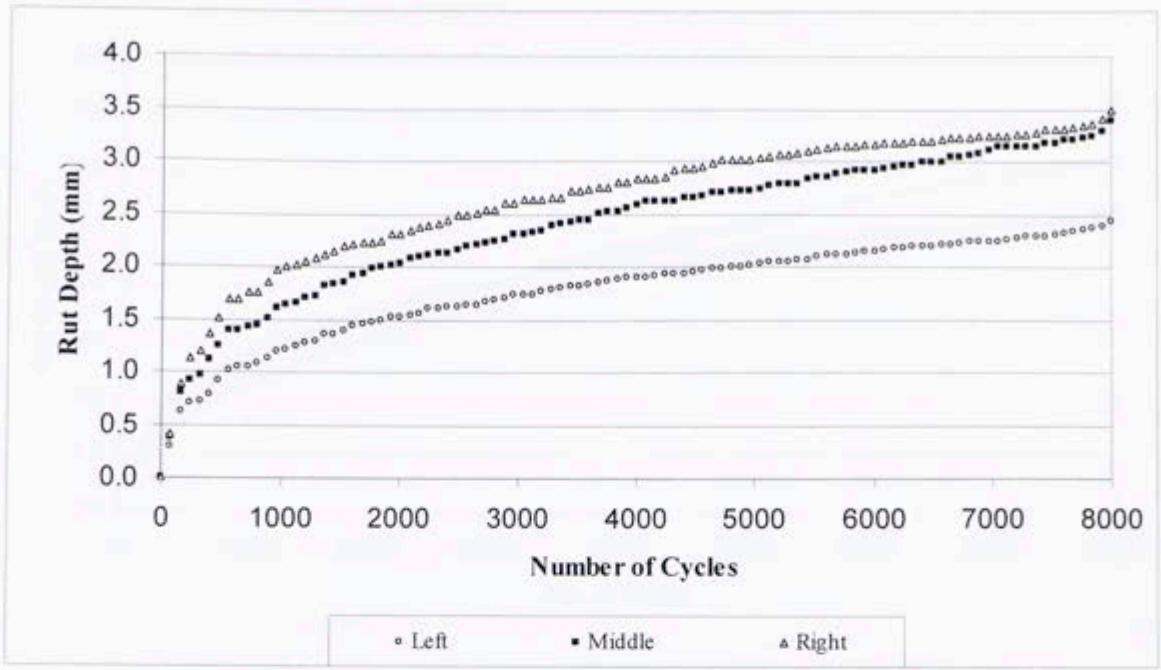


Figure C.5: APA Rut with Number of Cycles for Davis Cores

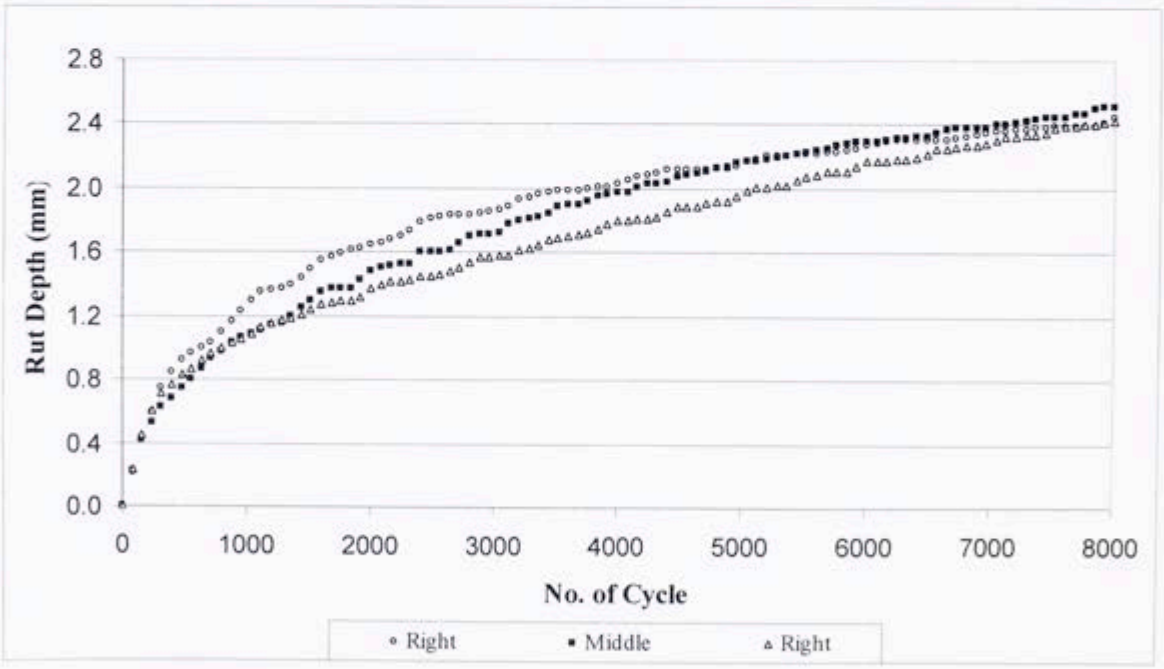


Figure C.6: APA Rut with Number of Cycles for OKC Base Mix

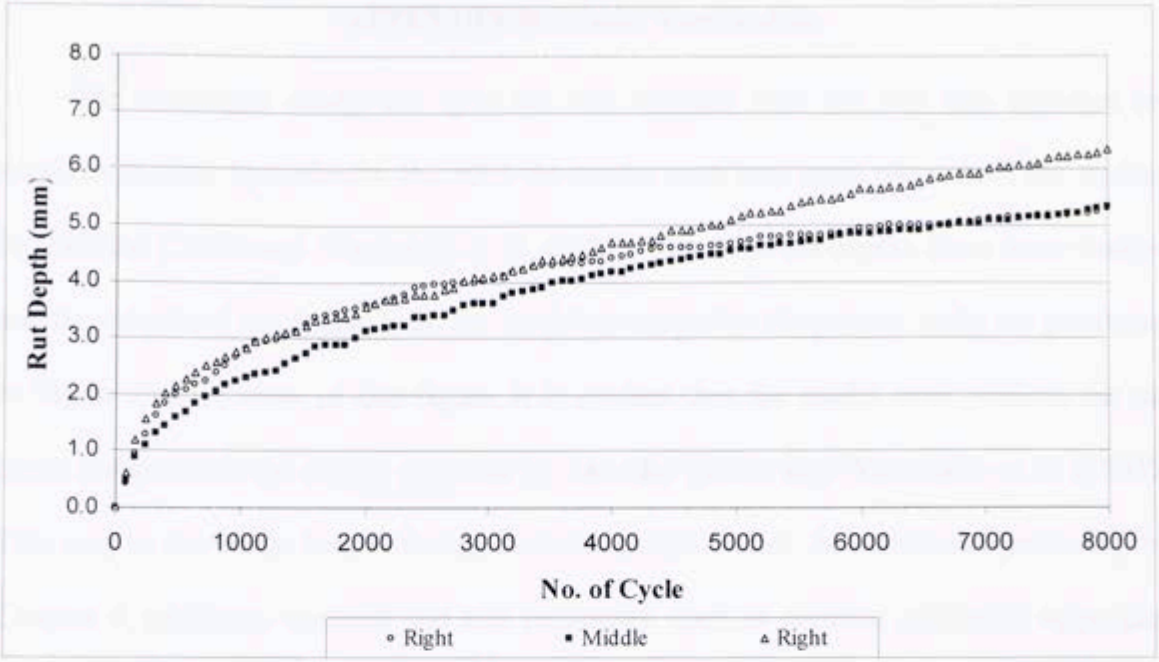


Figure C.7: APA Rut with Number of Cycles for OKC Cores

APPENDIX D: Model Verification

The developed model for APA rut was verified with the test data reported by previous studies. Specifically, the APA rut results used here were taken from the studies by Tarefder (2003) and Wasiuddin et al. (2005). The APA rut depths from these studies and the calculated rut depths from the model developed in the present study are presented in Figure D.1. In view of this figure, it is evident that the model over predicts the rut depth compared to the results reported by Tarefder (2003) and Wasiuddin et al. (2005). This may be due to the lack of factors included in this model. As mentioned previously in Chapter 4, additional material and mix properties, such as nominal maximum aggregate size and binder type were not examined in the present study. Only PG 64-22 binder was used in all four mixes. However, Tarefder (2003) and Wasiuddin et al. (2005) used different types of binders, as shown in Table D.1. To verify the present model further, it is recommended that additional comparisons be made.

Table D.1: Rut Depths from Literature and Developed Model

	Mix ID	PG Grade	AC	N_{200}	Rut Depth	
					Literature	Model
Wasiuddin et al. (2005)	SM40	PG 70-28	6.1	4.5	1.0	9.3
	SM60	PG 70-28	6.8	5.7	1.4	7.6
	SM80	PG 70-28	7.0	6.0	1.8	7.3
	BM40	PG 64-22	5.0	4.1	4.9	6.9
	BM50	PG 64-22	5.4	5.7	4.9	4.2
	BM70	PG 64-22	6.8	4.7	7.2	11.4
Tarefder (2003)	1	PG 64-22	4.6	4.5	2.8	5.0
	2	PG 64-22	4.8	4.2	1.4	6.1
	3	PG 64-24	5.6	5.7	4.3	4.6
	4	PG 70-28	4.9	4.7	1.9	5.2
	5	PG 70-28	3.8	4.7	2.3	3.3
	6	PG 76-28	4.7	4.6	2.1	5.0
	7	PG 70-28	4.1	4.7	1.9	3.7
	8	PG 64-22	6.3	5.7	3.2	6.2
	9	PG 70-28	5.2	5.4	3.5	4.4
	10	PG 70-28	4.5	5.3	2.0	3.5

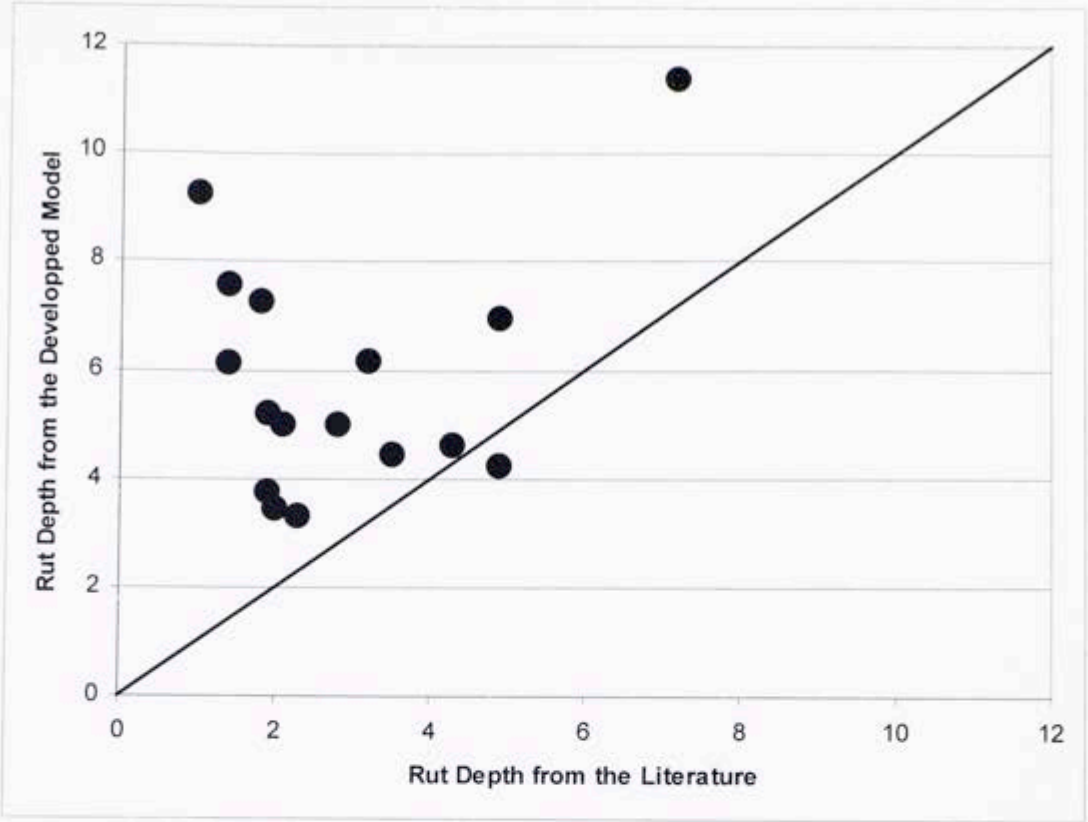


Figure D.1: Comparison of Rut Depths from Literature and Developed Model

This volume is the property of the University of Oklahoma, but the literary rights of the author are a separate property and must be respected. Passages must not be copied or closely paraphrased without the previous written consent of the author. If the reader obtains any assistance from this volume, he must give proper credit in his own work.

I grant the University of Oklahoma Libraries permission to make a copy of my thesis upon the request of individuals or libraries. This permission is granted with the understanding that a copy will be provided for research purposes only, and that requestors will be informed of these restrictions.

NAME [redacted]

DATE

A library which borrows this thesis for use by its patrons is expected to secure the signature of each user.

This thesis by SINNIAH KARUPPIAH NAVARATNARAJAH has been used by the following persons, whose signatures attest their acceptance of the above restrictions.

NAME AND ADDRESS	DATE

OU-139